Occupant sensing in buildings : methods for occupant number, location and activity

Chen, Zhenghua

2017

Chen, Z. (2017). Occupant sensing in buildings : methods for occupant number, location and activity. Doctoral thesis, Nanyang Technological University, Singapore.

http://hdl.handle.net/10356/70606

https://doi.org/10.32657/10356/70606

Occupant Sensing in Buildings: Methods for Occupant Number, Location and Activity

Zhenghua Chen

School of Electrical & Electronic Engineering

A thesis submitted to the Nanyang Technological University
in partial fulfillment of the requirements for the degree of
Doctor of Philosophy

2017

Statement of Originality

I hereby certify that the intellectual content of this thesis is the product of my original research work and has not been submitted for a higher degree to any other University or Institution.

....

Date Zhenghua Chen

Acknowledgements

First of all, I would like to give my greatest gratitude to my supervisor, Professor Yeng Chai Soh, who guided me throughout my entire PhD study. He provides me a wonderful platform for learning, and encourages me to explore challenging and interesting research fields. I have really benefited a lot on research methods and directions of my research from every discussion and meeting with him. I also want to thank Professor Lihua Xie, who provided me a lot of help during my application to NTU. Moreover, he gives me many useful suggestions on my research during our combined group meetings.

I appreciate the help of Dr Jinming Xu who is brilliant and erudite. We have many deep discussions on various research problems, where I learnt how to do research. I also would like to thank Mr Qingchang Zhu and Mr Mustafa K. Masood. We collaborated on many interesting research topics, and delivered several wonderful outcomes. In the meantime. I want to thank all the guys in Machine Learning and Internet Of Things laboratories for their help and kind friendships. I have had a wonderful time there because of them.

I would like to thank Mr Shuai Wang, who teaches me the way of fitness in my struggling time of PhD study. The workouts keep me fit and make me fear nothing. I meet a lot of hard-working guys who influenced me to work hard as well. I am very appreciative of the joyful time I spent with all the guys in our fitness group.

Last but not least, I must thank my girlfriend for her very supportive trust on all my decisions. She is very kind and has the purest of heart I ever seen. I am very lucky that I have met her in my life. I must also thank my dear family, my father and my mother. They supported me and understood me without any doubt. They always give their best to me without hesitation. They are certainly the best!

Abstract

Since buildings account for some 40% of total energy usage in the world, great attentions have been paid on energy efficient buildings. To achieve this objective, occupant sensing is a key factor, which includes knowing the number of occupants, their locations and their performed activities in buildings. In this dissertation, we attempt to give solutions to the three corresponding questions of occupant sensing: How many occupants are there in a zone? Where are they located? What are they doing?

Occupancy, i.e. the number of occupants, is a coarse information for the control of energy efficient buildings. We develop novel inhomogeneous Markov chain models which utilize the incremental information of occupancy for building occupancy modeling under two scenarios of multi-occupant single-zone (MOSZ) and multi-occupant multi-zone (MOMZ). In this way, we can dramatically simplify the calculation of model parameters, i.e. transition probability matrices. The proposed models have been evaluated using actual occupancy data. After that, we explore the more valuable information of real-time occupancy estimation that can be used for real-time building environment control. Since occupancy models can provide the information of occupancy pattern, we present a fusion framework of combining occupancy models with data-driven models for occupancy estimation using environmental parameters. Real experiments showed the effectiveness of the proposed approach. For some applications, such as smart scheduling, pre-heating and pre-cooling, they require the knowledge of occupancy level in future, known as occupancy prediction. We compare the prediction performance of existing occupancy models with some popular linear and non-linear data mining approaches. The experimental results allow us to deduce a guideline on how to choose a proper method for the prediction of occupancy in buildings under different prediction horizons.

One of the detailed aspects in occupant sensing is the locations of occupants in buildings. Outdoor localization can be resolved using GPS (Global Positioning

System). However, since GPS signals are blocked in indoor environments, the performance of GPS is greatly degraded. The most widely used technique for indoor localization is based on WiFi technology. We propose a fusion framework of WiFi, smartphone sensors and landmarks for indoor localization. Instead of using the popular WiFi fingerprinting approach which requires a labor intensive and time consuming site survey of the environment, we apply a weighted pass loss model for WiFi localization. We formulate the fusion in a linear perspective. Then, the Kalman filter which is computational light can be applied. Moreover, we use landmarks such as turns, stairs and elevators, which can be detected using smartphone sensors to further improve the performance of the proposed system. Significant improvements were demonstrated in real experiments. In situations where WiFi signals are not available, or the application is sensitive to power consumption, which makes WiFi based approaches not suitable because of the power hungry property of WiFi scanning, we present another localization and tracking system using smartphone sensors with occasional iBeacon corrections. Based on the detailed analysis of iBeacon technology, we define a calibration range where the extended Kalman filter is formulated. Real experiments have been conducted in two different environments. The experimental results demonstrated the effectiveness of the proposed approach. We also tested the localization accuracy with respect to the number of iBeacons. Another detailed aspect in occupant sensing is the activity performed by occupants. This activity information can be used to identify landmarks for indoor localization and, more importantly, to determine the metabolic rate which is a key parameter in calculating human comfort index. We propose an orientation independent activity recognition system based coordinate transformation and principle component analysis using smartphone acceleration data. The experimental results indicated that the proposed approach significantly improve the detection accuracy with regard to orientation variations. Moreover, the results also showed some improvements of our proposed approach on placement and subject variations.

Contents

List of Figures

Chapter 1

Introduction

1.1 Background and Motivation

Due to global energy crisis and the awareness of sustainable development, a great deal of attention has been paid on energy efficiency in buildings which account for some 40% of total energy consumption in the world [2] and one-third of total global greenhouse emissions [3]. This implies that large potential energy saving can be achieved in building sectors if more efficient control and management strategies are implemented. Occupants influence the indoor environment due to the emissions of heat and CO_2. Moreover, since occupants may trigger the use of appliances such as computers and lighting, they have a great impact on energy consumptions in buildings. Thus, occupancy information is vital for building control systems such as HVAC (Heating, Ventilating, and Air Conditioning). For instance, if there are no or few occupants in a zone, the HAVC systems can be turned off or running in an energy saving mode. If a large number occupants enter a zone (such as meetings or classes), we can immediately adjust the power of the HVAC system to create a comfortable environment. Moreover, if we can predict the occupancy for the zone, pre-cooling or pre-heating strategies can be applied to provide a comfort indoor environment and, at the same time, save energy. Therefore, occupant sensing is vital in achieving energy efficiency in buildings. It can be resolved in three aspects of occupant number, location and activity. The number of occupants, known as occupancy, is a coarse information in occupant sensing. We handle this in terms of

three aspects of occupancy modeling, estimation and prediction. Occupancy modeling can reveal the patterns of occupants, which can be used as inputs of energy simulation tools, such as EnergyPlus [4], DeST [5] and TRNSYS [6]. With these tools, we can simulate energy consumption of a building before construction. And, based on the simulation results, we can size the facilities of the building in advance. Current building control systems do not take real-time occupancy information into consideration. This leads to, for example, regularly air-conditioning of unoccupied areas, which wastes a large amount of energy. Occupancy-driven control can save up to 15% of the total energy usage in buildings [7], and adaptive lighting control based on real-time occupancy information is also shown to be effective and can reduce $35-75\%$ of energy usage for lighting in buildings [8]. These applications require the monitor of occupancy levels and the states of presence and absence in real-time in a non-intrusive way. Thus, occupancy estimation is necessary and important for energy efficient buildings. Knowing only the real-time occupancy information is not adequate to achieve high energy efficiencies in buildings. The goal of building control systems is to be able to respond optimally on the changes of indoor requirements. A slow response control system, e.g. HVAC, using current occupancy measurements generally will lag behind. This makes the prediction of occupancy vital so as to arrive at an optimal response [9]. If we can accurately predict future occupancy, known as occupancy prediction, optimal real-time building climate control strategies, e.g. model predictive control (MPC), can be leveraged to save energy without compromising occupants' comfort [10–12]. In addition, smart preheating or precooling strategies [13–15] and load prediction [16] also require an accurate occupancy prediction. The prediction accuracy and horizon will determine the type of application. For real-time MPC, it requires accurate prediction of occupancy level in short prediction horizons. For other applications such as preheating or precooling and load prediction, accurate long-term (hours) occupancy prediction is necessary. Therefore, the ability to accurately predict occupancy with different prediction horizons is also meaningful for building energy efficiency.

Besides the coarse information of occupant number, the more detailed information of occupant location and activity is also vital for energy efficiency in buildings. A typical application of location information is adaptive lighting control which is convenient for users and energy efficiency [8]. Meanwhile, we can also control appliances based on users' locations to save energy, known as location based control. For these applications, real-time meter-level localization accuracy is compulsory,

which is one of our objectives. The authors in [17] have shown that their location based control system can save 50% of energy consumed by lighting systems and around $140Wh$ per computer for a typical working day. In the meantime, the location information is useful for emergency evacuation and personalized services in buildings, which may only require room level localization accuracy [18]. The performed activity of occupant is another crucial information for building control systems. Recent intelligent building research attempts to save energy and, at the same time, maintain a comfort thermal environment [19]. One popular thermal comfort index, i.e. predicted mean vote (PMV), can be calculated based on user activity information, such as static, walking and running. We attempt to accurately identify these daily activities for real-time estimation of thermal comfort index. Utilizing real-time thermal comfort index, the control systems in building can save 30% of energy and maintain thermal comfort [20].

In a word, with the coarse information of occupant number and detailed information of occupant location, we can achieve energy saving in buildings through occupancy driven control, preheating or precooling, localized control and adaptive lighting control without compromising human comfort which can be estimated using the detailed information of occupant activity.

1.2 Objectives

The objectives of this thesis are to solve the specific problems in occupant sensing in buildings, and these includes occupancy modeling, estimation and prediction, occupant indoor localization and occupant activity recognition. For occupancy modeling, we attempt to simplify models and make them feasible for real-time implementations in two complicated scenarios of multi-occupant single-zone (MOSZ) and multi-occupant multi-zone (MOMZ). When performing occupancy estimation, we intend to combine occupancy models with conventional data-driven approaches using non-intrusive environmental sensors to improve the estimation accuracy. After that, we compare the prediction capabilities of occupancy models and data mining approaches for building occupancy prediction. Occupancy is a coarse information for building control systems. More detailed information consists of occupant location and activity. We try to improve the localization and tracking accuracy of occupants in indoor environments using WiFi, iBeacons, landmarks and portable

smart devices, such as smartphones. Finally, we also attempt to eliminate the effect of orientations variations of smartphones for recognizing occupant's simple activities indoors.

1.3 Major Contributions

Our main contributions can be stated as follows:

- *Occupancy Modeling, Estimation and Prediction*:

  For building occupancy modeling, there are three typical scenarios of Single-Occupant Single-Zone (SOSZ), MOSZ and MOMZ. In the case of SOSZ, it is easy to model, because only one occupant is involved and no interactions (other occupants or zones) need to be considered. Moreover, this simple case has already been well studied in literature. Here, we considered the two more complicated scenarios of MOSZ and MOMZ. In these two scenarios, the interactions between occupants and zones make the occupancy dynamics more difficult to model. And few works have handled these two scenarios, thus more researches need to be done. Two novel stochastic inhomogeneous Markov chain models were proposed to model building occupancy under the two scenarios. In the MOSZ scenario, instead of using the number of occupant in a zone as the state, we defined the state as the increment of occupancy in the zone. In the MOMZ scenario, by taking into account interactions among zones, we proposed another inhomogeneous Markov chain whose state is a vector where each component represents the increment of occupancy in each zone. In this way, we can significantly simplify the calculation of transition probability matrix which is a key parameter in Markov chain models. For building occupancy estimation, a non-intrusive method based on environmental parameters is presented. First, data-driven models that include extreme learning machine (ELM), support vector machine (SVM), artificial neural network (ANN), k-nearest-neighbors (KNN), Linear Discriminant Analysis (LDA) and Classification And Regression Tree (CART) were employed to achieve an initial estimation of building occupancy. Then, we fused the results of data-driven models with well-developed occupancy models which can

extract occupancy patterns to improve the estimation accuracy. For building occupancy prediction, we explored the prediction of occupancy level in multi-occupant commercial buildings. The prediction methods can be divided into two categories of occupancy models and data mining approaches. The occupancy models leveraged on the existing multi-occupant models, i.e. inhomogeneous Markov chain (IMC) and multivariate Gaussian (MG), which were proposed for occupancy modeling, to predict building occupancy. For the data mining approaches, the occupancy prediction problem is addressed in the form of time series prediction, and three popular linear and non-linear models, i.e. autoregressive integrated moving average (ARIMA), artificial neural network (ANN) and support vector regression (SVR), were proposed and evaluated. All the proposed approaches have been evaluated using real occupancy data in buildings.

- *Occupant Indoor Localization*:

  For indoor localization and tracking, we proposed a sensor fusion framework that combines WiFi, smartphone sensors and landmarks. Since the whole system will be running on a smartphone which is resource limited, we formulated the fusion problem in a linear perspective, then, a Kalman filter algorithm which is computationally light can be applied. Landmarks which can be detected using smartphone sensors were employed to restart the algorithm and reset the accumulative error of the system. Moreover, instead of using the labor-intensive and time-consuming WiFi fingerprinting approach, we applied a weighted pass loss (WPL) approach for WiFi based localization, which is efficient and simple for implementation. In situations where WiFi signals are not available, or the algorithm will be running on a battery sensitive smartphone, we proposed a smartphone inertial sensor based indoor localization and tracking system with occasional iBeacon corrections. By analyzing iBeacon measurements, we defined an efficient calibration range where an extended Kalman filter is formulated. We evaluated these algorithms in real environments to show the effectiveness of the propped approaches.

- *Occupant Activity Recognition*:

  For occupant activity recognition, we presented an orientation independent approach based on coordinate transformation and principal component analysis (CT-PCA). The activities of interest include static, walking, running,

going upstairs and going downstairs, which are the most common activities in our daily life. Our experimental results have showed the effectiveness of the proposed CT-PCA technique on orientation variation. Moreover, we also demonstrated impressive improvements on placement and subject variations using our proposed approach.

1.4 Outline of the Thesis

Chapter 1 starts with the background and motivation of this thesis, followed by the objectives of this research and the key contributions that we have made. Chapter 2 reviews the related works of Part I that deals with occupancy modeling, estimation and prediction. Chapter 3 presents our proposed occupancy models under two scenarios of MOSZ and MOMZ. Chapter 4 presents a non-intrusive occupancy estimation system using environmental parameters. Chapter 5 compares occupancy models and data mining approaches in predicting building occupancy under different prediction horizons. Chapter 6 presents the reviews of works related to Part II that deals with occupant indoor localization and activity recognition. Chapter 7 presents an indoor localization scheme based on WiFi, smartphone sensors and landmarks using the Kalman filter. Chapter 8 demonstrates another indoor localization approach which utilizes smartphone sensors with occasional iBeacon corrections. Chapter 9 shows an orientation independent activity recognition system by using coordinate transformation and principal component analysis. Finally, Chapter 10 concludes this thesis, and presents the limitations and some potential ideas for future works.

Part I

Occupancy Modeling, Estimation and Prediction

Chapter 2

Literature Review of Occupancy Modeling, Estimation and Prediction

In Part I of the thesis, we focus on the coarse information of occupant number in buildings. This will reveal the distributions of occupants which can be used for building climate control. The methods for occupant number can be divided into three aspects, i.e. occupancy modeling, estimation, and prediction.

2.1 Occupancy Modeling

Occupancy modeling that reveals occupancy patterns has been performed under scenarios of single-occupant single-zone (SOSZ), multi-occupant single-zone (MOSZ) and multi-occupant multi-zone (MOMZ) in the literature. To model occupant's presence and absence in single person offices, Wang et al. [21] proposed a non-homogeneous Poisson process with two exponential distributions for occupied and vacant intervals respectively. However, the goodness-of-fit test rejects the assumption of the exponential distribution for occupied intervals. Page et al. [22] presented an inhomogeneous Markov chain with two states of presence and absence to model occupancy state in single person offices. A parameter of mobility

which denotes the changing rate of the two states is defined to calculate the transition probability matrix of the inhomogeneous Markov chain model. However, the extension of their model into multi-occupant or multi-zone situations is non-trivial.

Due to the interactions among occupants, multi-occupant modeling can be much more challenging. Gunathilak et al. [23] presented a generalized event-driven and group-based framework to model occupants in buildings. They defined users into different groups based on similar characteristics. Then, the mobility of a user will be driven by group and personal events. Wang et al. [24] also reported an event-driven based approach for simulating building occupancy. They divided one day into the events of walking around, going to office, getting off work and lunch break. Within each event, a homogeneous Markov chain was formulated to simulate occupancy dynamics. The parameter of the homogeneous Markov chain, i.e. transition probability matrix, is determined based on the properties of each event. These two approaches suffer from the same problems of unclear definitions of events and unconvincing evaluation using simulation data instead of actual occupancy data. Richardson et al. [25] presented a Markov chain model whose state is the number of active occupants for occupancy modeling in residential buildings. Their model will not be feasible in the case where the number of active occupants is large.

Erickson et al. [26] presented a multivariate Gaussian model and an agent-based model for extracting occupancy patterns in buildings. The multivariate Gaussian model attempts to fit a Gaussian distribution for building occupancy at each time step. It does not take previous occupancy into consideration. While the agent-based model tries to model each occupant's behaviour individually. This approach does not consider inter-room correlations. To improve the generalization performance of their previous work, Erickson et al. [27] constructed an inhomogeneous Markov chain where the state is a vector in which each component represents the number of occupants in each zone. In this case, the dimension of transition probability matrix that is a key parameter of a Markov chain will increase exponentially with the increase of the number of zones or occupants. Liao et al. [28] proposed an agent-based model with four modules to simulate building occupancy. Based on the occupancy property, a damping process, which claims that occupants tend to stay at their working place for a long time, and an acceleration process, which claims that occupants tend to leave hallways or restrooms quickly, are presented.

Since the four modules are intuitively defined and lack of theoretical support, the performance of the model is limited, especially in the MOMZ scenario. To compensate this, they presented a graphical model in the MOMZ scenario, which is similar to the multivariate Gaussian model that is mentioned previously. Thus, it will suffer from the same problem. Yang et al. [29] modeled personalized occupancy profiles for each day of week using four different techniques, i.e. regression modeling, time-series modeling, pattern recognition modeling and stochastic process modeling. Note that, if the occupancy profiles for two days of week have no significant difference, they will be combined as a single occupancy profile. The four modeling techniques are applied to calculate the expected presence statues. The experimental results indicated that the four techniques outperform the fixed designed profile and the observation-based method.

Some other works deal with some special properties of occupancy dynamics. Stoppel and Leite attempted to describe occupants' long vacancy using probabilistic models [30]. The results were utilized for energy simulation, and the simulation results were compared with original energy models. Sun et al. presented a stochastic modeling of overtime occupancy in an office building [31]. They first applied a binomial distribution to represent the total occupancy in overtime, and then, utilized an exponential distribution to represent the duration of working overtime. The generated overtime occupancy schedules can be used as an input of energy simulations to improve their performance.

In this thesis, we propose two novel inhomogeneous Markov chain models under two complicated scenarios of MOSZ and MOMZ for modeling occupancy in buildings. In the MOSZ scenario, an inhomogeneous Markov chain model where the state is defined as the increment of occupancy in a zone is presented. Assume that the maximal number of occupants moving into or out of a zone in a short interval is one, we can obtain a simple transition probability matrix with a dimension of 3×3, regardless of the total number of occupants in a zone. In the MOMZ scenario, by taking interaction among zones into consideration, we presented another inhomogeneous Markov chain where the state is a vector in which each component represents the increment of occupancy in each zone. In this manner, a greatly simplified model that can be practically implemented is able to be obtained.

2.2 Occupancy Estimation

Occupancy estimation can be achieved using different sensors. Dodier et al. leveraged on binary sensors, i.e. passive infrared, to detect occupant's presence and absence [32]. However, more important information of the number of occupants cannot be derived by using their approach. Erickson et al. applied a wireless network of cameras [33], which may have privacy concerns for occupants. Labeodan et al. employed chair sensors in a conference room situation [34], which cannot detect occupants who are standing. Zhao et al. inferred building occupancy based on appliance power consumption data [35]. However, the occupants who are not using appliances will be missing. Some recent works tend to use wearable sensors, e.g. RFID [36], WiFi [37] and Bluetooth [38]. These solutions are intrusive for users and cannot detect visitors who do not take RFID tags or users who do not turn on WiFi or Bluetooth.

A recent tend is to use environmental sensors for occupancy estimation, which are non-intrusive, relatively inexpensive and can be applied to all occupants in a zone. With environmental sensor data, useful features that can capture changes of occupancy can be extracted. Then, data-driven models can be applied to estimate the occupancy level. Dong et al. applied a wireless sensor network system to measure environmental parameters, such as CO_2, carbon-monoxide, total volatile organic compounds (TVOC), small particulates (PM2.5), acoustics, illumination, motion, temperature, and humidity, to estimate the number of occupants in an open-plan office building [39]. An information gain theory was employed to perform feature selection. They concluded that the most relevant parameters are CO_2 and acoustic. Yang et al. explored different combinations of sensors, i.e. motion, sound, door, temperature, humidity, CO_2, light, and passive infrared, to detect occupancy in both single-occupancy and multi-occupancy offices by using six data-driven models [40]. The contributions of each sensor were evaluated based on information gain theory. It turned out that CO_2, door status and light level are the three most informative variables. Khan et al. presented an accurate occupancy detection system based on a wireless sensing system which is able to measure temperature, light, humidity, PIR and audio level [41]. They also developed a novel hierarchical analysis framework which combines meeting schedules and computer activity to increase the estimation accuracy. Real-world experiments demonstrated a significant improvement compared to a baseline non-hierarchical approach. Another

relevant work can be found in [42] where the authors employed light, temperature, humidity and CO_2 measurements to estimate the occupied/unoccupied state of an office room by using statistical learning models. Experimental results showed that the light sensor has the largest relative variable importance. They also concluded that the proper selections of features and models will have an important impact on the detection accuracy.

In this thesis, we only employ environmental sensors, i.e. temperature, humidity, CO_2 and air pressure, which are widely available in modern HVAC systems [43]. No specific occupancy sensors, e.g. PIR, motion or light sensors, are required in the environment, and no particular devices, e.g. RFID tags or smartphones, are required to be worn by occupants. Feature selection has been proved to be effective in increasing estimation accuracy [39, 40, 42]. In this work, we perform an ELM-based wrapper method for feature selection. The data-driven models we used include ELM, SVM, ANN, KNN, LDA and CART. To further enhance the performance of the detection system, we propose a fusion framework which combines data-driven models with occupancy models for building occupancy estimation.

2.3 Occupancy Prediction

Some advanced works have been done to predict occupants' presence and absence in homes or single person offices. Scott et al. predicted the occupied and unoccupied states in home environments based on the matching of current patterns with the historical ones [44]. The prediction results are utilized for preheating control of the houses. In experiments, they can save gas and, at the same time, reduce the unconformable time with the occupancy prediction. Kleiminger et al. compared schedule-based and context-aware methods for home occupancy prediction and applied the prediction results for smart heating control [15]. The investigated states are the presence of at least one occupant within a home and the absence of it. The experiments were conducted using actual occupancy schedules of 45 homes. They achieved a prediction accuracy of over 80% using schedule-based approaches. Moreover, a trade-off between energy saving using the prediction results and the risk of comfort loss was investigated. Mahdavi et al. presented a non-probabilistic occupancy model to predict future presence of occupants and compared with two probabilistic occupancy models [45]. Real experiments were conducted with the

data from eight workplaces for 90 days. The experimental results showed that the predictive performances of the three models are limited, especially the probabilistic ones. Several earlier models dealing with the modeling of occupants' presence and absence also have prediction ability. For example, Page et al. proposed an inhomogeneous Markov chain to model occupants' presence and absence in single person offices [22]. All these approaches only handle occupancy prediction with two states, i.e. presence and absence, instead of the more valuable information of occupancy level for applications in commercial buildings.

Some existing multi-occupant models can be applied for predicting building occupancy level. Richardson et al. extended the two-states inhomogeneous Markov chain that was presented by the authors in [22] into a multi-states inhomogeneous Markov chain where the state is the number of occupants [25]. Given the current occupancy level, one can predict future occupancy based on their proposed inhomogeneous Markov chain model. Erickson et al. presented a multivariate Gaussian model to fit room occupancy at each time step [26], which is similar to the graphical model used in [28]. The prediction abilities of these two models have not been studied yet.

Existing works mainly focused on the prediction of occupants' presence and absence in homes or single person offices. In this thesis, we shall explore the prediction of regular occupancy level in multi-occupant commercial buildings deployment scenario. The prediction methods can be divided into two categories of occupancy models and data mining approaches.

Chapter 3

Occupancy Modeling Using Novel Inhomogeneous Markov Chain Approaches

This chapter introduces two novel inhomogeneous Markov chain models for building occupancy modeling. Specifically, in Section 3.1, we will introduce the basic theory of Markov chain and the calculation of Markov transition probability matrix. After that, the modeling processes will be presented in Section 3.2. Finally, in Section 3.3, we present the data for simulation, variables and criteria for evaluation, followed by the simulation results.

3.1 Preliminaries

3.1.1 Markov Chain Theory

A Markov chain is established upon the assumption that the future state only depends on the current state [46]. Suppose X is the state variable, and Ω is the set of all states of X. Then, a discrete time Markov chain $\{X_k\}$ can be formulated as

$$P(X_{k+1} = s_{k+1}|X_1 = s_1, \cdots, X_k = s_k) = P(X_{k+1} = s_{k+1}|X_k = s_k) \tag{3.1}$$

where X_k is the state variable, $s_k \in \Omega$ is the state, and k is the time step. The most important parameter of a Markov chain is the transition probability which describes the transition of two states as follows:

$$P(X_{k+1} = s_{k+1}|X_k = s_k), s_k \in \Omega. \tag{3.2}$$

Since a transition from s_k at time step k to a state at time step $k+1$ must be happening with probability one, we have

$$\sum_{s_{k+1}\in\Omega} P(X_{k+1} = s_{k+1}|X_k = s_k) = 1. \tag{3.3}$$

This property is very helpful in calculating Markov transition probability matrix. If the transition probability matrix is fixed, expressed as $\Psi(k) = \Psi$ for all time step k, the Markov chain is homogeneous. Conversely, a Markov chain is inhomogeneous when the transition probability matrix, $\Psi(k)$, is time varying.

3.1.2 Calculation of Markov Transition Probability Matrix

We adopt maximum likelihood estimation (MLE) to calculate Markov transition probability matrix. Let's define two states, 0 and 1 for a state variable Y_k in a Bernoulli experiment. Assume that the probability of $Y_k = 1$ is p. Then, the likelihood function of p given the observation, y_k, can be expressed as

$$L(p \mid y_k) = \Pr(Y_k = y_k) = \begin{cases} p, & y_k = 1 \\ 1-p, & y_k = 0 \end{cases} \tag{3.4}$$

We use log-likelihood function, $\ln L(p \mid y_k)$, which can simplify the calculation by converting product operation into summation. The MLE can be achieved by maximizing the log-likelihood function [47]. Assume that the log-likelihood function is differentiable and the MLE exists. Then, the following partial differential equation, named *likelihood equation*, must be satisfied:

$$\frac{\partial \ln L(p \mid y_k)}{\partial p} = 0 \tag{3.5}$$

The solution of the above equation will be the MLE solution. The likelihood equation is only a necessary condition for the existence of an MLE solution. An

additional condition is required to guarantee that the solution is the maximum to the likelihood equation. This can be tested by utilizing the second derivative of the log-likelihood function. For the purpose of maximizing, the second derivative of the log-likelihood function should be less than zero at the maximum point, which can be shown as

$$\frac{\partial^2 \ln L(p \mid y_k)}{\partial p^2} < 0 \tag{3.6}$$

In an inhomogeneous Markov chain model, the transition from the state s_k to the state s_{k+1} at one time step can be treated as a Bernoulli experiment happening with the probability $\Pr(X_{k+1} = s_{k+1} | X_k = s_k)$. Note that the likelihood function of this conditional probability is only based on the data $X_k = s_k$ from different days at time step k with the assumption of the independence of the data. Let Ω denote the data set that we collected, M the total number of days where $X_k = s_k$. Within these days, let W be the total number of days where $X_{k+1} = s_{k+1}$, and p the probability $\Pr(X_{k+1} = s_{k+1} | X_k = s_k)$. Then, the log-likelihood function can be expressed as

$$\begin{aligned} \ln L(p \mid \Omega) &= \ln \frac{M!}{W!(M-W)!} p^W (1-p)^{M-W} \\ &= \ln \frac{M!}{W!(M-W)!} + W \ln p + (M-W) \ln(1-p) \end{aligned} \tag{3.7}$$

The corresponding *likelihood equation* is

$$\frac{\partial \ln L(p \mid \Omega)}{\partial p} = \frac{W}{p} - \frac{M-W}{1-p} = 0 \tag{3.8}$$

By solving the above equation, the MLE solution can be obtained as $p_{MLE} = W/M$. To make sure that the solution is the maximum to the likelihood equation, the second derivative of the log-likelihood function at point $p = p_{MLE} = W/M$ is checked, which yields

$$\frac{\partial^2 \ln L(p \mid \Omega)}{\partial p^2} = -\frac{W}{p^2} - \frac{M-W}{(1-p)^2} < 0 \tag{3.9}$$

and it is negative, as expected. Thus, the solution is the MLE. For each transition probability, $\Pr(X_{k+1} = s_{k+1}|X_k = s_k)$, we can calculate it separately using an MLE estimator. The entire transition probability matrix can be obtained in this manner.

3.2 Modeling

Occupancy dynamics have some unique properties. For example, the occupancy at current time is quite related to the occupancy at previous time. Assume the occupancy is low at this time instance, there will be a high probability that the occupancy will still be low at next time instance, which can be regarded as Markov property. Thus, Markov chain can be an efficient method in modeling occupancy dynamics. Meanwhile, the occupancy dynamics strongly relate to the time of day. For instance, the occupancy increases in the morning for arrival and decreases in the afternoon for departure. Therefore, the inhomogeneous Markov chain is a good candidate for occupancy modeling. However, traditional methods [22, 25] which apply the number of occupants as the state of inhomogeneous Markov chain are not feasible in real implementations with many occupants. Therefore, in the MOSZ scenario, we define the state of the inhomogeneous Markov chain as the increment of occupancy in a zone, which can be expressed as $N_k^i - N_{k-1}^i$, where N_k^i is the occupancy level in zone i at time step k. We assume that the maximum number of occupants moving into or out of a zone is one within a short interval. This short interval can be determined based on actual occupancy data. Under this assumption, the case where multiple occupants move into the zone simultaneously can be transferred to another case where multiple occupants move into the zone sequentially within a short interval. Due to the slow response of building control systems, this very short interval (for example several seconds) has minor influence. Thus, this assumption will has very minor influence on the building control systems. This indicates the reasonability of this assumption. Figure 3.1 illustrates a simple example of the proposed approach. Precisely, the occupancy level in a zone is 6 at time step k, then, one occupant has moved out of the zone at time step $k+1$. Therefore, the current state is -1 according to our state definition, and the next reachable state would be 1, 0 or -1. In this manner, we obtain the transition probability matrix with a dimension of 3×3 independent of the maximum number of occupants in the zone. As a comparison, assuming that the maximum number

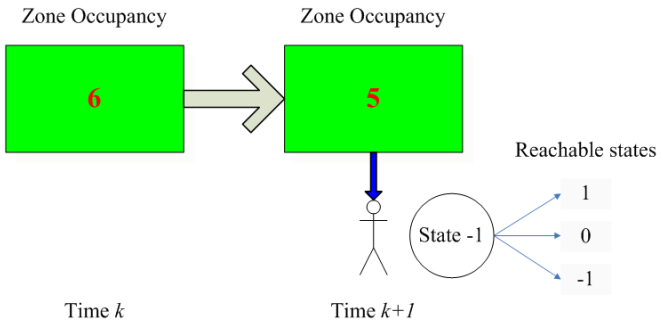

FIGURE 3.1: The occupancy state representation in the MOSZ situation.

of occupants in the zone is 20, then with the approach in [25], the state of the Markov chain can be 0 to 20, resulting in 21 states. The corresponding transition probability matrix will be of dimension 21×21, which is much more complicated.

In the MOMZ situation, by taking interactions among zones into consideration, we construct another inhomogeneous Markov chain model where the state is defined as a vector in which each component is the increment of occupancy in each zone. We make the same assumption that the maximum number of occupants moving into or out of a zone is one within a short interval. Therefore, the component of a state (vector) can be 1, -1 or 0. Figure 3.2 shows an example of four zones in the MOMZ situation. The occupancies of Zone1, Zone2, Zone3 and Zone4 are 8, 4, 3 and 0 respectively at time step k. At time step $k+1$, one occupant moved out of Zone1, one occupant moved into zone2, no occupants moved into or out of Zone3, and one occupant moved into zone4. Thus, the corresponding state is $\{-1, 1, 0, 1\}_{k+1}$. Since the total number of states is $3^4 = 81$ in terms of our state definition, the final transition probability matrix has the dimension of $3^4 \times 3^4$ independent of the number of occupants in a zone. In the same MOMZ situation, assuming that the maximum number of occupants in each zone is 20, if the advanced model in [27], which defined the state as a vector whose component is the number of occupants in each zone, is employed, each zone will contain 21 states. Therefore, the dimension of the transition probability matrix will be $21^4 \times 21^4$, which is huge and impossible to solve.

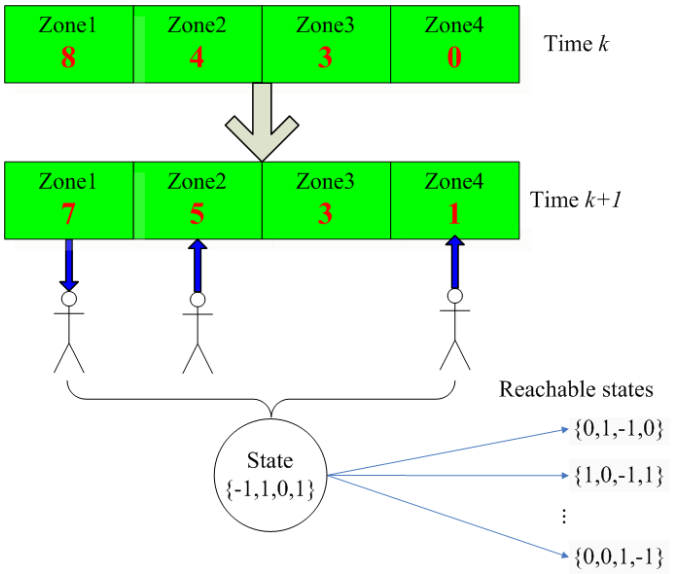

FIGURE 3.2: The occupancy state representation in the MOMZ situation.

3.3 Evaluation

To evaluate the performance of our proposed models, simulations with actual occupancy data have been done under two scenarios of MOSZ and MOMZ. First, we briefly introduce the data for simulation. Then, we define some variables related to occupancy properties and two evaluation criteria. Finally, we present the simulation results and discussions under the two scenarios.

3.3.1 Data

In the MOSZ scenario, the data that was provided by the authors in [28] was collected by using a wireless camera near the entrance of a zone from January 2010 to April 2010, a span of around four months. The occupancy level is manually counted from the video. Due to certain technical issues, only 70 days of data were collected. We compare our results with the agent-based model in [28], which applied the same data in model verification. In the MOMZ scenario, we have 31 days of data from 57 cubicles with 2 minutes resolution. The data spans from August 2009 to January 2010. According to the detailed analysis in [48], the data at a few cubicles (6, 20, 26, 56, 57) is considered abnormal with respect to the others, which has been discarded first. Then, we uniformly divide the remaining 52 cubicles into 4 zones, namely "Zone1", "Zone2", "Zone3" and "Zone4", for the

simulations. The four zones are decided based on the proximity, and they are uniformly distributed.

3.3.2 Variables and Criteria

To evaluate the performance of the proposed model, five variables related to occupancy properties are defined. The definitions of the variables are similar to those in [28]. Assume, $Q_{occupied}$ and $Q_{unoccupied}$ are the thresholds of occupied and unoccupied states respectively, and I is the time interval. The five variables are defined as follows:

- *Mean occupancy*: The mean occupancy of zone i at time step k is defined as $E(X_k^i)$, where $E(\cdot)$ is the expectation operation.
- *Time of first arrival*: The time of first arrival is the first time when the zone becomes occupied. Precisely, for zone i, if $X_k^i \geqslant Q_{occupied}$ and $X_t^i \leqslant Q_{unoccupied}$ for all $t < k$, then, k is the time of first arrival.
- *Time of last departure*: The time of last departure is the time from which the zone becomes unoccupied. For zone i, if $X_k^i \geqslant Q_{occupied}$ and $X_t^i \leqslant Q_{unoccupied}$ for all $t > k$, then, $k+1$ is the time of last departure.
- *Cumulative occupied duration*: The cumulative occupied duration is the total length of time when the zone is occupied. For zone i, it is the number of the elements of the set $\{k|X_k^i \geqslant Q_{occupied}, 1 \leqslant k \leqslant 24 \times 60/I\}$ for each day.
- *Number of occupied/unoccupied transitions*: The number of occupied/unoccupied transitions is the total number of transitions between "occupied" and "unoccupied" status of a zone. For zone i, it is the number of elements of the set $\{k|X_k^i \geqslant Q_{occupied}, X_{k+1}^i \leqslant Q_{unoccupied}, 1 \leqslant k \leqslant 24 \times 60/I\} \bigcup \{k|X_k^i \leqslant Q_{unoccupied}, X_{k+1}^i \geqslant Q_{occupied}, 1 \leqslant k \leqslant 24 \times 60/I\}$ for each day.

To quantify the performance of our proposed models in terms of the defined variables, two evaluation criteria are chosen. The first criterion of normalized root mean square deviation (NRMSD) is defined to compare the difference between mean occupancy profiles predicted by models and estimated from measurements which is the ground truth occupancy measured by using occupancy sensors. Given

two time series, $x(k)$ and $y(k)$, $k = 1, 2, ..., K$, the NRMSD between x and y is defined as

$$NRMSD(x, y) = \frac{\|x - y\| / \sqrt{K}}{max(z) - min(z)}, \tag{3.10}$$

where $x = [x(1), x(2), ..., x(K)]^T$, $y = [y(1), y(2), ..., y(K)]^T$, $z = [x^T, y^T]^T$, T is the vector transpose operation, $\|\cdot\|$ is the Euclidean norm and K is the length of the sequences.

The second criterion is Kullback-Leibler (K-L) divergence which is used to compare two distributions of the random variables predicted by models and estimated from measurements [49]. The K-L divergence between two random variables of p and q represents the difference of them and is defined as

$$d(p \parallel q) = \sum_k p_k \log(\frac{p_k}{q_k}), \tag{3.11}$$

where p_k and q_k are two probability mass functions (pmfs).

3.3.3 Simulation Results and Discussions

Since the increment information is applied instead of the exact number of occupants, we can significantly simplify the calculation of Markov transition probability matrices. But one problem arises because of using this increment information. That is, the simulation results may diverge when transferring the increment value into the final occupancy level. To handle this problem, we employ maximal and minimal occupancy constraints which can be derived from actual occupancy data. During simulations, if the current occupancy level after transferring violates these constraints, we will set the current state to the boundaries. Precisely, suppose, O_k^{max} and O_k^{min} are the maximal and minimal constraints of occupancy at time step k, the current state is s_k, and the current occupancy is o_k after transferring the increment information into occupancy. If $o_k > O_k^{max}$, we keep the o_k at the current maximum, O_k^{max}. Similarly, if $o_k < O_k^{min}$, we keep the o_k at the current minimum, O_k^{min}.

Since the agent-based model in [28] run the simulation of one thousand weeks, we performed one thousand simulations, each with a duration of one week, using our

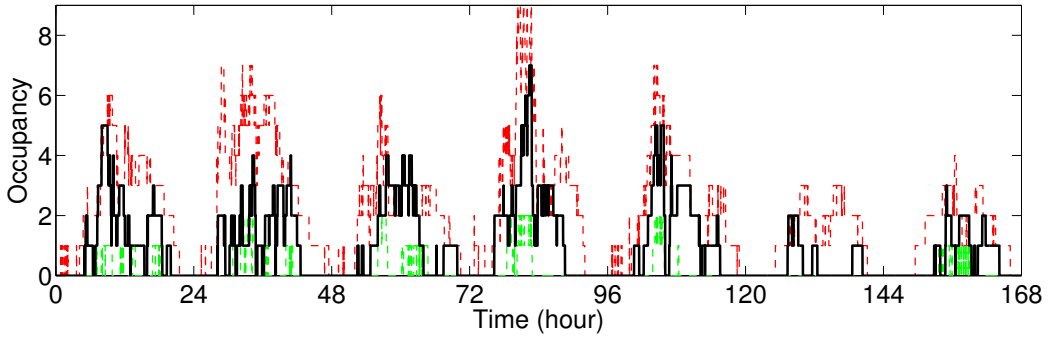

FIGURE 3.3: The output of the proposed model (black) for one week, the maximal occupancy constraint (dashed red) and the minimal occupancy constraint (dashed green).

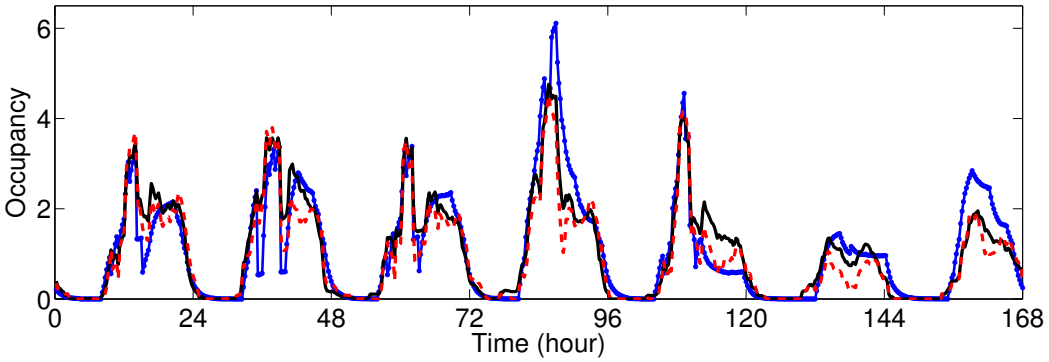

FIGURE 3.4: Mean occupancy profiles estimated from measurements (dashed red), predicted by the agent-based model (dotted blue) and the proposed model (black) in the MOSZ scenario.

proposed model in the MOSZ scenario. We compared the mean occupancy profiles estimated from the measurements, predicted by the agent-based model and our proposed model by using the criterion of NRMSD. Moreover, the four random variables of time of first arrival, time of last departure, cumulative occupied duration and number of occupied/unoccupied transitions, of the proposed model and those of the agent-based model are evaluated using the criterion of K-L divergence. Note that, only the data for weekdays is chosen for the two criteria, and the thresholds are $Q_{unoccupied} = Q_{occupied} = 0.5$.

Figure 3.3 shows the output of our proposed model with the maximal and minimal occupancy constraints for one week. Since the model is stochastic, the model output for each run would be different. The comparison of the mean occupancy profiles estimated from measurements, predicted by the agent-based model and the proposed model is illustrated in Figure 3.4. It can be found that the proposed

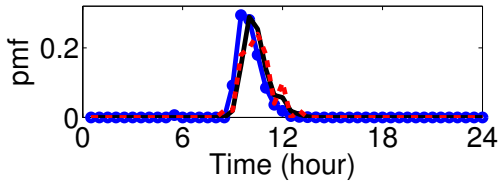

(a) Time of first arrival

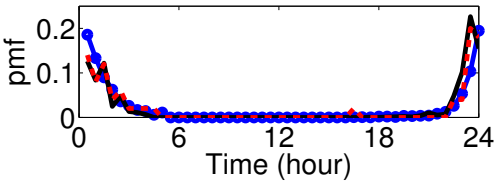

(b) Time of last departure

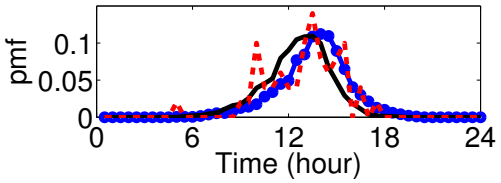

(c) Cumulative occupied duration

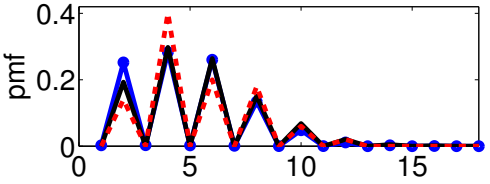

(d) No. of occupied/unoccupied transitions

FIGURE 3.5: The pmfs of the four random variables estimated from the measurements (dashed red), predicted by the agent-based model (dotted blue) and the proposed model (black). Comparison is for weekdays only, and the binsize is 1/2 hour.

TABLE 3.1: NRMSD of the mean occupancy and K-L divergence of the four random variables in the MOSZ scenario.

Criteria	Variables	Agent-based model	Proposed model
NRMSD	Mean occupancy	0.0867	0.0577
K-L divergence	Time of first arrival	0.2388	0.0484
	Time of last departure	0.1900	0.0411
	Cumulative occupied duration	0.3261	0.2394
	No. of occupied/unoccupied transitions	0.0748	0.0348

model matches the measurements much better than the agent-based model. Figure 3.5(a) and Figure 3.5(b) demonstrate the pmfs of time of first arrival and time of last departure. Our proposed model performs much better, and it can also capture certain peaks of the pmfs of the measurements, while the agent-based model cannot achieve that. The comparison of cumulative occupied duration estimated from measurements, predicted by the agent-based model and the proposed model, is shown in Figure 3.5(c). Both models could not capture the peaks of the pmf, but the trend of the pmf is predicted correctly. Figure 3.5(d) gives the pmf of the number of occupied/unoccupied transitions. The agent-based model matches very well, but our proposed model still performs better. Table 3.1 shows the NRMSD

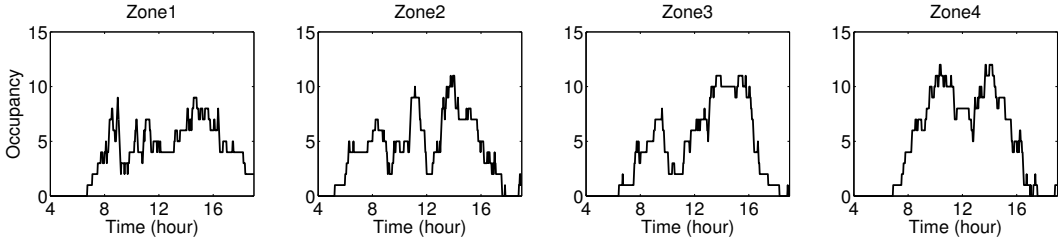

FIGURE 3.6: The output of the proposed model of the four zones for one day.

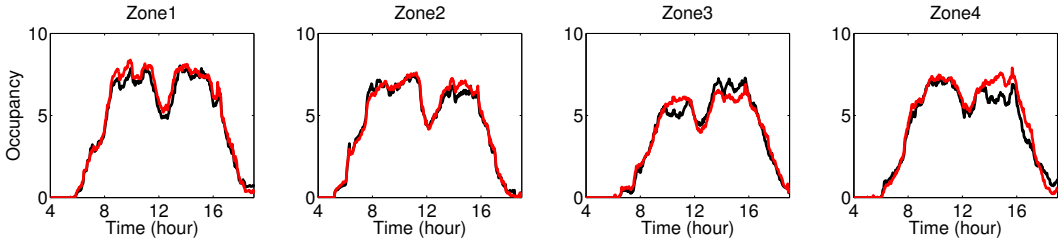

FIGURE 3.7: Mean occupancy profiles of the four zones estimated from measurements (red line) and predicted by the proposed model (black line) in the MOSZ scenario.

TABLE 3.2: NRMSD of the mean occupancy and K-L divergence of the three random variables for the four zones in the MOMZ scenario.

Criteria	Variables	Zone1	Zone2	Zone3	Zone4
NRMSD	Mean occupancy	0.0453	0.0336	0.0573	0.0735
K-L divergence	Time of first arrival	0.1220	0.0932	0.1373	0.1209
	Cumulative occupied duration	0.5247	0.1193	0.3515	0.2118
	No. of occupied/unoccupied transitions	0.2505	0.0647	0.1086	0.2864

of the mean occupancy and the K-L divergence of the four random variables under the MOSZ scenario. It can be found that the proposed model performs much better than the agent-based model for the variables of mean occupancy, time of first arrival, time of last departure and number of occupied/unoccupied transitions. In the meantime, both the proposed model and the agent-based model could not predict cumulative occupied duration very well, but our proposed model still performs better. These conclusions tally with the observations of Figure 3.4 and Figure 3.5. One possible reason for the big fluctuations in cumulative occupied duration could be due to the limited size of the measurement data. The data generated by the agent-based model and the proposed model involves 1000 weeks. So the pmfs predicted by both models are much smoother.

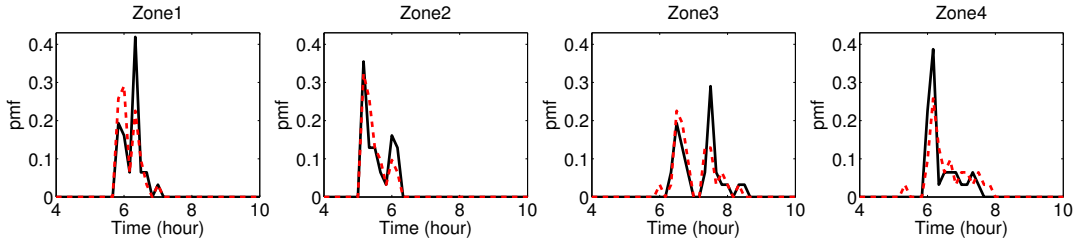

(a) Time of first arrival

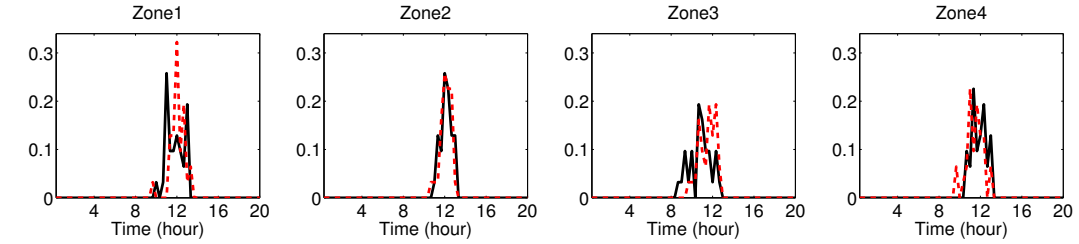

(b) Cumulative occupied duration

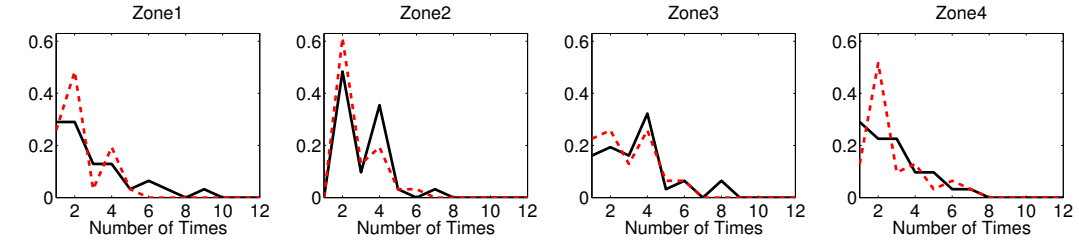

(c) No. of occupied/unoccupied transitions

FIGURE 3.8: The pmfs of the three random variables estimated from the measurements (dashed red) and predicted by the proposed model (black).

In the MOMZ scenario, even though our proposed approach can dramatically reduce the dimension of the transition probability matrix as compared to existing approaches, the dimension of the transition probability matrix will still increase exponentially with the increase of the number of zones. The relationship can be presented as $dimension = 3^m$, where m is the number of zones. According to the observations of the real occupancy data, we find that, although the possible number of states can be very large, only a small portion of the states appear in one time step. This phenomenon is mainly caused by the topology constraints of the building. For example, assuming that we have four zones with cascaded connection (shown in Figure 3.2), if one occupant intends to go to Zone3 from Zone1, then he/she need to go to Zone2 first. Because of this physical constraint, we will only consider the states that have appeared in the real occupancy data in simulations for simplification. For the MOMZ scenario, we divided 52 cubicles into 4 zones.

According to the analysis in [48], workdays have similar occupancy profile. And, due to the limited data size, we treat all working days as the same instead of separating them from Monday to Friday in the MOSZ scenario. The analysis in [48] also provides a possible reason for high occupancy after $7pm$. It may be caused by a security guard walking around the zones. Thus, we only model occupancy from $4am$ to $7pm$. In this case, the random variable of time of last departure cannot be obtained. Only the remaining three random variables are analyzed.

In order to match the number of days to actual measurement data, we perform thirty-one simulations, each has a duration of one day, using the proposed model under the MOMZ scenario. The output of the proposed model for one day of the four zones is shown in Figure 3.6. Due to the stochastic property of our proposed model, the result would be different for different days. Figure 3.7 shows the mean occupancy profiles estimated from the measurements and predicted by the proposed model. Our proposed model matches the measurements very well for the four zones. Note that the mean occupancy profiles are not as smooth as that in the MOSZ scenario. This may be because the number of days for the measurements and simulations is only 31, which is much smaller than the number of days in the MOSZ scenario. Figure 3.8 illustrates the three random variables of time of first arrival, cumulative occupied duration and number of occupied/unoccupied transitions estimated from the measurements and predicted by the proposed model. We conclude that the proposed model captures the properties of actual occupancy data very well. Table 3.2 shows the quantified results with the two evaluation criteria for the four zones. The proposed model performs very well for all the variables under the two criteria in each zone, which is consistent with the observations of Figure 3.7 and Figure 3.8.

3.4 Summary

In this chapter, we proposed two novel inhomogeneous Markov chain models for building occupancy modeling under two scenarios of MOSZ and MOMZ. In the MOSZ scenario, we defined the state of the inhomogeneous Markov chain as the increment of occupancy in a zone. Under the assumption that the maximal number of occupants moving into or out of a zone is one within a short interval, the transition probability matrix will be of dimension 3×3 which is much smaller than

existing approaches in the literature. We remark that the proposed approach can be readily extended to the case where the number of occupants moving into or out of a zone within a short interval can be 2 or 3, with the dimensions of the transition probability matrices increased to 5×5 and 7×7, respectively. In the MOMZ scenario, by taking the interactions among zones into consideration, we defined the state the inhomogeneous Markov chain as the vector in which each component is the increment of occupancy in each zone. In this way, we can dramatically simplify the calculation of the key parameters, i.e. Markov transition probability matrices, based on the detailed analysis. We have conducted real simulations to evaluate the performance of the proposed approaches and compared the simulation results with the agent-based model under the MOSZ scenario. Simulation results showed that our proposed model performs very well under the two scenarios and outperforms the agent-based model under the MOSZ scenario.

Chapter 4

Occupancy Estimation with Environmental Parameters Using a Fusion Framework

Occupancy models reveal the patterns of occupants which can be used in real-time occupancy estimation. In this chapter, we will present a fusion framework which combines the results of data-driven models with occupancy models for building occupancy estimation using environmental parameters. In Section 4.1, we first introduce the six data-driven models. Then, feature engineering which consists of feature extraction and feature selection is presented. After that, we present a proper occupancy model for our case. Finally, the fusion of the outputs of data-driven models and the occupancy model is shown. In Section 4.2, we introduce data acquisition process. Then, variables and criteria for evaluation are presented, followed by experimental results and discussions.

4.1 Methodology

4.1.1 Data-driven Models

Extreme Learning Machine: Extreme Learning Machine (ELM) was developed for single-hidden layer feedforward neural networks (SLFNs), it randomly

chooses the parameters of hidden layer neurons and analytically determines the weights of output neurons [50]. Given training samples $(\mathbf{x}_k, \mathbf{y}_k)$, where $\mathbf{x}_k = [x_{k1}, x_{k2}, \cdots, x_{km}]^T \in \mathbb{R}^m$ and $\mathbf{y}_k = [y_{k1}, y_{k2}, \cdots, y_{kn}]^T \in \mathbb{R}^n$, the activation function $g(\cdot)$ and the number of hidden nodes L, the output of SLFNs is given by

$$\sum_{j=1}^{L} \mathbf{w}_j g(\alpha_j, \mathbf{x}_k, \beta_j) = \mathbf{t}_k \tag{4.1}$$

where $k = 1, ..., N$, N is the total number of samples, L is the number of hidden neurons, α_j is the weight of input nodes to the hidden node j, β_j is the threshold of hidden node j, and $\mathbf{w}_j \in \mathbb{R}^n$ is the weight of the hidden node j to output nodes. Assume that the activation function $g(\cdot)$ can approximate these N samples with no error, which means $\sum_{k=1}^{N} \|\mathbf{t}_k - \mathbf{y}_k\| = 0$, i.e., there exist $\mathbf{w}_j$, α_j and β_j such that

$$\sum_{j=1}^{L} \mathbf{w}_j g(\alpha_j, \mathbf{x}_k, \beta_j) = \mathbf{y}_k \tag{4.2}$$

We can rewrite the above equation into matrix form as

$$\mathbf{H}\mathbf{w} = \mathbf{Y} \tag{4.3}$$

where

$$\mathbf{H} = \begin{bmatrix} g(\alpha_1, \mathbf{x}_1, \beta_1) & \cdots & g(\alpha_L, \mathbf{x}_1, \beta_L) \\ \vdots & \cdots & \vdots \\ g(\alpha_1, \mathbf{x}_N, \beta_1) & \cdots & g(\alpha_L, \mathbf{x}_N, \beta_L) \end{bmatrix}_{N \times L}, \tag{4.4}$$

$$\mathbf{w} = \begin{bmatrix} \mathbf{w}_1^T \\ \vdots \\ \mathbf{w}_L^T \end{bmatrix}_{L \times n} \quad \text{and} \quad \mathbf{Y} = \begin{bmatrix} \mathbf{y}_1^T \\ \vdots \\ \mathbf{y}_L^T \end{bmatrix}_{N \times n} \tag{4.5}$$

As named by Huang et al. [50], H is called hidden layer output matrix; the k-th column of H is the k-th hidden node output with respect to all the inputs. According to [50], the smallest least-squares solution of equation (4.3) can be expressed

as

$$\hat{\mathbf{w}} = \mathbf{H}^{\dagger}\mathbf{Y} \tag{4.6}$$

where $\mathbf{H}^{\dagger}$ is the *MoorePenrose generalized inverse* of matrix $\mathbf{H}$. Based on [51], an orthogonal projection method can be employed to calculate $\mathbf{H}^{\dagger}$ in two cases: when $H^T H$ is nonsingular, $\mathbf{H}^{\dagger} = (H^T H)^{-1} H^T$, or when HH^T is nonsingular, $\mathbf{H}^{\dagger} = H^T (HH^T)^{-1}$. To avoid the singularity of $H^T H$ or HH^T, the authors in [51] suggest to add a positive value to the diagonal of $H^T H$ or HH^T, which can be expressed as

$$\hat{\mathbf{w}} = \left(\frac{\mathbf{I}}{C} + H^T H\right)^{-1} H^T \mathbf{Y} \qquad \text{or} \tag{4.7}$$

$$\hat{\mathbf{w}} = H^T \left(\frac{\mathbf{I}}{C} + HH^T\right)^{-1} \mathbf{Y} \tag{4.8}$$

where $\mathbf{I}$ is the identity matrix, and C is the regularization term. In this way, the solution will be stabler and tend to have better generalization performance [51].

In summary, the implementation of ELM can be divided into three steps:

(1) Randomly assign hidden nodes parameters, i.e. α_j and β_j where $j = 1, 2, \ldots, L$.

(2) Calculate the hidden layer output matrix $\mathbf{H}$.

(3) Calculate the output weight $\mathbf{w}$.

Support Vector Machine: Support Vector Machine (SVM) was developed under the principles of structural risk minimization which not only minimizes the training error, but also reduces the system complexity [52].

Artificial Neural Network: Another widely used data-driven approach is Artificial Neural Network (ANN). The neurons in ANN are computational models inspired by natural neurons. The ANN model applies these neurons to process information.

K-Nearest Neighbors: K-Nearest Neighbors (KNN) algorithm is quite popular for classification because of its simple structure and easy interpretation.

Linear Discriminant Analysis: Linear Discriminant Analysis (LDA), also known as Fisher Linear Discriminant [53], is a popular data-driven approach in pattern

Feature	Description
First order difference	$fd(i) = raw(i) - raw(i-1)$
Second order difference	$fd2(i) = fd(i) - fd(i-1)$
First order shifted difference	$fds(i) = raw(i) - raw(i-2)$
Five-minute moving average	$mavg = \left(\sum_{j=i-4}^{i} raw(j)\right)/5$
Ten-minute shifted difference	$fds10(i) = raw(i) - raw(i-10)$

TABLE 4.1: List of features extracted from sensor data

recognition area. It aims at finding a projection hyperplane for features that minimizes the variance within each class and maximizes the means of classes after projection, which means the best separability in the new feature space [54].

Classification And Regression Tree: Classification And Regression Tree (CART) is established upon the principle of recursively partitioning feature space and fitting a simple threshold model within each partition [55].

4.1.2 Feature Engineering

The raw environmental sensor data may be noisy and is not likely to give accurate classification results if used directly. Thus, we need to extract more representative information, known as features. Among all the extracted features, some of them may be redundant, which will lead to poorer performance and incur unnecessary computational time. Therefore, feature selection is necessary. In this work, feature engineering contains two parts of feature extraction and feature selection.

Feature Extraction: The features extracted from the raw environmental sensor data are shown in Table 4.1. The first order difference (fd), second order difference ($fd2$) and first order shifted difference (fds) are selected to capture the temporal variations in the data. The moving average ($mavg$) and ten-minute shifted difference ($fds10$) features take into account the time delay in the build-up and decay of the environmental parameters.

Feature Selection: In general, feature selection can be accomplished by leveraging on two approaches, i.e. the filter method and the wrapper method. In the filter method, the merit of the features can be assessed using criteria, such as Information Gain [40, 56] and Symmetric Uncertainty [57], that are independent of

classifiers. This makes the feature selection quite fast, but compromises the estimation accuracy. In the wrapper method, classifiers are employed to assess the merit of features. The feature selection is thus optimized for classifiers. This generally yields better performance when compared to the filter method. One issue of the wrapper method is that the computational burden is quite high, because multiple classifier models are created in the feature selection process. Most previous works that estimated occupancy using environmental parameters used filter methods. We instead apply a wrapper method [58]. To address the issue of high computational time, we perform an ELM-based wrapper method which is quite fast owing to the extremely fast learning speed of the ELM algorithm [59]. We conduct the feature selection in two stages. First, we select the best features for each sensing domain, named individual domain analysis. Secondly, we combine these best features to form a multi-domain feature set, where we search exhaustively for the final feature set, named multi-domain analysis.

The objective of the individual domain analysis is to select the best features for each environmental sensor. This reduces the feature space to a more manageable number. To begin with, we have six features (that is, including the raw data) for each of the four environmental parameters. We thus have 24 features. We attempt to select the three best features from each sensing domain, thus yielding 12 features. To determine the best features, we apply a wrapper-based ranking. That is, we use the estimation accuracy of a classifier, in our case the ELM, as the criterion to rank features.

The algorithm of the individual domain analysis is outlined in Figure 4.1. Note that the algorithm shown applies for a single domain. Let $\{f_i\}$ be the set of features of an environmental parameter. Let N be the size of the combination of features and n the total number of features. In our case, $n = 6$. For each $N = 2, 3, ..., n$, all combinations of features are evaluated for their estimation accuracy. In each iteration, the set of features S^c represents a combination of N features. S^c is taken as the input and the occupancy O is made the target output of an ELM. A^c is the accuracy obtained with S^c. We note the combination S^{c^*} that yields the highest accuracy. The rank of each feature is the number of times it appears in the highest accuracy combination.

The algorithm described above was implemented on the extracted features. The

1 **for** $N = 2$ *to* n
2 **for** $c = 1$ *to* ${}_{N}C_{n}$
3 $S^{c} \Leftarrow feature\_combo^{c}; size(S^{c}) = N$
4 $A^{c} \Leftarrow ELM(S^{c}, O)$
5 **end for**
6 $S^{c^*} \Leftarrow argmax_{f_n^c} A$
7 **end for**
8 $Rank(f_i) \Leftarrow Count(f_i \in S^{c^*})$

FIGURE 4.1: The ELM-based wrapper algorithm

Domain	Best Feature Set
CO_2	CO_2_fds; CO_2_fd; $CO_2(raw)$
Relative Humidity	RH_fds10; RH_fd2; RH_$mavg$
Temperature	Temp_fds10; Temp(raw); Temp_fds
Pressure	Press_fds; Press_$mavg$; Press_fd

TABLE 4.2: Results of individual domain analysis for the ELM-based wrapper method

algorithm was implemented in MATLAB R2015a on a 1.80 GHz CPU. The approximate running time for the analysis in MATLAB was 7 minutes and 24 seconds. The results of the analysis are shown in Table 4.2.

With the feature space reduced to half by the individual domain analysis, the obtained best features are combined into a multi-domain feature set. All possible combinations of the elements of this set were evaluated for their estimation accuracy with an ELM. The best features were CO_2_fd, Temp_fds10, Temp(raw) and Press_fds. It is notable that the pressure data, which has not generally been considered for occupancy estimation, is deemed a relevant feature by the algorithm.

4.1.3 Occupancy Model

To obtain the exact number of occupants in a multi-occupant area is quite difficult, especially when the occupancy is relatively high. In most situations, for example, discriminating 10 occupants from 11 occupants in one thermal zone is not very meaningful. Also, this discrimination would require high cost devices such as cameras. Normally, the information of occupancy range, i.e. zero, low, medium and

high, will be enough for the control systems in buildings. In this work, we consider the estimation of these four states which can be defined based on different deployment scenarios in one thermal zone. We present an an inhomogeneous Markov chain where the states are the defined four occupancy ranges, which is similar to the model developed by Richardson et al. [25] where they defined the state as the number of active occupants. Recent occupancy models developed by Liao et al. [28] and Chen et al. [60] mainly deal with the simplification of the inhomogeneous Markov chain with a huge dimension of transition probability matrix. They are not suitable for our case. When we consider different deployment scenarios, proper occupancy models need to be chosen. Due to the slow response of the building control system, 15 minutes resolution will be adequate [22, 28]. Finally, an inhomogeneous Markov chain model with 96 transition probability matrices of dimension 4×4, where the 4 states are zero, low, medium and high, is constructed for building occupancy modeling.

4.1.4 Fusion Algorithm

Data-driven models estimate the current occupancy level only based on the real-time environmental sensor data. They do not take occupancy patterns into consideration. A large number of works have been done for occupancy modeling, which indicates that occupancy dynamics have some unique properties. These properties can be utilized for a better estimation of real-time building occupancy. In this work, we propose a fusion framework which combines the conventional data-driven approaches with occupancy models to improve the estimation accuracy of building occupancy. Here, we consider the outputs of data-driven models as individual observations without taking occupancy dynamics into consideration, and the occupancy model which can reveal occupancy patterns is utilized to form system dynamics.

We propose a particle filter for fusing the outputs of data-driven models and the occupancy model. The particle filter attempts to represent the posterior distribution by using a set of particles [61]. In our case, the state of i-th particle at time step k is defined as x_k^i which represents the occupancy of a zone. The implementation of the particle filter in this work consists of three steps shown as follows:

Propagation: The occupancy model we presented is a first-order inhomogeneous Markov chain model. Given i-th particle state at time step $k-1$, x_{k-1}^i, the particle can reach the state, $\hat{x}_k^i$, with the transition probability $P(\hat{x}_k^i|x_{k-1}^i)$, $i = 1, 2, ..., M$.

Weight calculation: The observation, o_k, can be derived from data-driven models with current environmental sensor data. Given the occupancy model output, $\hat{x}_k^i$, the i-th particle weight at time step k can be calculated as

$$\hat{w}_k^i = w_{k-1}^i P(o_k|\hat{x}_k^i) \tag{4.9}$$

where $P(o_k|\hat{x}_k^i) = \frac{1}{\sqrt{2\pi\sigma^2}} e^{-\frac{(o_k - \hat{x}_k^i)^2}{2\sigma^2}}$. Then, we normalize the weight for each particle as

$$w_k^i = \frac{\hat{w}_k^i}{\sum_{i=1}^M \hat{w}_k^i} \tag{4.10}$$

Resampling: We draw M new particles from the current particle set, $\hat{X}_k = \left\{\hat{x}_k^1, \hat{x}_k^2, ..., \hat{x}_k^M\right\}$, proportional to the weight of each particle and set the weights of all particles to $1/M$. Then, this new particle set, $X_k = \left\{x_k^1, x_k^2, ..., x_k^M\right\}$, is the desired one to determine the final occupancy of the zone at time step k, y_k, which can be expressed as

$$y_k = \frac{1}{M} \sum_{i=1}^{M} x_k^i \tag{4.11}$$

4.2 Experiments

4.2.1 Data Acquisition

In this work, we recorded the CO_2, humidity, temperature and pressure levels in the Process Instrumentation Lab at Nanyang Technological University (NTU), Singapore. The lab contains an office space with 24 cubicles and 11 open seats. The room seats 9 PhD students and 11 research staff. About 6 to 10 of them are regularly present during working hours. Additionally, there are 6 PCs for final year undergraduate students and 5 PCs open to all students. Since it is a lab environment with research students and staffs, the occupancy is regular. During

Sensor	Measured parameter	Resolution	Accuracy
Rotronic CL11	CO_2	1 ppm	±5% of the measured value
	Temperature	0.05 °C	±0.3 °K
	Relative Humidity	0.1 %RH	< 2.5 %RH
Lutron MHB-382SD	Pressure	0.1 hPa	±2 hPa

TABLE 4.3: The resolution and accuracy of the environmental sensors.

working days, the morning arrival will start from 8am and the departure will last to 11pm. In this work, we set the occupancy range of low (1-5 occupants), medium (6-10 occupants), and high (more than 10 occupants). The room is conditioned using both Active Chilled Beam (ACB) and the conventional Variable Air Volume (VAV) systems, and is mechanically ventilated using Air Handling Unit (AHU) which delivers a constant supply of fresh air.

The measurements of CO_2, relative humidity and temperature were done using the CL11 sensor from Rotronic. Pressure levels were measured using the MHB-382SD sensor from Lutron. The sampling time was one minute. The resolution and accuracy of the sensors are shown in Table 4.3. The sensors are attached on the wall at a height of $1.1m$ from the ground. We applied one sensor per environmental parameter. To record ground truth occupancy, three Internet Protocol (IP) cameras were installed. The layout of the zone is shown in Figure 4.2. The main door (referring to the location of camera 1) opens to an outer office space for administrative staffs. Another door (referring to the location of camera 2) opens to a lab area, while the third door remains closed. All the windows are closed. The size of the zone is $20m$ long, $9.3m$ wide and $2.6m$ high. Note that the locations of the sensors are randomly chosen. The optimal placement of the sensors is out of the scope of this work and will be one of our future works.

The data collected from the sensors was transferred to a laptop using a USB cable. Preprocessing of the data was done in MATLAB. This involved removing missing values, synchronizing the time stamps of the sensors and synchronizing the sensor data with occupancy values. Since the occupancy dynamics on weekdays and weekends are different, we only consider occupancy estimation on weekdays in this work. Note that the occupancy estimation method for weekends is the same. Finally, we collected 32 days of data in weekdays for performance evaluation. Among them, we utilize 25 days of data for training and the last 7 days of data for testing.

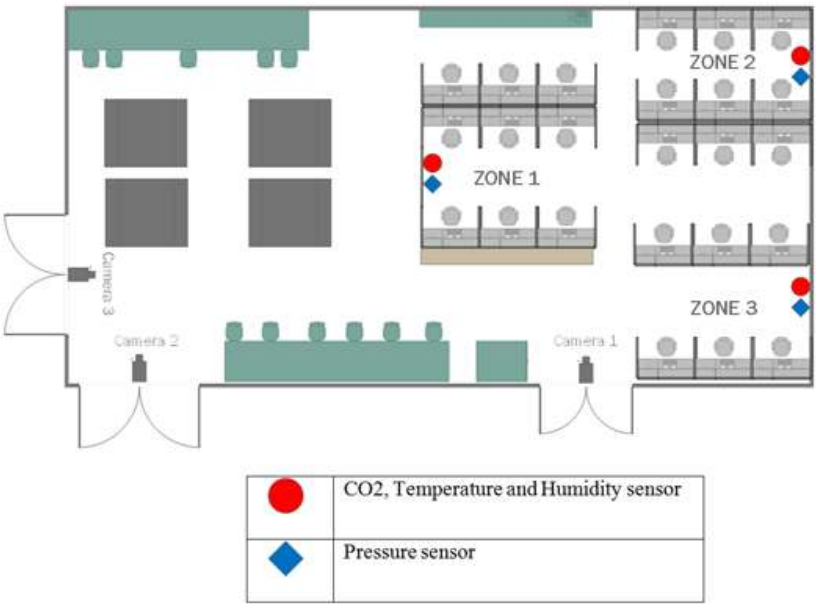

FIGURE 4.2: Layout of the zone

4.2.2 Variables and Criteria

The estimation of building occupancy is treated as a classification problem. Thus, one basic criterion is classification accuracy which is defined as the correctly estimated results against the total number of samples. Another evaluation metric that we used is Normalized Root Mean Square Error (NRMSE) which indicates the magnitude of the estimation error [62]. Time of first arrival (TOFA) and time of last departure (TOLD) which has been defined in Section 3.3.2 are the two most important parameters for building control systems. They will determine the operation period of the control systems. Therefore, the estimation accuracy of these two parameters is vital for an occupancy estimation system. The normalized mean errors of TOFA and TOLD will be evaluated to demonstrate the performance of the proposed framework.

4.2.3 Results and Discussions

The overall results can be found in Table 4.4 which presents the classification accuracy, the NRMSE, the normalized mean errors of TOFA and TOLD for the six methodologies with and without fusion. The values of the parameters of some data-driven models, i.e. ELM, SVM, ANN and KNN, are presented in Table 4.5.

Model		Accuracy	NRMSE	TOFA (%)	TOLD (%)
ELM	WO	0.6885	0.2490	7.6340	4.1369
	W	0.7418	0.2099	0.8184	1.2351
SVM	WO	0.6592	0.2660	1.0417	7.4405
	W	0.7167	0.2125	0.8035	1.6369
ANN	WO	0.6427	0.2692	6.6965	3.2441
	W	0.7037	0.2295	1.8899	1.2351
KNN	WO	0.6100	0.2687	14.3452	7.8125
	W	0.7074	0.2126	0.8482	1.5774
LDA	WO	0.6964	0.2450	0.8928	2.2322
	W	0.7390	0.2133	0.7441	1.0417
CART	WO	0.6250	0.2722	14.4345	7.7381
	W	0.7188	0.2176	0.7441	1.4583

TABLE 4.4: The classification accuracy, the NRMSE, the normalized mean errors of time of first arrival and time of last departure for the six approaches with and without fusion. Here, W denotes the approach with fusion and WO denotes the approach without fusion.

ELM		SVM			ANN		KNN	
No. of hidden neurons	Activation function	C	ε	Kernel function	No. of hidden neurons	Activation function	Distance metric	No. of neighbors
50	Sigmoid	1.7	0.01	RBF	50	Sigmoid	Euclidean	20

TABLE 4.5: The values of the parameters of some data-driven models, i.e. ELM, SVM, ANN and KNN.

All these parameters are adjusted based on grid-search with cross validation of the training data. Specifically, for example, the number of hidden neurons of the ELM algorithm needs to be tuned. We selected the number of hidden neurons from 1 to 100. Five-fold cross validation was employed on the training data with different number of hidden neurons. Then, we chose the optimal number of hidden neurons based on the mean testing accuracy of the five-fold cross validation. The same strategy was applied for determining the optimal parameters for the other data-driven approaches.

After fusion, all the approaches show impressive improvements on the estimation accuracy and reductions on the NRMSE. Among all the approaches, the ELM with fusion outperforms the others under the two criteria of the estimation accuracy and the NRMSE, which demonstrates the effectiveness of applying this algorithm for building occupancy estimation. For the criteria of the normalized mean errors of TOFA and TOLD, all the approaches with fusion show great reductions. In addition, the LDA and CART with fusion have the lowest estimation error on the

normalized mean error of TOFA, and the LDA with fusion has the lowest estimation error on the normalized mean error of TOLD.

Figure 4.3 shows the classification results of the 7 testing days for the six methodologies with and without fusion. The results after fusion are smoother. Thus, they are more suitable for building control systems. Meanwhile, the proposed fusion framework eliminates the errors in midnight which may be caused by the slow spread of the environmental parameters, i.e. CO_2, temperature, humidity, after becoming unoccupied. Due to these wrong detections at midnight in the methodologies of ELM, ANN, KNN and CART without fusion, the normalized mean errors of TOFA for the four approaches are quite large. After fusion, the four approaches show significant improvements of the normalized mean errors of TOFA. The SVM and LDA do not contain this wrong detection at midnight. But our fusion approach still shows encouraging improvements. One example of error cumulative distribution functions (CDF) of TOFA for the ELM approach with and without fusion is shown in Figure 4.4(a). Note that each step refers to 15 minutes. The large error is caused by the wrong estimation of occupancy range at midnight.

Figure 4.5 presents the confusion matrix of the estimation result of the ELM with fusion. We can find that the detections of zero and high occupancy are easier than the detections of low and medium occupancy. The possible reason can be that, since the environmental parameters are smoothly changing, the low and high thresholds can be easily identified, but the low and medium ones can be confusing. Moreover, the confusion matrix also indicates a high detection accuracy of presence and absence.

Another observation is that the normalized mean error of TOLD is larger than that of TOFA in most cases after fusion. To explain this phenomenon, we take the environmental parameter of CO_2 as an example. When the zone becomes first occupied in the morning, the CO_2 level will increase to indicate occupancy change. After that, the zone will become occupied for almost the entire day, thus, the CO_2 level accumulates to a relatively high level in the evening. Then, after all occupants have left, the CO_2 level will take some time to decrease to a low level which indicates vacancy. That is the main drawback of the environmental parameter based occupancy estimation method. Nevertheless, according to Figure 4.4(b), the mean error of TOLD has been greatly reduced by our proposed fusion algorithm, as compared to that without fusion.

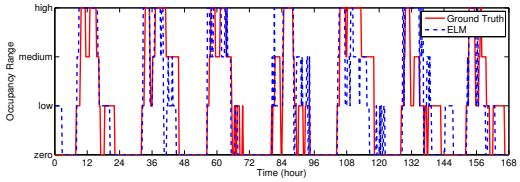

(a) ELM without fusion

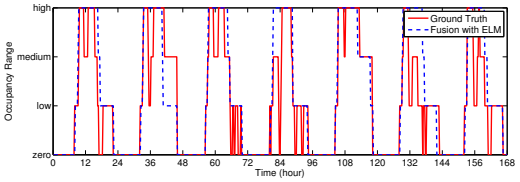

(b) ELM with fusion

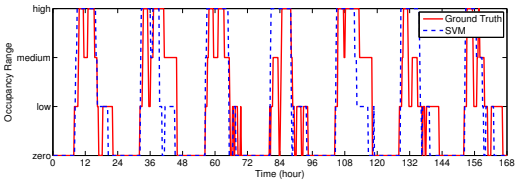

(c) SVM without fusion

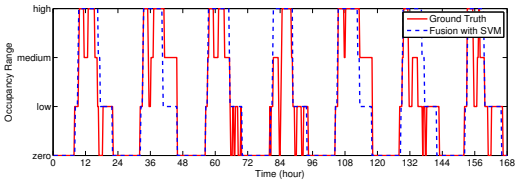

(d) SVM with fusion

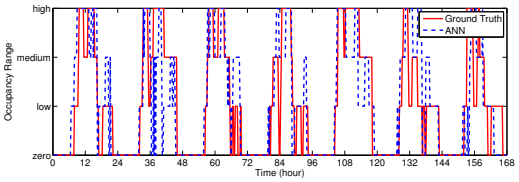

(e) ANN without fusion

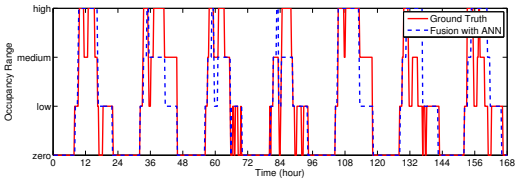

(f) ANN with fusion

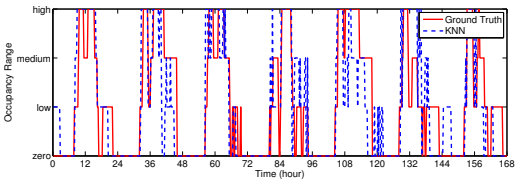

(g) KNN without fusion

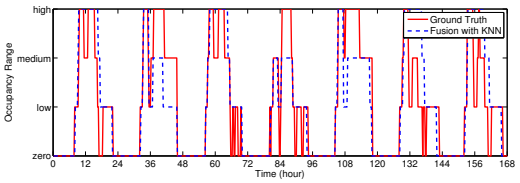

(h) KNN with fusion

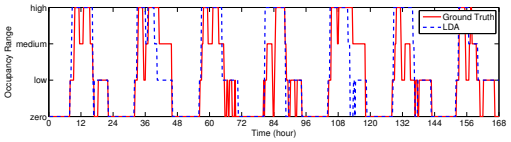

(i) LDA without fusion

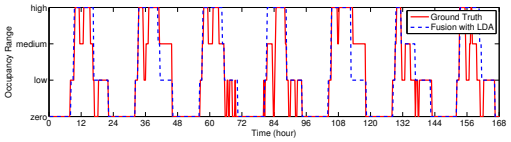

(j) LDA with fusion

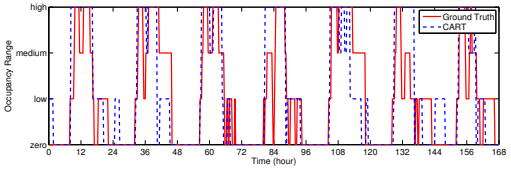

(k) CART without fusion

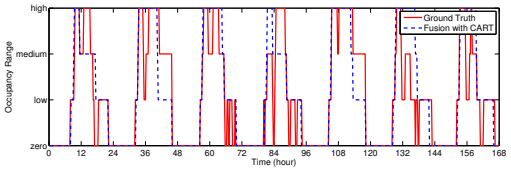

(l) CART with fusion

FIGURE 4.3: The classification results of the six methodologies with and without fusion

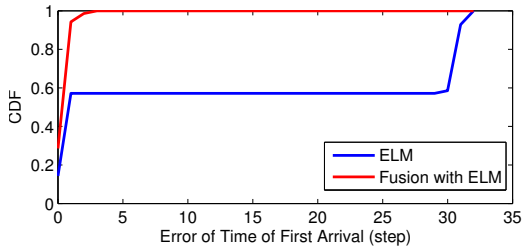

(a) TOFA for ELM with and without fusion

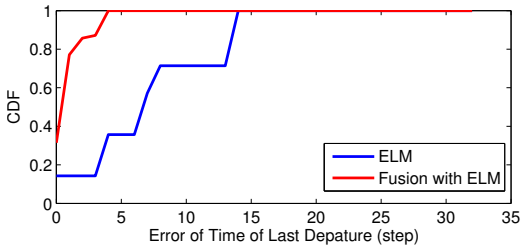

(b) TOLD for ELM with and without fusion

FIGURE 4.4: The CDFs of TOFA and TOLD for the ELM approach with and without fusion

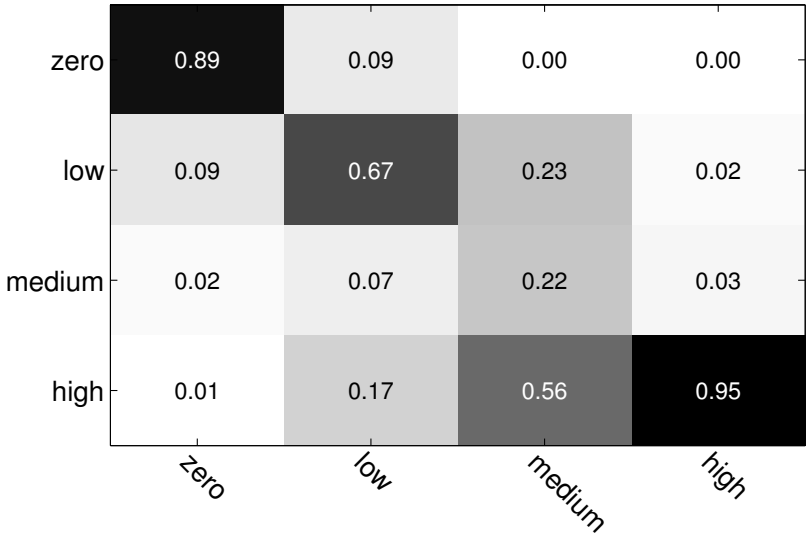

FIGURE 4.5: Confusion matrix of the estimation result of the ELM with fusion

	ELM		SVM		ANN		KNN		LDA		CART	
	WO	W	WO	W	WO	W	WO	W	WO	W	WO	W
Accuracy	0.8729	0.9318	0.8586	0.9281	0.8728	0.9345	0.8152	0.9278	0.9033	0.9345	0.8125	0.9304

TABLE 4.6: The classification accuracy of presence/absence for the six methodologies with and without fusion.

Presence and absence of occupant information is important for applications such as lighting control. The classification accuracies of presence/absence for the six methodologies with and without fusion are also tested and shown in Table 4.6. The fusion algorithm demonstrates an impressive improvement of around $3-12\%$ among different approaches. Among all the approaches, ANN and LDA with fusion perform the best. The average detection accuracy for all the approaches after fusion is as high as some 93% with only the environmental sensors, rather than any extra occupancy related sensors, e.g. motion sensor [39, 40], acoustic sensor [39–41], PIR sensor [40, 41] and light sensor [41, 42]. In summary, the proposed fusion algorithm is quite effective in improving the performance of the pure data-driven approaches in the estimation accuracy, the magnitude of the estimation error and other variables, i.e. the mean errors of TOFA and TOLD.

4.3 Summary

In this chapter, we presented a fusion framework using non-intrusive environmental sensors for building occupancy estimation. Traditional approaches relies on data-driven approaches which do not consider occupancy dynamics. Since the occupancy model can reveal the patterns of occupants, we attempted to fuse the results of data-driven models treating as observation and the occupancy model treating as system dynamics using a particle filter. Experiments have been conducted to verify our proposed scheme in a research lab environment. The experimental results demonstrated impressive enhancement of the estimation accuracy of occupancy and significantly reduction of detection errors of the two important random variables, i.e. time of first arrival and time of last departure.

Chapter 5

Comparing Occupancy Models and Data Mining Approaches for Building Occupancy Prediction

This chapter explores the prediction abilities of occupancy models and compares with some popular linear and nonlinear data mining approaches. In Section 5.1, we present the problem overview. The prediction methods are introduced in Section 5.2. In Section 5.3, we show the data for simulation and the evaluation criteria. Then, we present the simulation results and discussions in this section.

5.1 Problem Overview

Previous works on occupancy modeling attempt to extract occupancy patterns. The prediction abilities of occupancy models need to be explored. On the other hand, since the occupancy data is a typical time series, some time series prediction models can be applied. The basic idea is to construct a relationship between the future occupancy and the past ones using a linear or nonlinear mapping. Thus, we divide the occupancy prediction methods into two categories of occupancy models and data mining approaches. The two widely used models for multi-occupant modeling are the inhomogeneous Markov chain (IMC) model and the multivariate Gaussian (MG) model. The investigated data mining models include a linear model, i.e. ARIMA, and two nonlinear models, i.e. ANN and SVR. In this work,

we shall investigate and compare the effectiveness of these methodologies for occupancy prediction in commercial buildings.

5.2 Methodology

The investigated occupancy models are the IMC model and the MG model. The introductions of the IMC model and the calculation of its key parameters can be found in Section 3.1. The explanations of the ANN and SVM methods have been shown in Section 4.1.1. And the SVR approach was developed as the implementation of SVM for regression purpose [63]. Thus, in this section, we only present the introduction of the MG model and the linear data mining approach of ARIMA.

5.2.1 Multivariate Gaussian

The multivariate Gaussian model developed by Erickson et al. [26] attempts to fit the occupancy at each time step using a Gaussian model. The idea is similar to the Graphical model proposed by Liao et al. [28]. The MG model contains two important parameters, i.e. mean and standard deviation, at each time step. Assume that y_k^i, $i \in 1,\ 2, \cdots,\ D$, is the occupancy at time step k on day i, and D is the total number of days, the mean $\bar{y}_k$ and standard deviation s_k at time step k can be calculated as

$$\bar{y}_k = \frac{1}{D}\sum_{i=1}^{D} y_k^i \tag{5.1}$$

$$s_k = \sqrt{\frac{1}{D}\sum_{i=1}^{D}(y_k^i - \bar{y}_k)^2} \tag{5.2}$$

During testing, a value at time step k will be randomly selected from the Gaussian distribution with mean $\bar{y}_k$ and standard deviation s_k.

5.2.2 Autoregressive Integrated Moving Average

The autoregressive integrated moving average model is the most widely used linear model for time series prediction, e.g. in stock market [64], traffic volume [65], electricity prices [66], etc. Assume that y_k is the occupancy time series at time step k, an ARIMA(p, d, q) model can be expressed as

$$\left(1-\sum_{i=1}^{p}\varphi_i L^i\right)(1-L)^d y_k = \left(1-\sum_{j=1}^{q}\psi_j L^j\right) \tag{5.3}$$

where p is the order of autoregressive process, d is the degree of differencing, q is the order of moving average process, φ_i and ψ_j are coefficients of autoregressive and moving average processes respectively, and L is the lag operator. The parameters p and q can be determined by partial autocorrelation and autocorrelation of the signal respectively, and the parameter d is the minimal order of differentiation that makes the signal stationary. The coefficients φ_i and ψ_j can be specified using least-squares fit.

5.3 Evaluation

To have a comprehensive analysis of the prediction abilities among the different models, we define four prediction horizons which are $15mins$, $30mins$, $1h$, and $2h$. The prediction horizons of $15mins$ and $30mins$ are treated as short-term prediction of occupancy which can be applied for MPC based real-time building climate control. And the prediction horizons of $1h$ and $2h$ are treated as long-term prediction of occupancy which can be employed for smart preheating or precooling strategies. Note that, the length of time step of data is consistent with prediction horizon. Thus the prediction is always one step ahead under different prediction horizons. The prediction performances of the different methodologies are compared in each horizon. Moreover, we will give an analysis on how to choose a proper and efficient prediction model under different prediction horizons. Note that the outputs of MG, ARIMA, ANN and SVR are decimal format. Since the occupancy value must be non-negative integer, so if the occupancy value is less than zero, it will be manually set to zero, and if the occupancy value is in decimal format, a rounding operation will be performed.

5.3.1 Data for Evaluation

Data for evaluation is generously provided by the authors in [28], and it was collected by using video cameras from January 2010 to April 2010, a span of about four months, in a multi-occupant room which contains 5 graduate students and 3 undergraduate research assistants. In this work, only workdays of occupancy data is considered. Note that the prediction of weekends' occupancy data is the same. Due to certain technical issues, only 60 workdays of occupancy data (14 days for Monday, 12 for Tuesday, 9 for Wednesday, 12 for Thursday and 13 for Friday) were derived from 16 weeks of video data. The more detailed description of the data can be found in [28]. The raw occupancy time series data has a resolution of one minute. If the prediction horizon is H minutes, the data needs to be transferred into H minutes time-resolution by using mean and rounding operations. For instance, given a time series, $y_1,\ y_2, \cdots,\ y_H$, with length H, the obtained occupancy value can be expressed as $\left\lfloor \frac{1}{H}\sum_{k=1}^{H} y_k \right\rceil$, where $\lfloor\cdot\rceil$ is the rounding operation. We choose first half of the data from each weekday for training (i.e. 7 days for Monday, 6 for Tuesday, 5 for Wednesday, 6 for Thursday and 7 for Friday). Totally, we have 32 days of data for training and the remaining for testing.

5.3.2 Evaluation Criteria

To quantify the performance of the models, we shall apply two widely used evaluation criteria of root mean square error (RMSE) and mean error (ME) under the rational that RMSE indicates the magnitude of occupancy prediction errors and ME indicates overestimation or underestimation of occupancy prediction [67]. The definitions of RMSE and ME are as follows

$$\mathrm{RMSE} = \sqrt{\frac{1}{N}\sum_{k=1}^{N}(y_k - \hat{y}_k)^2} \tag{5.4}$$

$$\mathrm{ME} = \frac{1}{N}\sum_{i=1}^{N}(y_k - \hat{y}_k) \tag{5.5}$$

where y_k and $\hat{y}_k$ are the actual and predicted occupancy at time step k, and N is the total length of the data.

Horizon	Baseline	Occupancy Models		Data Mining Approaches		
	SDP	IMC	MG	ARIMA	ANN	SVR
$15mins$	1.0009	0.8361	1.3007	0.5321	0.5473	0.5323
$30mins$	0.9815	0.9582	1.2735	0.6825	0.7106	0.6840
$1h$	0.9619	1.1063	1.2448	0.8954	0.9188	0.8836
$2h$	0.9018	1.0568	1.1612	1.1251	1.0554	0.9112

TABLE 5.1: The RMSE of different models under four prediction horizons.

Horizon	Baseline	Occupancy Models		Data Mining Approaches		
	SDP	IMC	MG	ARIMA	ANN	SVR
$15mins$	-0.0851	-0.0857	-0.0733	0.0014	-0.0466	-0.0014
$30mins$	-0.1171	-0.1024	-0.0713	0.0518	-0.0678	-0.0613
$1h$	-0.0690	-0.1428	-0.0807	0.1379	-0.0697	-0.2047
$2h$	-0.0833	-0.1299	-0.0836	0.1214	-0.0814	-0.2000

TABLE 5.2: The ME of different models under four prediction horizons.

Horizon	ARIMA			ANN		SVM		
	p	d	q	order	f	order	C	ε
$15mins$	1	0	0	3	6	3	256	0.0118
$30mins$	1	0	1	11	5	5	16	0.0118
$1h$	1	0	1	12	5	12	3.0314	0.068
$2h$	2	0	2	15	8	18	1.7411	0.0206

TABLE 5.3: The values of the parameters of the data mining models.

5.3.3 Results and Discussions

Experimental results under two criteria of four prediction horizons are shown in Tables 5.1 and 5.2 with different methodologies including a simple diversity profile (SDP) method which is widely used [45]. The SDP model adopts the mean occupancy profile of training data to predict future occupancy. At short term predictions of $15mins$ and $30mins$, the linear data mining approach that is ARIMA performs the best. The SVR approach and the SDP approach have superior performances under the prediction horizons of $1h$ and $2h$ respectively. The stochastic occupancy models, i.e. IMG and MG, have the worst performance. This indicates that the stochastic occupancy models have limited prediction performance in the commercial building deployment scenario, which is consistent with the conclusion of predicting occupant's presence and absence in single workplaces [45]. The performances of MG, ARIMA, ANN and SVR that utilize previous steps of occupancy to predict future occupancy degrades with the increase of the prediction horizons.

Horrizon	$15mins$	$30mins$	$1h$	$2h$
Smoothness rate	0.8104	0.7113	0.6050	0.4734

TABLE 5.4: The smoothness rate for different prediction horizons

This is because the correlation between each steps becomes weaker with a longer prediction horizon. But the SDP and MG models seem to be unaffected by the prediction horizon, which will be analyzed later. The ME of the SDP approach is stable and small, which indicates the data for training and testing has similar patterns. Since the maximal number of occupants in the zone is 8, the percentages of biases of all the methodologies are very small and can be neglect. This means that all the methodologies based on real measurements contain negligible biases, which is also consistent with the conclusions in [68]. The values of the parameters of the data mining approaches are listed in Table 4.5. The order represents the number of previous steps of occupancy that is used as model inputs. Note that these values were derived by using grid search with cross-validation of the training data. For example, for the ANN approach at each prediction horizon, we selected the order from 1 to 20. At each order, we chose the hidden nodes of ANN from 1 to 100. Five-fold cross validation was employed on each combination of parameters. The detection accuracy is chosen as a criterion in determining the optimal number of order and hidden nodes. Note that this process will cost some time (up to several hours), but it only requires to be done once. The same strategy was applied for determining the optimal parameters for SVR.

When the prediction horizons are $15mins$ and $30mins$, the ARIMA model outperforms the other models. The adjusted ARIMA models are ARIMA(1, 0, 0) and ARIMA(1, 0, 1) when the prediction horizons are $15mins$ and $30mins$ respectively, which suggests the high correlation between the current occupancy and the previous one step occupancy. Figure 5.1 shows an example of 100 testing samples under four different prediction horizons. We can find that the shorter the prediction horizon, the smoother the signal. In order to quantify the smoothness of the signal, we define a smoothness rate. Given a time series $y_1, y_2, \cdots, y_N$, the smoothness rate, r, can be expressed as

$$r = \frac{\sum_{k=1}^{N-1} \delta\left(y_k, y_{k+1}\right)}{N-1} \tag{5.6}$$

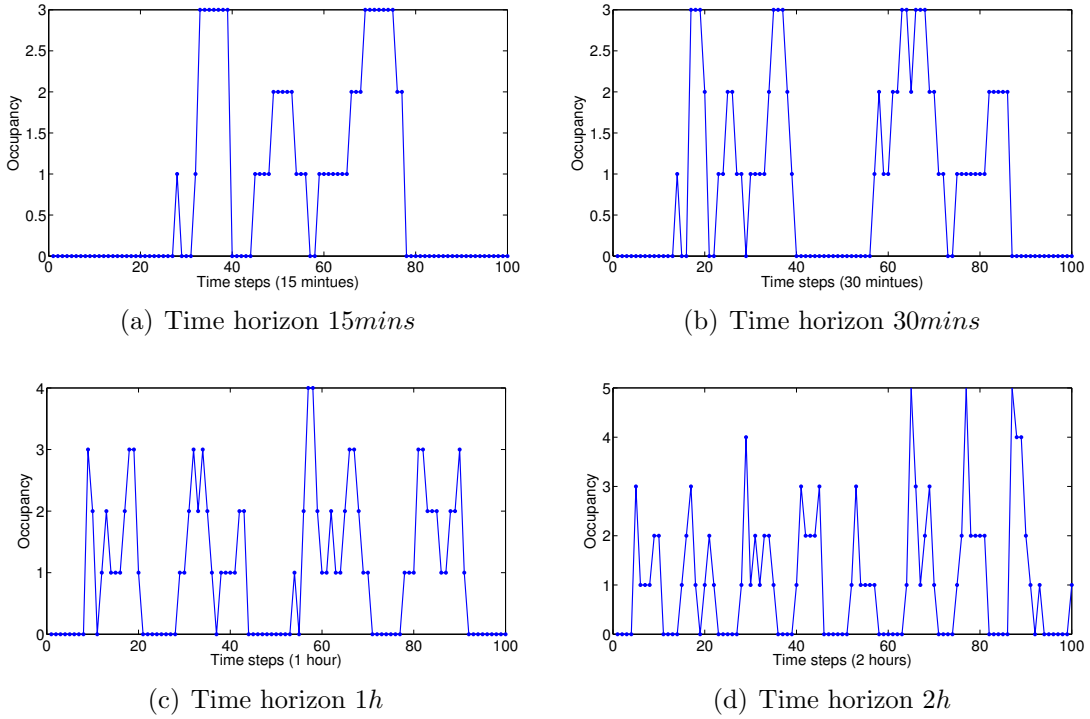

(a) Time horizon $15mins$

(b) Time horizon $30mins$

(c) Time horizon $1h$

(d) Time horizon $2h$

FIGURE 5.1: An example of 100 testing samples under four different time horizons

where $\delta(y_k, y_{k+1}) = \begin{cases} 1, & y_k = y_{k+1} \\ 0, & y_k \neq y_{k+1} \end{cases}$, and N is the total length of the time series. The smoothness rate of 1 indicates that the occupancy is equal for all time steps, and the smoothness rate of 0 indicates that the adjacent steps of occupancy are different for all time steps. Table 5.4 demonstrates the smoothness rate for different prediction horizons. It can be found that the smoothness rate decreases with the increase of prediction horizon. As mentioned before, the prediction accuracy decreases with the increase of prediction horizon, except for the SDP and MG models. According to the definition of the SDP and MG model, it does not take into consideration of the occupancy in the previous steps. Therefore, the adjacent occupancy predicted by these models will have a low probability to be equal, which makes its prediction performance increase with the decrease of the smoothness rate, or in other words, the increase of the prediction horizon. When the prediction horizons are $15mins$ and $30mins$, the smoothness rates are as high as 0.8104 and 0.7113 respectively, which means that first order linear property is dominant under these conditions. Thus, the linear ARIMA models using previous

one step occupancy can achieve a good performance, and the nonlinear model, i.e. ANN and SVR, cannot be expected to achieve better performance.

When the prediction horizons are $1h$ and $2h$, the smoothness rates decrease to 0.6050 and 0.4734 respectively, which means the linear property of the signal becomes weak. Therefore, the nonlinear data mining models, i.e. ANN and SVR, perform well, especially under prediction horizons of $1h$. The SDP method outperforms the other methods under prediction horizons of $2h$. This may be because it tends to provide predictions close to the average patterns. Moreover, due to the limited size of the training samples under the perdition horizon of $2h$ (12 samples per day), the nonlinear data mining approaches cannot be well trained, leading to a limited performance.

5.4 Summary

In this chapter, we compared occupancy models and data mining approaches for building occupancy prediction. We tested the prediction capabilities of two occupancy models in the multi-occupant situation, and presented three linear and nonlinear data mining approaches for predicting building occupancy. The performances of the occupancy models and the data mining approaches have been compared using actual occupancy data under the four prediction horizons of 15 minutes ($15mins$), 30 minutes ($30mins$), 1 hour ($1h$) and 2 hours ($2h$). The results showed that the prediction abilities of the occupancy models are limited and the data mining approaches are efficient in building occupancy prediction. We also presented a guideline on how to choose a proper model for predicting occupancy under different prediction horizons.

Part II

Indoor Localization and Activity Recognition

Chapter 6

Literature Review of Indoor Localization and Activity Recognition

In Part II of the thesis, we focus on the detailed information of occupant location and activity in buildings. The real-time locations of occupants can be utilized for lighting control and the activities of occupants can be used for the estimation of occupant comfort level which is important for building climate control. Two novel methods for indoor localization and one novel method for activity recognition are introduced.

6.1 Indoor Localization

One of the most popular indoor localization techniques is the WiFi fingerprinting approach, which consists of offline training and online testing. In online testing, a nearest neighbors algorithm and a probabilistic model are utilized for location estimation [69, 70]. However, fingerprinting approaches require a labor-intensive and time-consuming site survey for data collection. Li et al. presented two algorithms, i.e. Environment-Aware Sequence-Based Localization (EASBL) and Iterative Maximum Likelihood Estimation (IMLE), for WiFi based indoor localization in emergency situations where deployment cost needs to be considered [71, 72].

Real experiments have been conducted in [18], which indicated a high room identification accuracy and a significant reduction of deployment cost. However, due the fluctuations of WiFi signals, the performances of these approaches are limited. Smartphone embedded sensors can provide an alternative solution, i.e. Pedestrian Dead Reckoning (PDR), for indoor localization [73]. The PDR approach states that the current position can be derived from the previous position, the current walking length and direction. Unfortunately, this approach suffers from the drift problem with walking distance [74]. To improve the indoor localization performance, recent works tend to fuse WiFi and PDR to compensate the drawbacks of each method.

Evennou et al. [75] first integrated WiFi and PDR for indoor localization and navigation. They applied the WiFi fingerprinting approach with a k-closest neighbors algorithm. For the PDR approach, the key parameter of walking direction was derived from the integration of gyroscope data, which will drift with walking distance. They employed a Kalman filter to correct this drift by using WiFi based localization trajectories. Finally, a particle filter was leveraged to fuse WiFi and PDR. Another work can be found in [76]. The authors intended to fuse inertial sensors, indoor map and WLAN RSS (Received Signal Strength) to localize pedestrians in indoor environments. In the PDR approach, the walking direction was derived from gyroscope data. In terms of the estimation of walking length, they presented a linear fitting of step length with step frequency. To decrease the computational load of the system, they proposed an obstacle line grouping method for map information. Wang et al. [77] proposed a similar work which fuse PDR, WLAN RSS and map information for pedestrian tracking by using a particle filter. Fingerprinting approach was applied for RSS based localization, which is also treated as a benchmark for performance comparison in experiments. In the PDR approach, an empirical equation was employed to estimate walking length. And the walking direction was sampled from a uniform distribution. Waqar et al. [78] presented a fusion framework which combines motion information from smartphone sensors and the WiFi fingerprinting by using a Bayes filter. They applied the term of *belief* which represents conditional probability distribution over all possible states in terms of users' coordinates. In the motion model, the *belief* was updated based on the PDR approach. Then, the WiFi fingerprinting method which leverages on rank based scheme and Spearman's footrule distance instead of existing nearest neighbour method was employed to correct the *belief*. A WiFi-SLAM based on

Gaussian Process Latent Variable Model is introduced in [79]. It simultaneously considered the constrains of WiFi RSS measurements and the user's motion model obtained from smartphone inertial sensors. An improved version, i.e. Semantic-SLAM, can be found in [80]. It also utilized the landmarks sensed by smartphone sensors. Experiments indicated the good performance of their proposed approach on simultaneous localization and mapping.

Particle filter is widely used in fusing WiFi and the PDR approach. However, due to the high computational load of the particle filter, it is not suitable for a resource limited smartphone platform. In this work, we employ the Kalman filter algorithm which is computationally light by formulating the fusion problem in a linear perspective. For WiFi based localization, instead of using the fingerprinting approach which requires a time consuming training process, we apply a weighted path loss (WPL) [81] approach which has been shown to be efficient and simple for implementation. Novel approaches are employed in estimating several important parameters of the PDR approach. To avoid the influence of smartphone tilting in step detection, a quaternion is applied to obtain consistent vertical acceleration, and an efficient step detection scheme is presented. Another important issue in the PDR approach is walking direction estimation. The approaches that leveraged on magnetometers are easily distorted by metal and electronic facilities, and gyroscope integration approaches will accumulate errors. To overcome these problems, we apply a fusion framework using the Kalman filter. Moreover, we leveraged on landmarks which can be detected using smartphone sensors to reset system errors and restart the system.

The smartphone inertial sensor based approach is lightweight and requires fewer resources for indoor localization and tracking. However, without any corrections, it suffers from the drift problem. WiFi based corrections is shown to be effective. In situations where WiFi signals are not available, or the application is sensitive to battery consumption (WiFi scanning is power hungry), other corrections are required.

The authors in [82] combined PDR with GPS to enhance localization accuracy. They also constructed a neural network model to estimate the step length. A helmet containing the inertial measurement unit and the GPS antenna was used for real experiments. However, since GPS signals are degraded indoors, this solution is not feasible for indoor situations. Girard et al. [83] presented an ultrasound

ranging assisted PDR system. A particle filter was applied for the fusion of the PDR approach with ultrasound measurements. The portable ultrasound range sensors measured the distance between the pedestrian and adjacent walls, which eliminates the invalid particles to enhance the localization accuracy of the PDR approach. Ruiz et al. [84] proposed to fuse the PDR approach with active RFID measurements using the Kalman filter. Instead of employing a loose integration which leverages on the estimated position of a separate RFID system, they applied the residuals of PDR-predicted reader-to-tag ranges and the ranges derived from the RFID system. Lee et al. [85] presented an inertial sensor based localization system with Chirp Spread Spectrum (CSS) radio beacons whose locations are unknown. They performed a Simultaneous Location and Mapping (SLAM) technique to localize the pedestrian in indoor environments. Their system was tested using real experiments and achieved good accuracy with a small number of beacons. However, these three approaches requires extra devices and cannot be integrated into a portable smartphone which is widely available. The authors in [86] applied landmarks in environments, e.g. stairs, escalators, elevators and WiFi signatures, to calibrate the drift of the PDR approach. An unsupervised learning method was employed to identify landmarks in environments. Real experiments were conducted in three different environments with median localization errors of $1.69m$. However, the locations of landmarks need to be manually measured in advance. In this situation, we present a smartphone inertial sensor based PDR approach for indoor localization and tracking with occasional iBeacon calibrations. Since the PDR approach will drift with walking distance, we propose an iBeacon based calibration algorithm using the extended Kalman filter. By analyzing iBeacon measurements, an efficient calibration range is defined. In order to obtain the initial position, we propose a combination of existing WiFi routers and installed iBeacon tags using a WPL model [81].

6.2 Activity Recognition

Early human activity recognition R&D activities began with wearable devices. Bao et al. [87] applied five biaxial accelerometers worn on different parts of the body to recognize 20 daily activities. It was found that a decision tree classifier achieved the highest recognition accuracy of over 80%. They also concluded that

the recognition performance will drop slightly with only two accelerometers worn on thigh and wrist. Preece et al. [88] compared 14 methods to extract features from wavelet transformation, time and frequency domain of wearable acceleration signals in different placements. A nearest-neighbor classifier was used and two datasets were involved in the experiments. They concluded that frequency features are more efficient in recognizing human dynamic activities. However, wearable devices are intrusive for users and require additional cost for hardware.

With the development of smartphone technology, a large number of sensors, e.g. accelerometer, gyroscope, magnetometer, proximity, etc., are embedded. Thus, smartphone based activity recognition has emerged in the past decade. Kwapisz et al. [89] employed smartphone acceleration to identify human physical activities such as walking, jogging, climbing stairs, sitting, and standing. With the phone placed in pants' pocket, they achieved an average accuracy of over 90%. Figo et al. [90] investigated different features for human activity recognition using smartphone built-in accelerometers. In real-world experiments of recognizing three activities of walking, running and jumping, they made a conclusion that frequency-domain features are more robust and perform better. Bayat et al. [91] proposed an average of probabilities method to fuse five classifiers for human activity recognition. They also presented a new digital low-pass filter to isolate the gravity component in raw acceleration. With only a single triaxial acceleration data from smartphones, they achieved identification accuracy of up to 91.15% on six daily activities for two phone positions, i.e. in hand and in pants' pocket. These works did not consider a real problem of orientation variations of the smartphone.

Some advanced works have taken the orientation effects into consideration. Sun et al. [92] proposed an activity recognition approach with orientation and position variations. They treated the acceleration magnitude as the 4th data dimension together with triaxial acceleration to overcome the effect of orientation variations. To solve the effect of position variations, they trained a location-specific SVM classifier for each location. Experimental results showed a significant improvement compared with state-of-the-art approaches. Tao et al. proposed a Multi-column Bi-directional Long Short-Term Memory (MBLSTM) approach using two directional features for human activity recognition with smartphone accelerometer [93]. The two directional features are extracted from vertical component and the norm of horizontal components of three dimensional ($3D$) acceleration. The experiments

showed the effectiveness of these two directional features and their proposed learning algorithm.

Ustev et al. [94] proposed an activity recognition system independent of device orientation by transferring sensor data from the device coordinate system into the earth coordinate system. Experimental results demonstrated the effectiveness of their proposed scheme. They also tested the recognition accuracy in terms of device and user dependency and concluded that their impacts are minor compared to orientation effects. Guo et al. [95] presented smartphone based activity recognition regardless of device orientation and placement by using coordinate mapping. The Euler angles were leveraged to obtain the rotation matrix for coordinate mapping. Moreover, they presented a triaxial motif combination method and a motif-based activity classification algorithm. The experimental results showed the effectiveness of their proposed approach in reducing the negative effects of orientation and placement. All researchers did not realize one serious problem that has arisen after performing coordinate transformation. After transferring the acceleration into the fixed earth coordinate system, the directions of performed activities will have significant influence on the acceleration in horizontal axes, which shall degrade the performance of activity detection systems. Therefore, we presented an orientation independent approach based on coordinate transformation and principal component analysis (CT-PCA) techniques.

Chapter 7

Indoor Localization Using WiFi, Smartphone Sensors and Landmarks

The coarse information of occupant number is important for energy efficiency in buildings. In addition to that, the detailed information of occupant location is also very important for many applications related to energy efficient buildings. In this chapter, to achieve accurate indoor localization, we propose a localization and tracking system based on the fusion of WiFi, smartphone sensors and landmarks using the Kalman filter. In Section 7.1, we present a WiFi WPL method for coarse localization. Then, we introduce the PDR approach based on smartphone inertial sensors, together with some novel techniques for its key parameters. After that, the identification of landmarks using smartphone sensors is shown. Finally, we resolve the sensor fusion problem using the Kalman filter. In Section 7.2, we present the experimental setups, and show the experimental results and discussions under two different environments.

7.1 Methodology

7.1.1 Weighted Path Loss of WiFi

One of the most popular WiFi positioning techniques is the fingerprinting approach which consists of two phases, i.e. off-line training and on-line testing. In the off-line training phase, a large amount of data that contains the received signal strength (RSS) and the corresponding location is collected. Then, machine learning algorithms are employed to construct the relationship between the RSS and the location information. In the on-line testing phase, the location information can be derived based on real-time WiFi RSS value using the model obtained in the training phase. The WiFi fingerprinting approach requires a tedious manual collection of data for training and a re-training process when the environment changes.

In order to overcome the drawbacks of the fingerprinting approach in real implementation, we present a WPL algorithm which has already been successfully applied in RFID based localization system [81, 96]. Assume s_t^i is the RSS of the router i at time step t, then, based on signal propagation model in [97], we obtain

$$s_t^i = PL_0 + 10\alpha \log(d_t^i) \tag{7.1}$$

where PL_0 is the reference path loss coefficient, α is the path loss exponent, and d_t^i is the distance between the router i and the device at time step t. Based on Equation (7.1), d_t^i can be expressed as:

$$d_t^i = 10^{\frac{s_t^i - PL_0}{10\alpha}} \tag{7.2}$$

Suppose we have N routers, and the distance between the device and routers can be expressed as a vector $\{d_t^1, d_t^2, \cdots, d_t^N\}$ at time step t. Then the weight of each router can be calculated as:

$$w_t^i = \frac{\frac{1}{d_t^i}}{\sum_{i=1}^{N} \frac{1}{d_t^i}} \tag{7.3}$$

Finally, the location of the device, (x, y), can be expressed as

$$(x, y) = \sum_{i=1}^{N} w_t^i (x_i, y_i) \tag{7.4}$$

where (x_i, y_i) is the location of the i-th router.

Considering that our system will be running on a resource limited smartphone platform instead of a server, lightweight WPL algorithm is more suitable than the popular fingerprinting approach which requires manual collection of a huge data set for training and heavy load machine learning algorithms. Moreover, when the environment changes, the WPL algorithm only needs to adjust two parameters, i.e. PL_0 and α, in Equation (7.1), while the fingerprinting approach requires re-collection of the data and a re-training process. Therefore, the WPL algorithm is more suitable for real-time implementation.

7.1.2 Pedestrian Dead Reckoning

In the PDR approach, the current position is determined by the previous position, current walking length and walking direction, which can be expressed as

$$\mathbf{S}_{k+1} = \mathbf{S}_k + L_k \begin{bmatrix} \sin\theta_k \\ \cos\theta_k \end{bmatrix} \tag{7.5}$$

where $\mathbf{S}_k$ is the $2D$ coordinate of the pedestrian, L_k is the walking length and θ_k is the walking direction at time step k. Some critical issues need to be resolved, such as step detection, walking length estimation and walking direction estimation.

Initial Position Estimation: The PDR approach only provides relative information. Therefore, the accuracy in estimating the initial position will directly influence the accuracy of the entire localization process of the PDR approach. Since we do not have any prior information of the initial position, the only location information comes from the WiFi positioning system at the beginning. Due to the importance of the initial position estimation, we leverage on the landmarks, whose positions are known, as new starting points to restart the algorithm when the pedestrian reaches these landmarks. In addition, landmarks will be helpful in resetting accumulative errors of the system caused by unknown bias in sensors.

The detailed definition and identification of landmarks will be introduced in Section 7.1.3.

Step Detection: Since the feet hit the ground during walking, the vertical acceleration signal will contain periodic patterns which can be applied for step detection. To overcome the tilting effect and obtain consistent vertical acceleration values, we need to transfer the original acceleration from smartphone coordinate system (SCS) into a fixed reference, i.e. earth coordinate system (ECS). We leverage on a quaternion, i.e. a four-element vector, to represent any rotation in a $3D$ coordinate system [98]. According to [99], a software sensor, i.e. rotation vector sensor, will provide real-time quaternions referring to ECS. Based on [98], a rotation matrix, $\mathbf{R}$, can be calculated using a real-time quaternion. Assume that $\mathbf{A}_s$ and $\mathbf{A}_e$ are the $3D$ acceleration in SCS and ECS respectively, then we have

$$\mathbf{A}_e = \mathbf{R}\mathbf{A}_s \tag{7.6}$$

In this way, we can obtain a consistent $3D$ acceleration in ECS regardless of device orientation. But the obtained vertical acceleration contains gravity component that needs to be eliminated. Due to the stability of gravity, we leverage on a low-pass filter to obtain the gravity first, and then employ the vertical acceleration to subtract the gravity [99], which can be expressed as

$$\mathbf{G} = \alpha\mathbf{G} + (1-\alpha)\mathbf{A}_e \tag{7.7}$$

$$\mathbf{L} = \mathbf{A}_e - \mathbf{G} \tag{7.8}$$

where $\mathbf{G}$ is the gravity, α is the parameter of the low-pass filter, and $\mathbf{L}$ is the required linear acceleration. Due to the limited quality of smartphone sensors, the sensor outputs are very noisy. We perform a smoothing operation to reduce the noise effect. Assume that, $\{a_k, k = 1, 2, ..., N\}$ is the time series of vertical acceleration, and N is the total length of the data, the m-th order smoothed acceleration, $\hat{a}_k$, can be expressed as

$$\hat{a}_k = \frac{\sum_{i=k}^{k+m-1} a_i}{m} \tag{7.9}$$

Fig. 7.1 shows a simple example of vertical acceleration smoothing where the

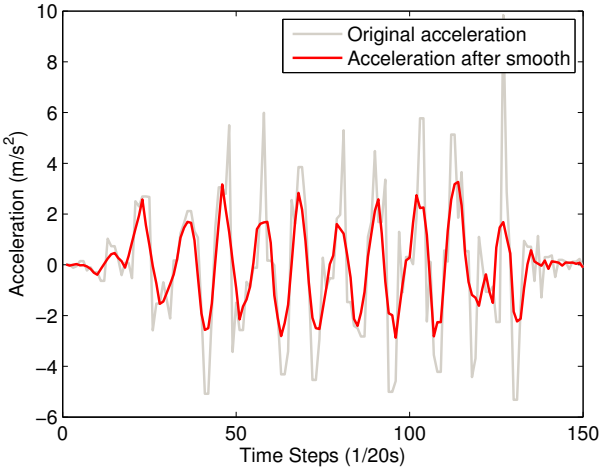

FIGURE 7.1: An example of acceleration smoothing.

sampling frequency is $20Hz$. After smoothing, most of high frequency noise is wiped off, which will make the step detection process more accurate and robust. One of the most popular step detection methods is based on peak detection, but it will be easily affected by noise. In this work, we present a simple and efficient threshold-based step detection algorithm. The set of valid step events for the proposed approach is as follows:

$$\{\hat{a}_k > a^+, \hat{a}_{k+p} < a^-, 0 < p < p_{max}\} \tag{7.10}$$

where a^+ and a^- are the positive and negative thresholds respectively, and p_{max} is the upper-bound of one step duration. In this work, we set a^+, a^- and p_{max} as $1.0m/s^2$, $-0.8m/s^2$ and 12 (corresponding to $12 * 1/20s = 0.6s$), respectively. Fig. 7.2 compares the peak detection with the proposed threshold-based algorithms using an example of 10 steps. The proposed approach is obviously more robust.

Step Length Estimation: One of the most influential parameters in the PDR approach is the walking length. It has large variance among different subjects. Even for the same subject, it varies significantly at different times during walking. The authors in [100] presented constant walking lengths for different activity modes, i.e. walking, jogging and running. Another work in [101] estimated walking length based on the height of a pedestrian. These approaches did not take into consideration the variations of walking length during walking. One sophisticated approach can be found in [102] where the author constructed a relationship between walking

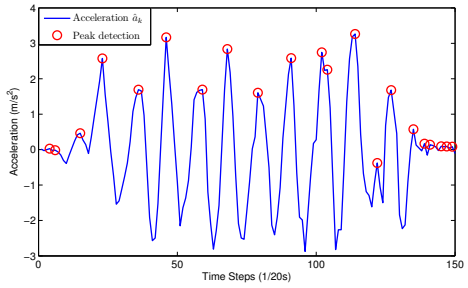

(a) The peak detection algorithm

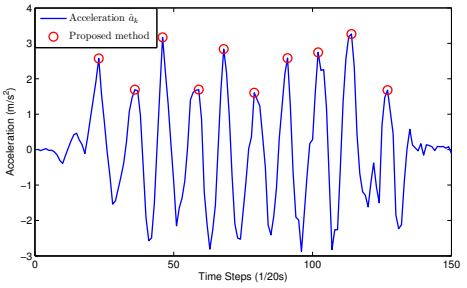

(b) The proposed threshold-based detection algorithm

FIGURE 7.2: Step detection based on (a) the peak detection algorithm and (b) the proposed threshold-based detection algorithm using an example of 10 steps.

length and vertical acceleration, which is given by

$$L = \beta(\hat{a}_{max} - \hat{a}_{min})^{1/4} \tag{7.11}$$

where $\hat{a}_{max}$ and $\hat{a}_{min}$ are the maximal and minimal smoothed vertical accelerations during one step respectively, and β is a parameter that needs to be specified for different subjects. Note that, since we have transferred the acceleration into ECS, the tilting of smartphones during walking will have no effect on this walking length estimation algorithm.

Walking Direction Estimation: One method for estimating pedestrian walking direction is based on the orientation sensor output which is a combination of magnetometer and accelerometer readings in smartphones [99]. One of the orientation sensor outputs, i.e. the azimuth reading, is the angle between smartphone pointing direction and the geographical north. Since this angle is determined by the magnetometer output which will be affected by electronic devices, we intend to compensate this effect by fusing the gyroscope output which provides the angular acceleration without any effect of electronic devices. The Kalman filter is applied for this fusion.

7.1.3 Identification of Landmarks

Landmarks with known positions have specific sensor patterns which make them identifiable in environments. The motivation of introducing landmarks is that the accuracy of the PDR approach highly relies on the estimation accuracy of

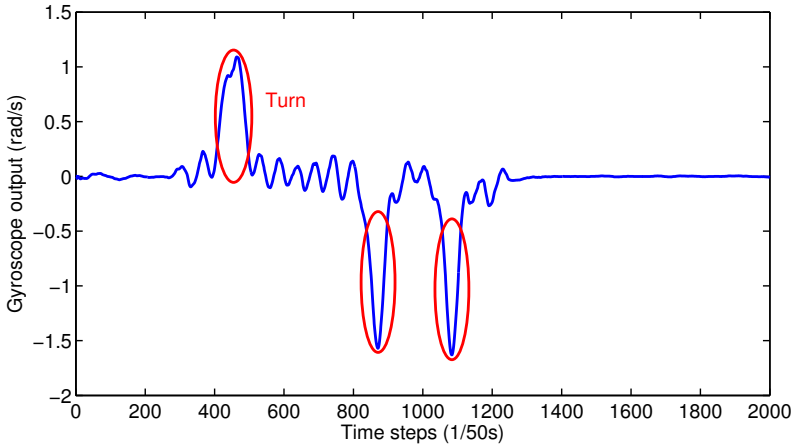

FIGURE 7.3: Identification of turns

initial location. Landmarks can provide accurate new starting points for the PDR algorithm when a pedestrian reaches these landmarks [86]. Moreover, they can also reset the cumulative errors of the system due to the biases of sensors.

The landmarks we investigated in this work include turns, elevators, escalators, stairs and doors. The sensors involved in the identifications of these landmarks include accelerometer, magnetometer, gyroscope, barometer and WiFi.

Turns: Due to topology constrains in indoor environments, turns can be identified using angular or direction related sensors. The most direct way to recognize turns is to use magnetometer reading. However, it may be affected by electronic devices, which makes it unstable for the recognition of turns. An alternative way to achieve that is leveraging on the gyroscope readings which measure angular acceleration without any interferences. After smoothing the gyroscope outputs, turns can be easily distinguished. An example is shown in Figure 7.3. In addition, based on the direction of the pulse in the figure, left or right turns can be separated. In real situations, many turns can be detected. If the distance of two turns is smaller than localization accuracy, we may make a wrong decision leading to a bias for the system. To avoid this, we only consider the turns that are unique in the path as landmarks.

Elevators: Based on the unique pattern of vertical acceleration, taking elevators can be easily identified. It contains a hyper-gravity and a hypo-gravity processes,

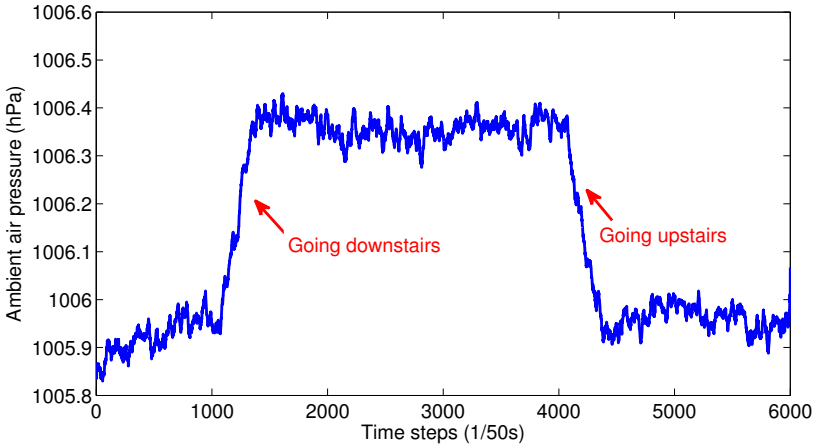

FIGURE 7.4: Ambient air pressure for going upstairs and downstairs

shown as a positive impulse and a negative impulse of vertical acceleration respectively [86]. Moreover, the length between the impulses reflects how many floors the pedestrian goes up or down, which would be important for multi-floor localization.

Escalators: The acceleration pattern of taking escalators is similar to stationary. We apply magnetometer data to distinguish them. In stationary condition, the variance of magnetometer data is small. while, due to the significant influence on magnetics of the motors in escalators, the variance of magnetometer readings will be large when taking escalators. We can identify these landmarks by using the variance of magnetometer readings.

Stairs: Going upstairs or downstairs has similar patterns of acceleration with normal walking. An effective way to distinguish these two activities is to use the barometers in smartphones [103]. It is well known that the higher the elevation, the lower the ambient air pressure. Therefore, there will be a decrease of ambient air pressure when going upstairs and an increase of that when going downstairs. Figure 7.4 shows an example of ambient air pressure change for going upstairs and downstairs.

Doors: The landmarks of doors contain two phases of acceleration, low acceleration for opening the door and periodic patterns of acceleration for walking out. If only based on this phenomenon, many false positive events will be produced. Another prominent property of passing through a door is the big change of received signal strength of WiFi, as shown in Figure 7.5. Based on this property, the landmarks of doors can be easily identified.

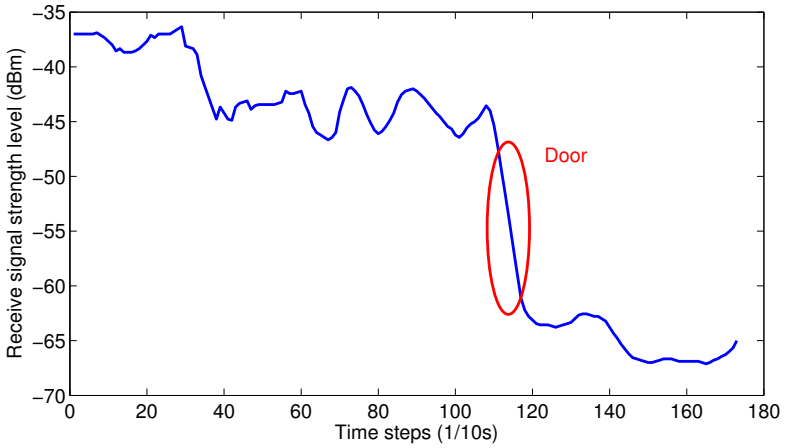

FIGURE 7.5: Receive signal strength of WiFi when passing through a door

7.1.4 Sensor Fusion Using the Kalman Filter

The WiFi WPL approach and the PDR approach have different properties for localization. In particular, the WiFi WPL approach can provide an exact location. But the localization results have large variations because of the variations of WiFi signals. While the PDR approach leveraging on relative location information can provide a smooth location, but the localization results will slowly drift with working distance. The combination of these two different approaches will compensate the weaknesses of each other. Specifically, the WiFi WPL approach will correct the drift of the PDR approach, while the PDR approach will smooth the variations of the WiFi WPL approach.

The potential sensor fusion techniques for combining the WiFi WPL approach with the PDR approach include particle filter [104], hidden Markov model [105], Kalman filter [106], etc. In real situations, users need to know their locations in real time for navigation. Therefore, the whole system should be running on smartphones instead of servers. Because of that, light computation algorithms will be preferred because of limited resources in smartphones. In terms of problem formulation, we tackle the problem in a linear perspective, then, the Kalman filter which is computationally light can be applied instead of the particle filter which is widely used in the literature.

Assume $\mathbf{X}_t$ is the $2D$ coordinate of a pedestrian and $\mathbf{d}_t = L_t \begin{bmatrix} \sin\theta_t & \cos\theta_t \end{bmatrix}^T$ is the input where L_t is the step length and θ_t is the walking direction at time step t. Then, based on the PDR approach, the state transition function of the sensor

fusion framework can be expressed as:

$$\mathbf{X}_t = \mathbf{F}\mathbf{X}_{t-1} + \mathbf{G}\mathbf{d}_t + \mathbf{v} \tag{7.12}$$

where $\mathbf{F}$, $\mathbf{G}$ are identity matrices, and $\mathbf{v}$ denotes the Gaussian noise of the motion model with zero mean and covariance matrix $\mathbf{M}$ [107]. The observation function can be obtained based on the output of the WiFi WPL approach, $\mathbf{Z}_t = \sum_{i=1}^{N} w_t^i(x_i, y_i)$ where w_t^i is the weight of router i at time step t and (x_i, y_i) refers to the location of router i. The observation function can be expressed as:

$$\mathbf{Z}_t = \mathbf{H}\mathbf{X}_t + \mathbf{p} \tag{7.13}$$

where $\mathbf{p}$ denotes the Gaussian noise of the WiFi WPL output with zero mean and covariance matrix $\mathbf{N}$ [108]. Since it is a direct observation problem, $\mathbf{H}$ is an identity matrix.

The Kalman filter [106] is employed for this sensor fusion. The algorithm contains two processes, i.e. predicting and updating.

Predicting:

$$\mathbf{X}_{t|t-1} = \mathbf{F}\mathbf{X}_{t-1|t-1} + \mathbf{G}\mathbf{d}_t \tag{7.14}$$

$$\mathbf{P}_{t|t-1} = \mathbf{F}\mathbf{P}_{t-1|t-1}\mathbf{F}^T + \mathbf{M} \tag{7.15}$$

Updating:

$$\mathbf{K}_t = \mathbf{P}_{t|t-1}\mathbf{H}^T(\mathbf{H}\mathbf{P}_{t|t-1}\mathbf{H}^T + \mathbf{N})^{-1} \tag{7.16}$$

$$\mathbf{X}_{t|t} = \mathbf{X}_{t|t-1} + \mathbf{K}_t(\mathbf{Z}_t - \mathbf{H}\mathbf{X}_{t|t-1}) \tag{7.17}$$

$$\mathbf{P}_{t|t} = (\mathbf{I} - \mathbf{K}_t\mathbf{H})\mathbf{P}_{t|t-1} \tag{7.18}$$

7.2 Evaluation

To evaluate the performance of our proposed approach, two experiments have been conducted in different environments. The comparisons have been made among the proposed fusion approach, the WiFi WPL approach and the PDR approach with landmarks.

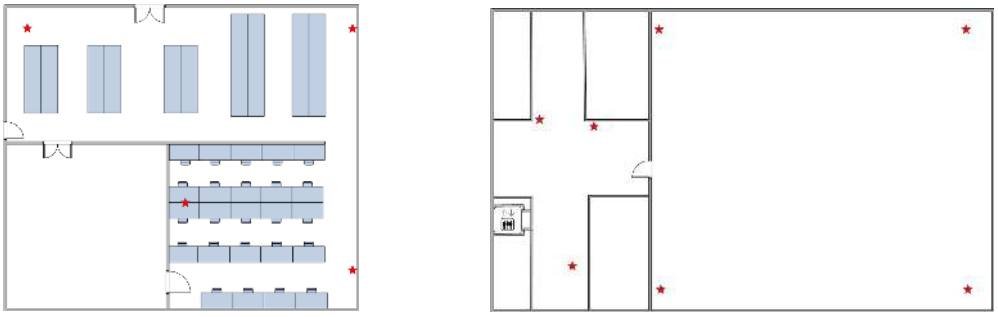

(a) The research lab (b) The testbed

FIGURE 7.6: Layouts

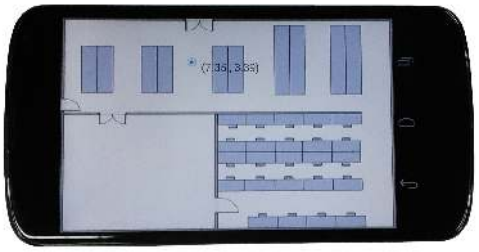

FIGURE 7.7: User Interface

7.2.1 Experimental Setup

The two experiments were performed in a typical research lab and a designed testbed in the campus of NTU (Nanyang Technological University, Singapore). The sizes of the lab and the testbed are $19.0m \times 16.3m$ and $27.5m \times 16.4m$, respectively. Figure 7.6 shows the layouts of the research lab and the testbed. The red stars represents the locations of APs (Access Points). The device involved in the experiments is a Google Nexus 4 smartphone. We developed an Android application for the experiments. The user interface is shown in Figure 7.7. The circle shows the position of the user and the number represents the corresponding coordinate. We define top left corner as coordinate origin, x-axis points to the right and y-axis points downwards. Note that we only consider hand-hold situation, the others situations, such as putting in pockets or bags, are our future works. To obtain the ground truth of the trajectory, we mark the ground with $1m$ grid and apply a camera to record the whole walking process, then, we manually measure the location of each step of the pedestrian.

7.2.2 Experimental Results and Discussions

The first experiment was conducted in the research lab. Due to the physical constraints caused by facilities, many physical turns are involved in the experiment. Based on the criterion introduced in Section 7.1.3, only one turn shown as magenta circle in Figure 7.8(a) satisfies. The second experiment has been performed in the designed testbed. Since the testbed is relatively empty, no physical turns are involved in the experiment. Therefore, no landmarks of turns can be used. According to the true trajectory in Figure 7.8(b), two landmarks of an elevator and a door are employed in the experiments.

Figure 7.8 shows the trajectories of the true path, the WiFi WPL model, the PDR approach with landmarks and our proposed fusion approach for the two experiment setups. The corresponding cumulative distribution functions (CDFs) of localization errors for the three approaches are demonstrated in Figure 7.9. In the first experiment, the mean localization errors of the WiFi WPL approach and the PDR approach with landmarks are $2.8977m$ and $1.7547m$, respectively, while that of our proposed fusion model with the Kalman filter is $0.9945m$. After sensor fusion of WiFi, smartphone sensors and landmarks, we reduce the localization errors by 65.7% and 43.3%, respectively, when comparing to the WiFi WPL approach and the PDR approach with landmarks. Since only one landmark is employed in the middle of the path in the first experiment, the localization error is relatively large before arriving at the landmark. After restarting from the landmark, PDR provides a high localization accuracy within a short range, and then slowly drifts, while the proposed algorithm corrects the drift by fusing the WiFi WPL outputs. Clearly, the proposed sensor fusion approach takes the advantages of the techniques including PDR, WiFi WPL and landmarks to achieve a high localization accuracy. In the second experiment, the mean localization errors of the WiFi WPL approach and the PDR approach with landmarks are $3.5189m$ and $1.7727m$, respectively, while that of the proposed approach is $0.8492m$. After sensor fusion, we reduce the localization errors by 75.9% and 52.1%, respectively, when comparing to the WiFi WPL approach and the PDR approach with landmarks. Note that we did not adjust the parameters of WiFi WPL in the new environment. Therefore, the localization accuracy of WiFi WPL is slightly poorer than that in the first experiment. However, the entail fusion system can still achieve a high localization accuracy, i.e. $0.8492m$, when combining with smartphone sensors and landmarks.

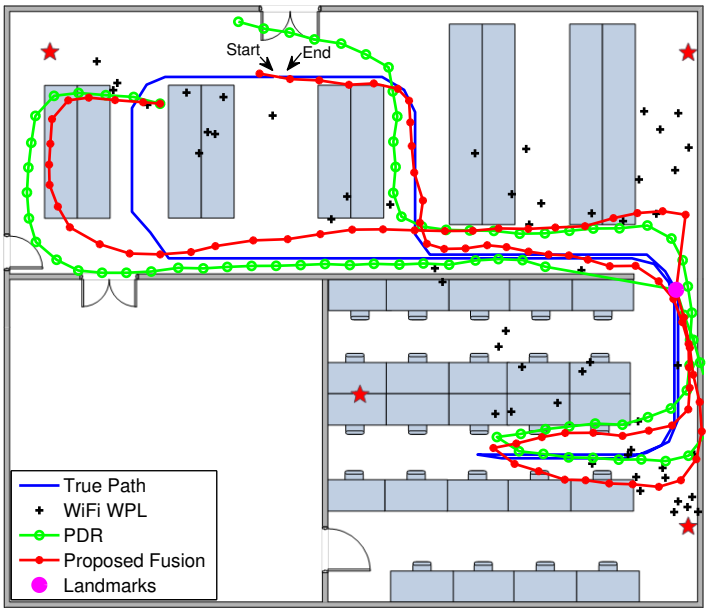

(a) The research lab

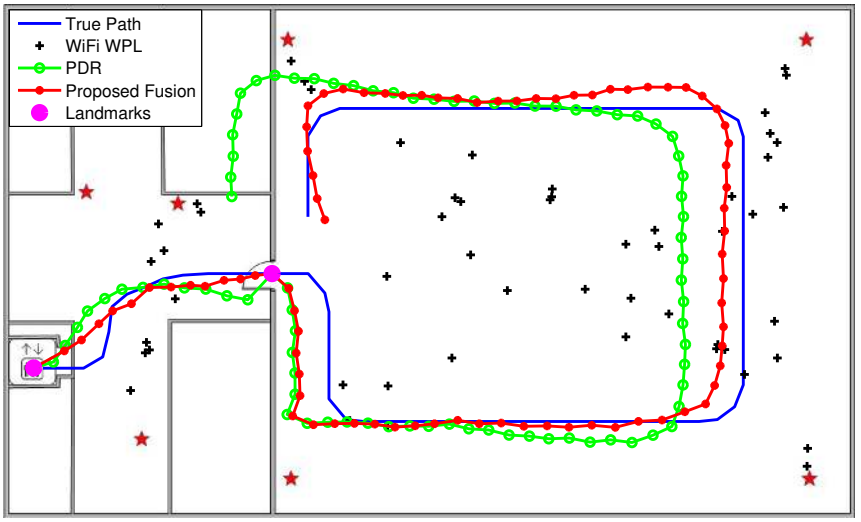

(b) The testbed

FIGURE 7.8: The trajectories of the true path, WiFi WPL model, PDR with landmarks, and the proposed fusion model for the two experiment setups.

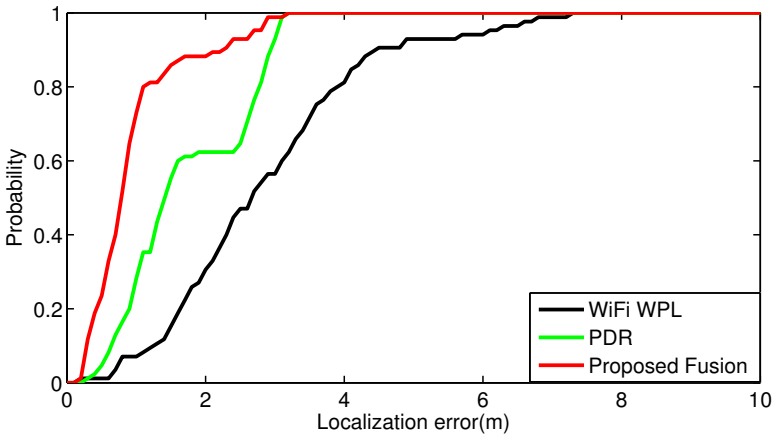

(a) The research lab

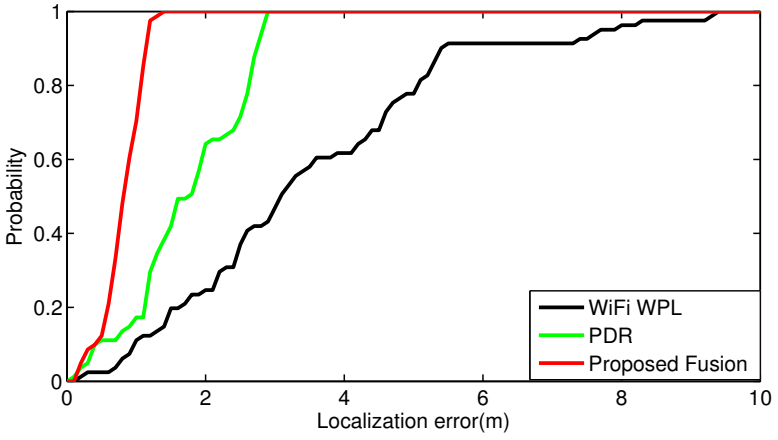

(b) The testbed

FIGURE 7.9: Cumulative distribution functions of localization error for the three approaches.

The tracking starts from an elevator which is a known landmark. Before arriving at the second landmark which is a door, PDR has relatively small localization error, but the walking direction has some deviations at the beginning, which may be caused by the magnetic effect of the motors in the elevator. However, the proposed fusion algorithm reduces the deviations by the correction of WiFi WPL. After passing through the door, PDR has high localization accuracy in a short range, and then slowly drifts. However, our proposed algorithm follows the true path very well. In summary, the proposed system has smaller variation than the WiFi WPL approach and lower drift than the PDR approach, and it provides an average localization accuracy of around $1m$.

With the accuracy of $1m$, the accurate occupancy distributions in a zone can be

obtained. Then, localized cooling or heating can be achieved for human comfort and energy saving. Moreover, with this high precision, automatic location-based lighting control can be performed to save energy. Another potential application is emergency response in fire and earthquake situations. Last but not least, with a localization accuracy of $1m$, personalized advertisement can be achieved when the occupants pass through a particular shop in a mall [109].

7.3 Summary

In this chapter, we proposed a combination of WiFi, smartphone sensors and landmarks using the Kalman filter for localizing occupants in indoor environments. Instead of using the tedious WiFi fingerprinting approach, we presented a weighted pass loss (WPL) model for WiFi based localization. A pedestrian dead reckoning (PDR) approach was leveraged for smartphone sensors based localization. Some important parameters including step detection, walking direction and walking length estimation have been specified. We also introduced the landmarks that can be detected using smartphone sensors to restart the system and reset cumulative errors of the system. Then, we formulated the fusion problem in a linear perspective. Thus, the Kalman filter which is computational light can be applied. Experiments have been conducted under two different environments. We can achieve a mean localization accuracy of around $1m$.

Chapter 8

Indoor Localization Using Smartphone Sensors with iBeacon Corrections

Since WiFi scanning is power hungry, WiFi based localization approaches will not be suitable for some applications on smartphones which are sensitive to battery consumption. Moreover, in some old buildings, WiFi signals may not be available, or WiFi APs are sparsely deployed leading to limited performances of WiFi based approaches. Thus, we present another localization and tracking system based on smartphone sensors with occasional iBeacon corrections. In Section 8.1, we first evaluate the estimation of one key parameter in the PDR approach. Then, we analyze iBeacon measurements and define an efficient calibration range where the extended Kalman filter is formulated. After that, a hybrid initial position estimation based on RSS measurements in environments is presented. In Section 8.2, we introduce the experimental setups and the experimental results as well as discussions under two different environments.

8.1 Methodology

The PDR approach based on smartphone sensors has been introduced in Section 7.1.2. But one important parameter of walking direction has not yet been well evaluated. Thus we present some details for walking direction estimation in

Section 8.1.1. Then, in Section 8.1.2, we analyze iBeacon measurements and define an efficient calibration range. After that, in Section 8.1.3, we present the extended Kalman filter based fusion algorithm for calibration. Finally, a hybrid initial position estimation based on RSS measurements in environments is shown in Section 8.1.4.

8.1.1 Walking Direction Estimation in PDR

The most direct way to estimate walking direction is based on magnetometer readings. However, they can be easily distorted by metal and electronic devices in indoor environments. An alternative way to estimate walking direction is based on the integration of gyroscope readings, i.e. angular velocities. Due to the sensor noise in smartphone gyroscope, the integration will slowly drift. In this work, we fuse these two approaches together using the Kalman filter which is computationally efficient. We assume that users will point their smartphones towards their walking direction in handheld situation, but the tilting of smartphones will have no effect because of the coordinate transformation. The corresponding state transition and observation functions are expressed as

$$\theta_t = \theta_{t-1} + \Delta t V_t + \mu \tag{8.1}$$

$$M_t = \theta_t + \varphi \tag{8.2}$$

where θ_t is the walking direction, V_t is the vertical gyroscope in ECS after coordinate transformation, M_t is the pointing direction derived from magnetometer outputs, Δt is the time interval, μ is assumed to follow Gaussian error with zero mean and variance P, and φ_t is assumed to follow Gaussian error with zero mean and variance Q.

Several simple tests have been conducted to evaluate the performance of this fusion approach. We fixed the route with three 90 degrees turns. The experiments were repeated 9 times using a Google Nexus 5 smartphone. Fig. 8.1 shows the experimental results. Since no prior knowledge of initial heading is available, we choose the initial magnetometer reading as the initial value for the gyroscope integration and the fusion approaches. Therefore, at the beginning with low drift of the

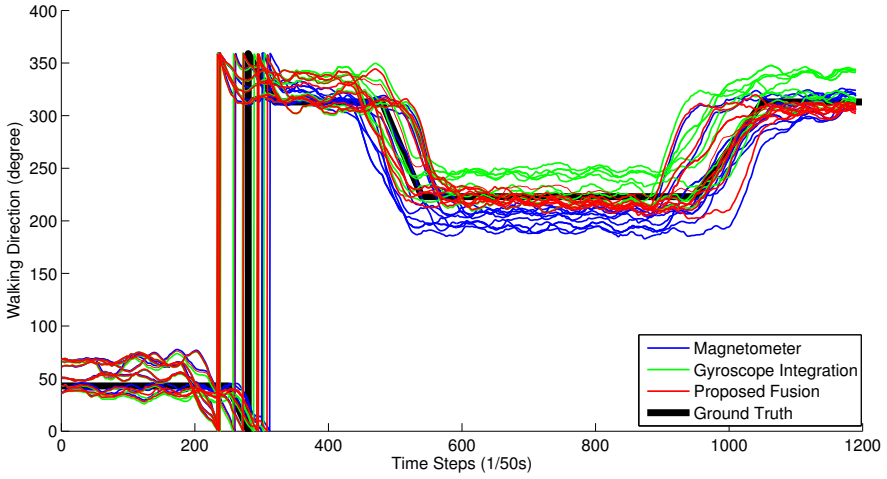

FIGURE 8.1: The test results of walking direction estimation.

gyroscope integration, the performances of the three approaches are very similar. After two turns, gyroscope based approach starts to drift, and the fusion algorithm outperforms the two individual methods in robustness and accuracy. Note that the exact turning times are different for different runs, so the curves shift forward or backward randomly. And the turning time of the ground truth path is chosen as the mean of all the runs.

8.1.2 iBeacon Measurements

According to Equation (7.5), only relative information is leveraged in the PDR approach. Therefore, errors will accumulate leading to the drift with walking distance. In this work, we apply a new technology, i.e. iBeacon, which is built upon Bluetooth Low Power (BLE). Comparing to WiFi, it is much more energy efficient. Since the localization is performed in a portable smartphone platform, power consumption is a big concern. Scanning BLE devices requires much less power than scanning WiFi routers [110], which makes iBeacon more suitable for our application. Owing to the low power consumption of BLE, a button cell can support an iBeacon for more than one year [111]. Thus, the iBeacon can be very small and easy to be deployed. An iBeacon package contains a unique ID, a reference RSS at one meter distance and the RSS between the iBeacon and a device. Various approaches, such as fingerprinting, triangulation and weighted pass loss, can be applied for iBeacon based localization, but the dense deployment of iBeacons is

required [110, 112]. Therefore, the deployment cost will be high, which is not suitable for industrial applications. In this work, we attempt to develop a low cost and high efficient localization and navigation system. Thus, the sparse deployment of iBeacons is recommended. Instead of utilizing iBeacons for precise localization, we employ them to calibrate the PDR approach occasionally with distance measurements. Based on Bluetooth signal propagation, the distance between the device and the iBeacon can be derived using a path loss model in [81], which can be expressed as

$$R_k^i = R^0 - 10\gamma \log\left(d_k^i / d^0\right) \tag{8.3}$$

where R_t^i is the RSS of i-th iBeacon, R^0 is the reference RSS value at one meter distance, γ is the path loss exponent, d_t^i is the distance between the device and i-th iBeacon, and d^0 equals to one meter. Then, the distance, d_t^i, can be derived as

$$d_k^i = 10^{\frac{R^0 - R_k^i}{10\gamma}} \tag{8.4}$$

To determine the parameters, R^0 and γ, we chose 14 reference points (0.1, 0.5, 1, 1.5, 2, 2.5, 3, 3.5, 4, 4.5, 5, 5.5, 6 and 6.5 meters) and collected 500 RSS values at each point. The parameter R^0 equals to the mean RSS value at one meter distance. And the parameter γ can be determined using a least-squares fit. In our experiment, the final estimated values of R^0 and γ are -77.39 and 2.1529, respectively. Figure 8.2 shows the RSS measurements at the reference points, the corresponding mean RSS values at each reference point and the curve of the least-squares model. We can find that the least-squares model fits the data very well. Another observation is that the differences of RSS values after 3 meters are minor. Since the RSS measurements of iBeacons are used for calibrating the drift of the PDR approach, accurate measurements are necessary. Therefore, we define that the calibration using iBeacon measurements will only be performed when the estimated distance between a device and an iBeacon is equal to or less than 3 meters.

8.1.3 Fusion Algorithm

The PDR approach is simple and effective, but it will drift with walking distance. With sparse deployment of iBeacons, we attempt to calibrate the PDR approach

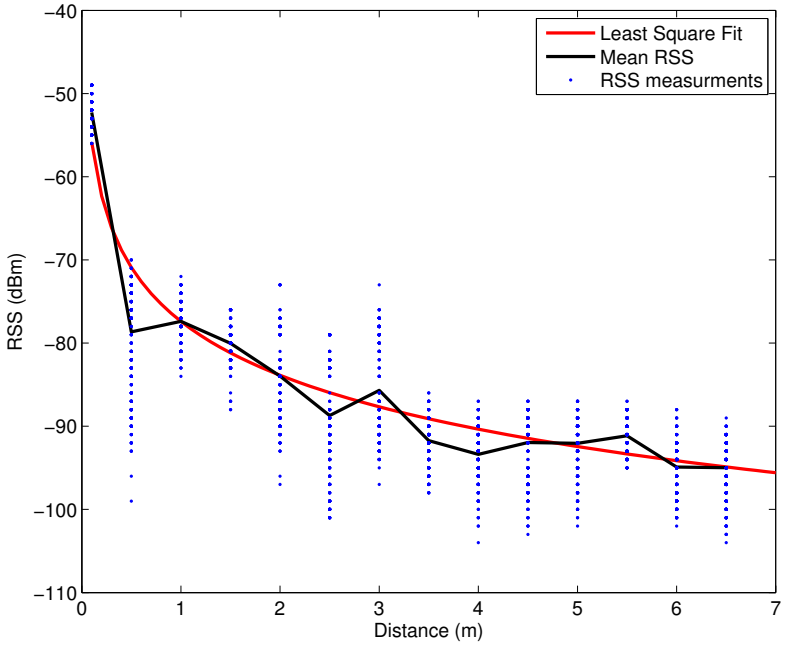

FIGURE 8.2: The RSS measurements at 14 reference points, the mean RSS values at each point and the curve of least-squares fit.

occasionally with iBeacon measurements. Based on the PDR approach, we formulate the system dynamics as

$$\mathbf{S}_{k+1} = \mathbf{S}_k + \mathbf{u}_k + \mathbf{w} \tag{8.5}$$

where $\mathbf{u}_k = L_k \begin{bmatrix} \sin\theta_k \\ \cos\theta_k \end{bmatrix}$, and $\mathbf{w}$ follows normal distribution with zero mean and variance $\mathbf{R}$. Based on the RSS between a device and an iBeacon, the distance between them can be derived using Equation (8.4). Then, the observation model can be formulated as

$$z_{k+1} = \|\mathbf{S}_{k+1} - \mathbf{S}^i\| + v \tag{8.6}$$

where z_{k+1} is the estimated distance between the device and the iBeacon, $\mathbf{S}^i$ is the location of i-th iBeacon, $\|\cdot\|$ is the Euclidean norm, and v follows a normal distribution with zero mean and variance G. Since the observation function is nonlinear, traditional Kalman filter cannot be applied. Particle filter is a good candidate, but due to its high computational load, it is not suitable for a resource limited smartphone platform. In this work, we leverage on the extended Kalman

filter which is much more computational efficient than a particle filter. Since the observation function (Equation (8.6)) is nonlinear, we need to calculate its Jacobian matrix. Assume that, $\|\mathbf{S}_{k+1} - \mathbf{S}^i\| = f(\mathbf{S}_{k+1} - \mathbf{S}^i)$, $\mathbf{S}_{k+1} = \begin{bmatrix} x_{k+1} & y_{k+1} \end{bmatrix}$ and $\mathbf{S}^i = \begin{bmatrix} x^i & y^i \end{bmatrix}$, the Jacobian matrix, $\mathbf{F}$, can computed as

$$\mathbf{F}_{k+1} = \left.\frac{\partial f}{\partial \mathbf{S}}\right|_{\mathbf{S}_{k+1|k}} = \begin{bmatrix} \frac{x_{k+1|k}-x^i}{f(\mathbf{S}_{k+1|k}-\mathbf{S}^i)} & \frac{y_{k+1|k}-y^i}{f(\mathbf{S}_{k+1|k}-\mathbf{S}^i)} \end{bmatrix} \tag{8.7}$$

The extended Kalman filter contains two phases shown below: **Predicting:**

$$\mathbf{S}_{k+1|k} = \mathbf{S}_k + \mathbf{u}_k \tag{8.8}$$

$$\mathbf{P}_{k+1|k} = \mathbf{P}_k + \mathbf{R} \tag{8.9}$$

$$\tag{8.10}$$

Updating:

$$\mathbf{K}_{k+1} = \mathbf{P}_{k+1|k}\mathbf{F}_{k+1}^T(\mathbf{F}_{k+1}\mathbf{P}_{k+1|k}\mathbf{F}_{k+1}^T + G)^{-1} \tag{8.11}$$

$$\mathbf{S}_{k+1} = \mathbf{S}_{k+1|k} + \mathbf{K}_{k+1}(z_{k+1} - f(\mathbf{S}_{k+1|k} - \mathbf{S}^i)) \tag{8.12}$$

$$\mathbf{P}_{k+1} = (\mathbf{I} - \mathbf{K}_{k+1}\mathbf{F}_{k+1})\mathbf{P}_{k+1|k} \tag{8.13}$$

where $\mathbf{P}$ is the estimate covariance, $\mathbf{K}$ is the Kalman gain, and $\mathbf{I}$ is the identity matrix.

In most of the cases, iBeacons are attached on walls. Thus, the iBeacon signals at the other side of the wall will be expected to be very weak. Once the estimated distance between the iBeacon and the device is in the calibration range (equal to or less than $3m$), we can ensure that the pedestrian is on the side where the iBeacon is attached. We can add this simple constraint into the fusion algorithm. If the output position of the fusion algorithm is at an invalid side of an iBeacon, we can mirror the position to the valid side. This is similar to the operation that kills the particles crossing a wall in the particle filter [113].

8.1.4 Initial Position Estimation

It is not practical to assume that the initial position is known [73, 86]. Various initial position estimation methods have been proposed. Errington et al. [114] presented a least-squares solution for initial position estimation using RFID. Their system requires extra devices, i.e. RFID receivers and readers. Woodman et al. [115] presented a WiFi-based initial position estimation for inertial pedestrian tracking. The WiFi RSS provided a prior knowledge of particle weights in a particle filter algorithm. This will increase the convergence rate of their map matching approach. Due to the sparse deployment of existing WiFi infrastructures in indoor environments, the accuracy of WiFi based approach is limited. In this work, we present an initial position estimation scheme using existing WiFi routers and iBeacons. One possible approach is fingerprinting which constructs a fingerprint database, and then performs localization according to the database. This approach requires a labor-intensive data collection process. When a new WiFi router or an iBeacon is added, or some facilities are changed, fingerprinting approach needs to re-collect the whole data. A more efficient and practical solution is the model-based weighted pass loss (WPL) algorithm. Since the mechanisms of WiFi and iBeacon are different, the RSSs of WiFi and iBeacon are not comparable. To solve this heterogeneous problem, we transfer the RSSs into distances using Equation (8.4) with different parameters for WiFi and iBeacon. Then, a WPL algorithm can be employed using the distances. The details are elaborated as follows: Based on Equation (8.4), the distance between a device and i-th iBeacon at time step k, d_k^i, can be calculated. The distance between the device and j-th WiFi routers at time step k, D_k^j, can be computed using the same equation of iBeacons with different parameters, i.e. R^0 and γ. Assume that we have N sensible iBeacons and M sensible WiFi routers, and the locations of i-th iBeacon, (a^i, b^i), and j-th WiFi routers, (A^j, B^j) are known. The weights of i-th iBeacon, w^i, and j-th WiFi router, W^j, can be expressed as

$$w_k^i = \frac{\frac{1}{d_k^i}}{\sum_{i=1}^{N} \frac{1}{d_k^i} + \sum_{j=1}^{M} \frac{1}{D_k^j}} \tag{8.14}$$

$$W_k^j = \frac{\frac{1}{D_k^j}}{\sum_{i=1}^{N} \frac{1}{d_k^i} + \sum_{j=1}^{M} \frac{1}{D_k^j}} \tag{8.15}$$

Then, the location of the device, (a_k, b_k) can be calculated as

$$(a_k, b_k) = \sum_{i=1}^{N} w_k^i (a^i, b^i) + \sum_{j=1}^{M} W_k^j (A^j, B^j) \tag{8.16}$$

Considering that our system is running on a resource limited smartphone platform, the WPL algorithm is simpler and more efficient compared with the fingerprinting approach. Since existing WiFi infrastructures and installed iBeacons are sparsely distributed, an approach that is only based on WiFi or iBeacons may not resolve the localization problem or will have low accuracy. Our proposed scheme leverages on all resources in the environment including WiFi routers and iBeacons. To solve the heterogeneous problem of the different facilities, i.e. WiFi routers and iBeacons, we transfer the RSSs into distances, and then perform a WPL algorithm to determine the location of the device.

8.2 Evaluation

In this section, we will first introduce the experimental setup. Then, the experimental results and discussions under two different environments will be presented.

8.2.1 Experimental Setup

Real experiments have been conducted to evaluate the performance of the proposed approach. The device used in the experiments is a Google Nexus 5 smartphone. And four Estimote iBeacons [111] are employed in the experiments. Moreover, an Android app has been developed for real-time localization and tracking. The user interface is shown in Figure 8.3 where the circle represents the location of the user, and the arrow inside the circle indicates the pointing direction of the smartphone. The coordinate of the user is shown in the top right corner. Note that we define the coordinate origin as the top left corner, the x-axis pointing to the right, and the y-axis pointing downwards. The experiments have been carried out under two environments, i.e. a research lab and an empty hall in the campus of Nanyang Technological University. The layouts are shown in Figure 8.4 where the yellow stars represent the locations of iBeacons. In order to obtain the ground truth

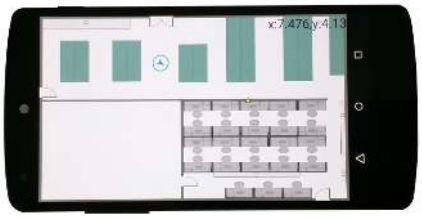

FIGURE 8.3: User interface.

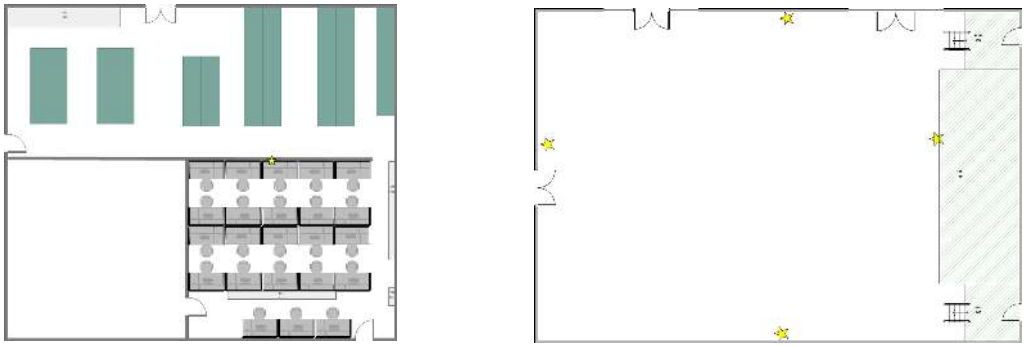

(a) A research lab (b) An empty hall

FIGURE 8.4: The Layouts of the experimental environments.

trajectory of a pedestrian, we use a camera to record the entire walking process and manually measure each step. In the experiments, we only consider handheld situation. This position is reasonable because a user should frequently check the current location on the screen of a smartphone in real-time navigation. Note that, in this situation, the walking direction of the user will almost be aligned with the pointing direction of the smartphone.

8.2.2 Experimental Results

The first scenario is a $19.0m \times 16.2m$ research lab (See Figure 8.4(a)). Due to the limited size of the environment, only one iBeacon is employed. Multiple experiments have been conducted in this scenario, and the average results are shown. Figure 8.5 shows the walking direction estimation using magnetometer, gyroscope and the fusion algorithm. Note that we leverage on the mean of direction values during each step as the final walking direction. In this way, the random noise effect is reduced. Due to the effects of electronic facilities, e.g. computers, printers and

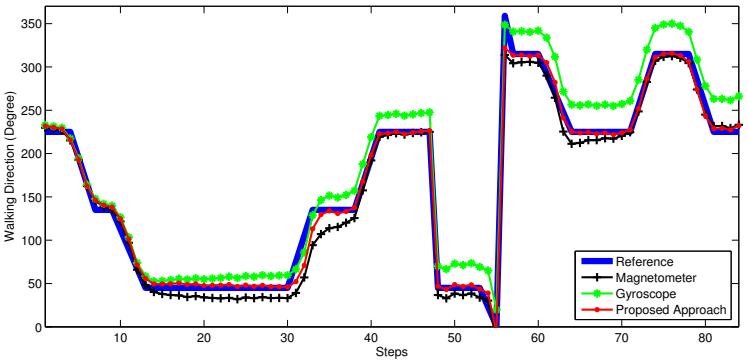

FIGURE 8.5: Walking direction estimation based on magnetometer, gyroscope and our proposed fusion approach.

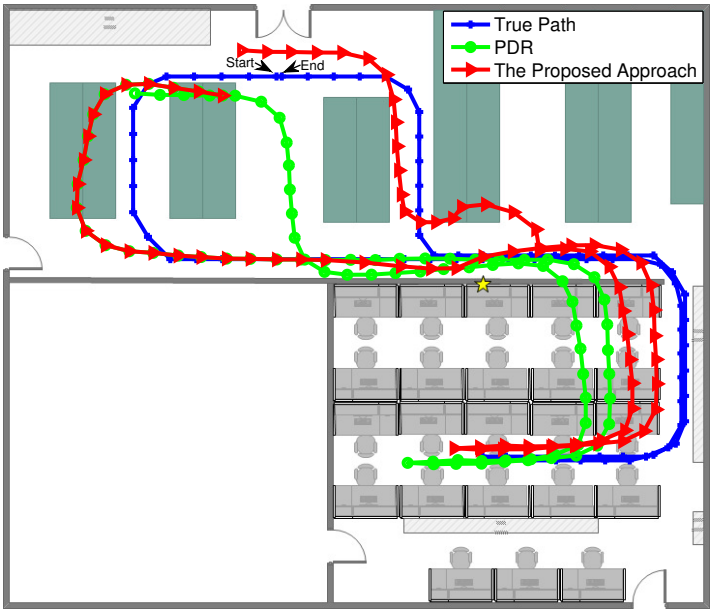

FIGURE 8.6: The trajectories of the true path, the PDR approach and the proposed approach.

the metal frameworks of cubicles, the magnetometer values are distorted. Moreover, vibrations during walking will also affect the measurements. The gyroscope based approach matches very well at the beginning, but it drifts after several turns. The fusion algorithm matches the ground truth reference direction very well. It is much more stable comparing to magnetometer based approach and avoids the drift problem in the gyroscope based approach. We can conclude that the fusion algorithm has the highest estimation accuracy and resolves the problems of individual sensors.

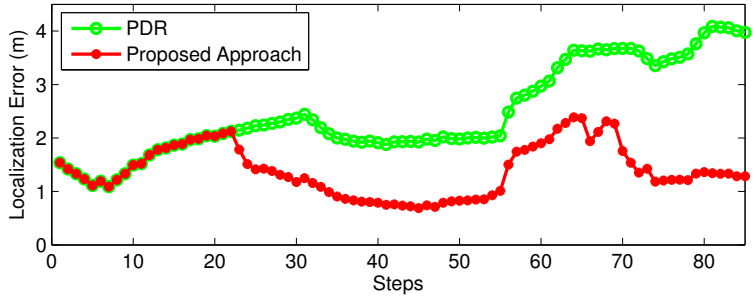

FIGURE 8.7: Localization error with respect to each step.

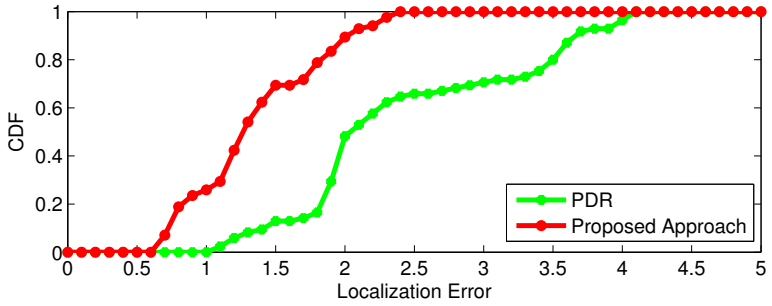

FIGURE 8.8: Cumulative error distributions of the PDR approach and our proposed approach.

Figure 8.6 illustrates the trajectories of the true path, the PDR approach and the proposed approach. Each step is shown in the figure where the start and end points are indicated. Based on WiFi measurements of existing routers and the measurement of the iBeacon, the initial location is estimated using the WPL approach mentioned in Section 8.1.4. According to the true trajectory, we can infer that the system will be calibrated twice when the estimated distance between the pedestrian and the iBeacon is equal or less than $3m$.

Figure 8.7 depicts the localization error with respect to each step. Generally, the localization errors of the PDR based approaches will increase with walking distance because of the estimation errors of step detection, walking length estimation and walking direction estimation. However, our proposed approach corrects the drift using occasional iBeacon measurements, which is shown as two significant reductions of localization errors in the figure. The cumulative error distribution of the results is shown in Figure 8.8. The mean localization accuracies of the PDR approach and the proposed approach are $2.46m$ and $1.39m$, respectively. This indicates the effectiveness of the proposed algorithm.

Another scenario is a $25.0m \times 17.0m$ empty hall environment whose layout is shown

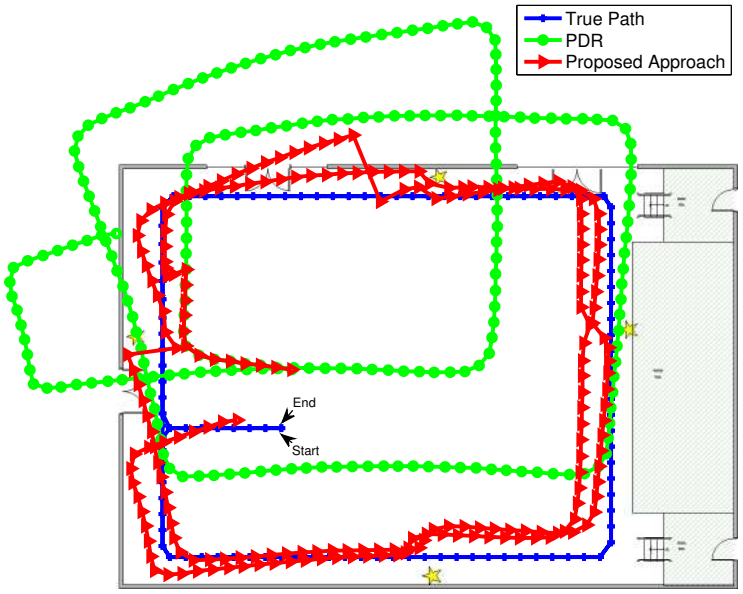

FIGURE 8.9: The trajectories of the true path, the PDR approach and the proposed approach with 4 iBeacons.

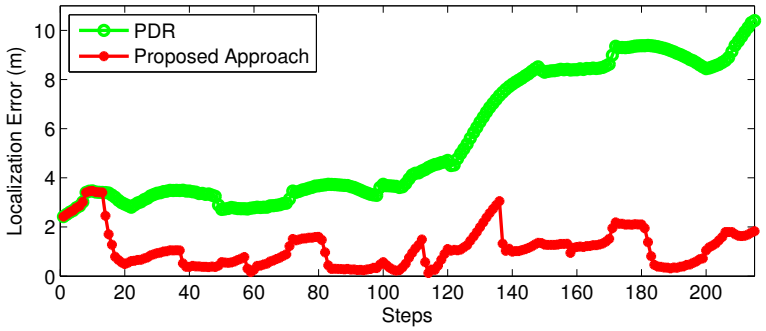

FIGURE 8.10: Localization error with respect to each step.

in Figure 8.4(b). The iBeacon in the right-hand side is attached on a tripod, therefore, this iBeacon cannot use the constraint mentioned in Section 8.1.3. And the others are attached on walls, which satisfies the required condition of applying the constraint. In the experiments, a pedestrian walks around the layout twice, producing a shape of two rectangles. Figure 8.9 depicts the trajectories of the true path, the PDR approach and the proposed approach. Starting and ending points are shown in the figure. Since no WiFi routers are contained in the environment, we only apply iBeacon measurements to determine the initial location using the WPL approach mentioned in Section 8.1.4. It can be found that the proposed

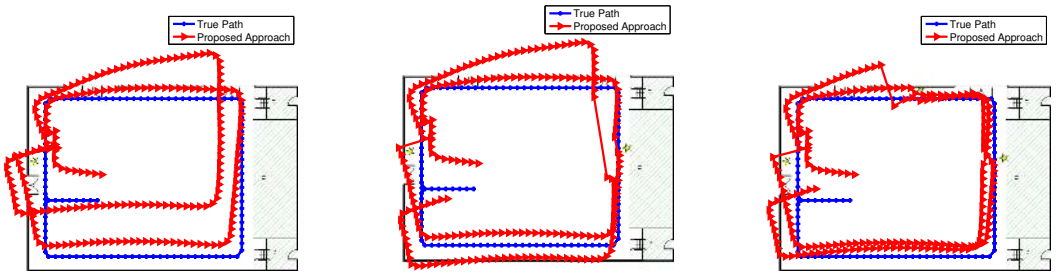

(a) The proposed approach with 1 iBeacon

(b) The proposed approach with 2 iBeacons

(c) The proposed approach with 3 iBeacons

FIGURE 8.11: The trajectories of the proposed approach with different number of iBeacons.

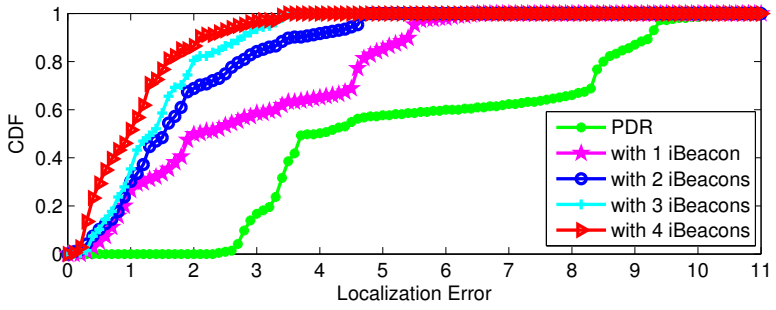

FIGURE 8.12: Cumulative error distributions of the PDR approach and our proposed approach with different number of iBeacons.

approach significantly reduces the drift when walking through iBeacons. The calibration will be performed when the estimated distance between the user and an iBeacon is equal or less than $3m$. Figure 8.10 illustrates the localization error with respect to each step. The PDR approach slowly drifts to more than $10m$ after 200 steps. Owing to the correction of iBeacons, the proposed algorithm achieves a high localization accuracy. The mean localization accuracies of the PDR approach and our proposed approach are $5.55m$ and $1.28m$, respectively. This result indicates that our proposed approach can be utilized for localized cooling or heating, location based lighting control, emergency evacuations and personalized services.

Next, we evaluate the number of iBeacons with respect to the localization accuracy. Figure 8.11 shows the trajectories of the proposed approach with different number of iBeacons, i.e. one to three iBeacons. The trajectories of the PDR approach and our proposed approach with four iBeacons are depicted in Figure 8.9. Figure 8.12 illustrates the cumulative error distribution of the PDR approach and the proposed approach with different number of iBeacons. As expected, the accuracy of the

proposed approach degrades with fewer iBeacons. But, even with one iBeacon, the proposed approach has yielded significant improvement over the PDR approach for the localization accuracy. When the number of iBeacons is larger than two, only slight improvements of localization accuracy is observed. Thus, if taking device (iBeacon) and deployment cost into consideration, the proposed approach with two iBeacons can achieve a reasonable accuracy in this environment. In conclusion, the localization error of the proposed approach will decrease with the increase of the number of iBeacons. And, we can roughly determine an optimal number of iBeacons when given a required localization accuracy.

8.2.3 Compared with WiFi fingerprinting

WiFi fingerprinting is the most popular technique for indoor localization and tracking. Thus, we compare our proposed approach with WiFi fingerprinting based approaches on three criteria, i.e. localization accuracy, calibration time and power consumption. The WiFi fingerprinting approach was performed in our first testing scenario (See Figure 8.4(a)). Five WiFi Access Points (APs) were used, and 40 reference points were selected for data collection. At each reference point, we collected 3000 samples in four different orientations. The APs that we used are TP-LINE WDR4300.

Localization accuracy: Each algorithm has been run for 5 times and the average results are shown. With the above experimental setting, the WiFi fingerprinting approach can achieve a mean localization accuracy of $2.2m$. Many researches have demonstrated the effectiveness of the fusion of WiFi based approaches with smartphone inertial sensors [116, 117]. Therefore, we attempted to fuse WiFi fingerprinting approach with PDR using a Particle filter which is the most popular algorithm in localization and tracking [116, 118]. One thousand particles were used in the experiment. The final mean localization accuracy of this fusion approach is $1.54m$. For our proposed approach, we only employed one iBeacon device and we achieved a mean localization accuracy of $1.39m$.

Calibration time: In the experiments, we set the sampling frequency of WiFi scanning and iBeacon scanning to be $1Hz$. The WiFi fingerprinting approach requires a collection of 40×3000 data samples (40 reference points and 3000 samples for each reference point), which requires approximately 33.3 hours. While our

proposed approach only needs to calibrate R^0 and γ in Equation (8.3) referring to 12×500 data samples (12 reference points and 500 samples for each reference point), which requires some 1.7 hours. In this regard, our proposed approach requires much less calibration time.

Power consumption: Since the whole system will be running on a portable smartphone, power consumption will be crucial. We developed a simple Android application to test the power consumption of WiFi scanning and iBeacon scanning. A Google Nexus 5 smartphone with a battery capacity of $2300mAh$ was used. The scanning frequency of WiFi and iBeacon is $1Hz$. First, we ran the application without scanning WiFi or iBeacon as the basic battery usage for 1 hour, and then, we performed WiFi scanning and iBeacon scanning separately for 1 hour. Finally, the basic battery usage was subtracted for the calculations of the power consumption of WiFi scanning and iBeacon scanning respectively. In the experiment, WiFi scanning for 1 hour consumes $115mAh$, while iBeacon scanning for 1 hour only consumes $46mAh$, which translates to a battery power saving of around 60%.

8.3 Summary

In this chapter, Considering the situations where WiFi signals are not available, or the application is sensitive to power consumption making WiFi based solutions not suitable because of the power hungry property of WiFi scanning, we then presented another indoor localization system using smartphone sensors with occasional iBeacon corrections. Based on the analysis of iBeacon measurements, we defined an efficient calibration range where the extended Kalman filter is formulated. We also proposed a hybrid initial point estimation approach based on existing RSS measurements in environments. Experiments have been performed under two different environments to evaluate the performance of the proposed approach. The results showed the effectiveness of the proposed approach. We also tested the influence of different number of iBeacons, and concluded that our proposed approach demonstrated a significant improvement of system performance even with just one iBeacon in the environment. Finally, we compared our proposed approach with the popular WiFi fingerprinting approach and the fusion of WiFi fingerprinting with smartphone sensors approach. Our proposed approach can achieve a higher localization accuracy with less calibration time and power consumption.

Chapter 9

Orientation Independent Activity Recognition via Coordinate Transformation and Principal Component Analysis

The activity performed by the user is another detailed aspect of occupant sensing. We present an orientation independent activity recognition system based on coordinate transformation and principle component analysis. In Section 9.1, we analyze the problems in activity recognition and resolve them using coordinate transformation and principle component analysis methods. Then, we extract relevant features based on the processed data and classify the activities. In Section 9.2, we describe the data collection process and show the experimental setups. After that, we present the experimental results and discussion in experiments on aspects of orientation, displacement and subject variations.

9.1 Methodology

In previous works, most of researchers assumed that the orientation of the device is fixed. However, it is not usually the case in real life. The basic idea of this study attempts to combine some other sensor information and signal processing techniques to eliminate the effect of orientation variation.

9.1.1 Data Preprocessing

The raw acceleration data of a smartphone is a combination of device linear acceleration and gravity. Human activity will impact the dynamic part of the acceleration, i.e. the device's linear acceleration. Therefore, the gravity effect from the raw acceleration has to be eliminated. Since the gravity effect is relatively stable, we intend to utilize a digital low pass filter to obtain the gravity component, and then apply the raw acceleration to subtract the gravity component to obtain the required linear acceleration. Assume that the three dimensional raw acceleration is denoted as $\mathbf{O}_t$, and the gravity component is denoted as $\mathbf{G}_t$. Then, the linear acceleration, $\mathbf{L}_t$, at time step t can be calculated as

$$\mathbf{G}_t = \alpha \mathbf{G}_{t-1} + (1-\alpha)\mathbf{O}_t \tag{9.1}$$

$$\mathbf{L}_t = \mathbf{O}_t - \mathbf{G}_t \tag{9.2}$$

where the parameter, α, needs to be specified. Practical values of α lay between 0.8 and 1.

For wearable-device based activity recognition systems, the orientation of the device is fixed. This condition is not feasible for smartphone based activity recognition systems. The orientation of smartphones will be different for different users because of clothing, and will be changing during the whole recognition process because of slip and rotation. Since the sensor output is along with the device coordinate system which is shown in Figure 9.1(a), it will change along with the changing coordinate system, which will dramatically degrade the accuracy of our activity recognition system. How to obtain a consistent sensor output regardless of smartphone orientation is a big challenge. One way to achieve that is to transfer the sensor output from the device coordinate system into a fixed coordinate system. A potential fixed coordinate system is the earth coordinate system which is shown in Figure 9.1(b).

The two most widely used coordinate transformation methods are based on Euler angle and quaternion. However, Euler angle based approaches will suffer from the problem of *gimbal lock* [119]. We employ a quaternion, which is more efficient and does not have such problem, for the coordinate transformation. It is a four-element vector that can represent any rotation in a $3D$ coordinate system [119]. According to Google API [1], a software sensor, named Rotation Vector Sensor, can provide

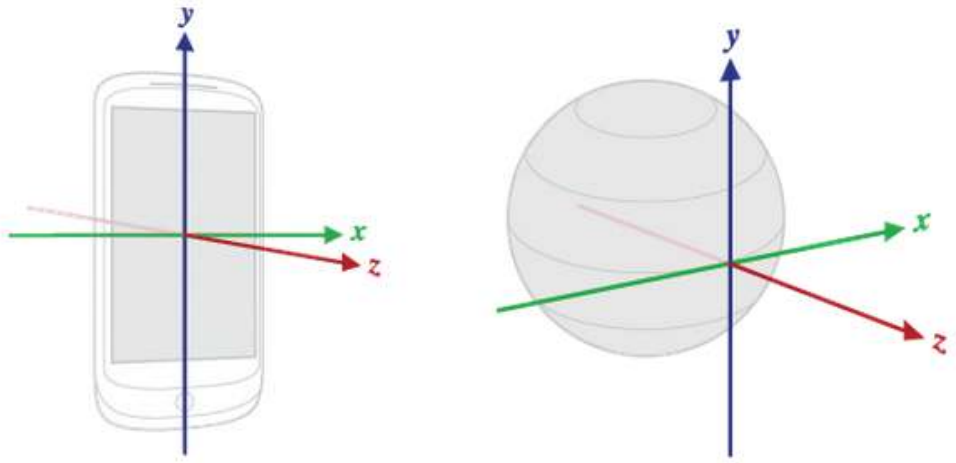

(a) Device coordinate system (b) Earth coordinate system

FIGURE 9.1: Coordinate systems [1]

real-time four elements of a quaternion. The quaternion, $\mathbf{q}$, can be expressed as

$$\mathbf{q} = \begin{pmatrix} a \\ b \\ c \\ d \end{pmatrix} = \begin{pmatrix} \cos(\theta/2) \\ v_x \sin(\theta/2) \\ v_y \sin(\theta/2) \\ v_z \sin(\theta/2) \end{pmatrix} \tag{9.3}$$

where v_x, v_y and v_z are unit rotation of three axes, and θ is the angle of rotation. Based on [119], a rotation matrix, $\mathbf{R}$, can be calculated as follows:

$$\mathbf{R} = \begin{pmatrix} 1-2c^2-2d^2 & 2bc-2ad & 2bd+2ac \\ 2bc+2ad & 1-2b^2-2d^2 & 2cd-2ad \\ 2bd-2ac & 2cd+2ad & 1-2b^2-2c^2 \end{pmatrix} \tag{9.4}$$

Then, the output in the earth coordinate system can be calculated as

$$\mathbf{V}_e = \mathbf{R}\mathbf{V}_d \tag{9.5}$$

where $\mathbf{V}_e$ is the output vector in the earth coordinate system, and $\mathbf{V}_d$ is the acceleration vector in the device coordinate system.

Figure 9.2 shows a comparison of acceleration patterns before and after coordinate transformation when a subject performs the activity of walking and the device is put in the backpack with three difference orientations (shown in Figure 9.3). Since

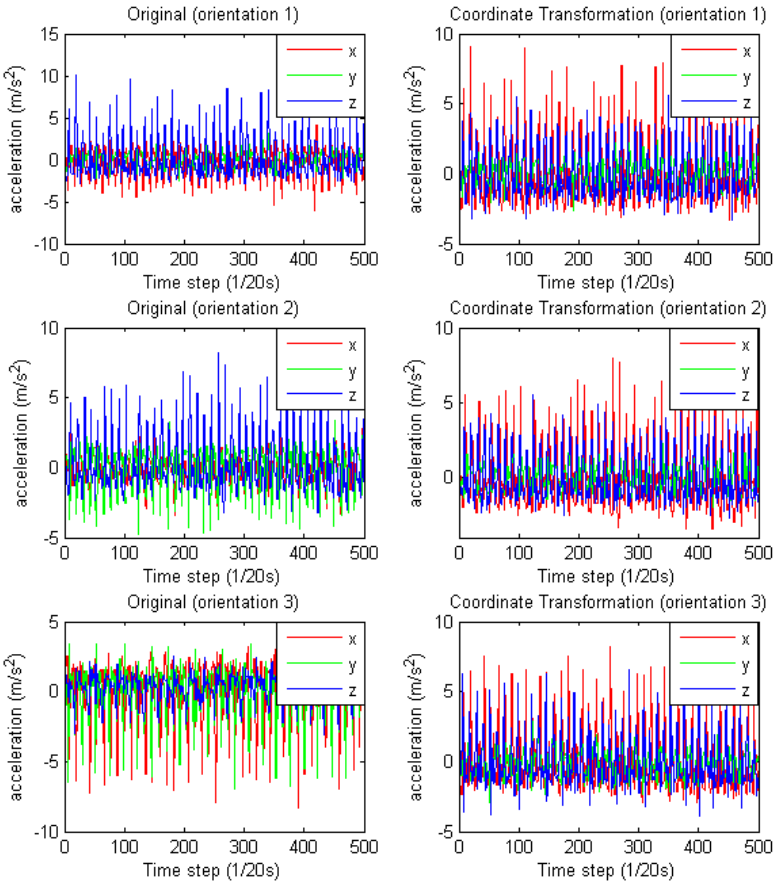

FIGURE 9.2: Before and after coordinate transformation. The performed activity is walking and the placement is the backpack with three different orientations (shown in Figure 9.3)

the orientation of the device has changed, the acceleration patterns are totally different for the raw data. However, after performing coordinate transformation, the patterns of triaxial acceleration are similar for three different orientations. Note that the subject walks to the same direction in this example, therefore, the acceleration in x-axis and y-axis are similar for the three different orientations after coordinate transformation. The reason why we emphasize this will be introduced in the following paragraph.

Other researchers have applied different approaches to achieve coordinate transformation [94, 95, 120, 121]. But, to the best of our knowledge, no one realized that one serious problem will arise after this coordinate transformation. As the earth coordinate system is fixed, precisely, x-axis which is tangential to the ground points to the East, y-axis which is tangential to the ground points to the North, and z-axis

(a) orientation 1 (O1) (b) orientation 2 (O2) (c) orientation 3 (O3)

FIGURE 9.3: Three different orientations in the backpack

which is perpendicular to the ground points to the sky [1], one subject performs certain activity in different directions will yield different acceleration patterns after coordinate transformation. The left portion of Figure 9.4 presents an example. The performed activity is walking and the walking directions are East, Northeast and North. We can find that the pattern of acceleration at x-axis and y-axis are totally different because of different walking directions. To eliminate this direction effect, we can project the acceleration from x-axis and y-axis into orthogonal bases. We leverage on a Principal Component Analysis (PCA) technique to achieve this objective.

Assume that $\mathbf{a}_x = \begin{pmatrix} a_x^1 & a_x^2 & \cdots & a_x^N \end{pmatrix}^T$ and $\mathbf{a}_y = \begin{pmatrix} a_y^1 & a_y^2 & \cdots & a_y^N \end{pmatrix}^T$ denote accelerations in x-axis and y-axis of an acceleration window and N is the window size. Combining the data from x-axis and y-axis in an acceleration window, we obtain matrix, $\mathbf{A}$, as follows

$$\mathbf{A} = \begin{pmatrix} a_x^1 & a_y^1 \\ a_x^2 & a_y^2 \\ \vdots & \vdots \\ a_x^N & a_y^N \end{pmatrix} \tag{9.6}$$

After that, we can calculate the corresponding covariance matrix, $\mathbf{\Omega}$, as

$$\mathbf{\Omega} = \frac{1}{N}(\mathbf{A} - \mathbb{E}(\mathbf{A}))(\mathbf{A} - \mathbb{E}(\mathbf{A}))^T \tag{9.7}$$

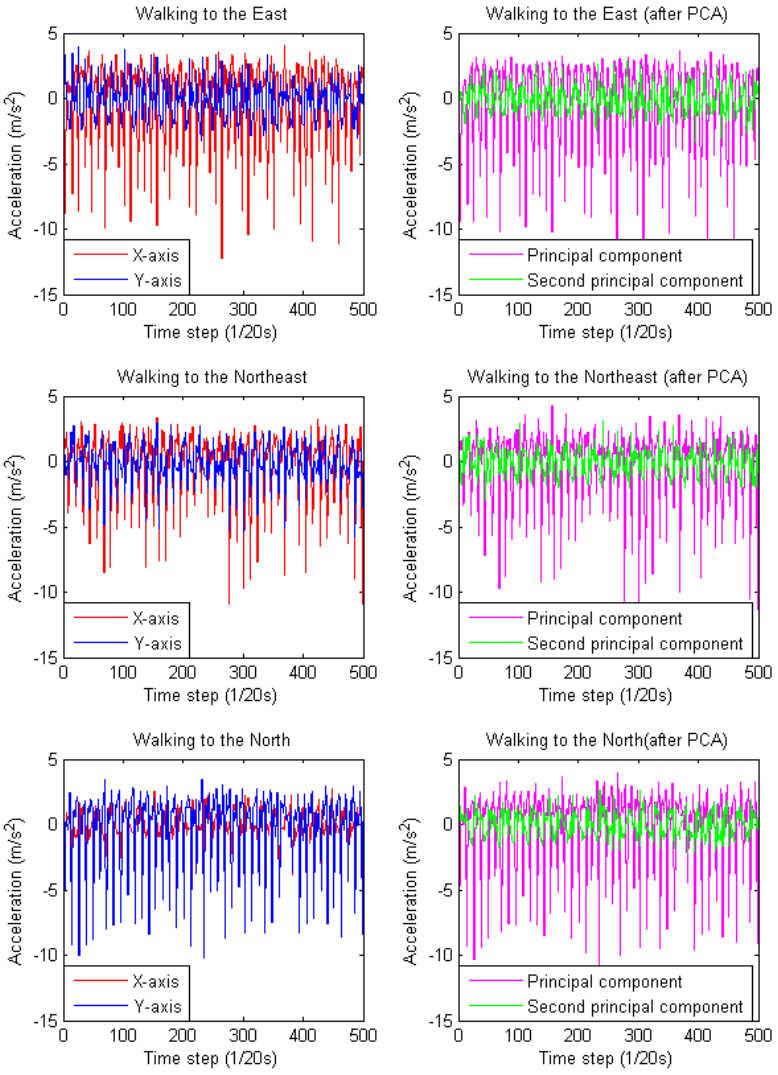

FIGURE 9.4: Before and after PCA analysis. The performed activity is walking and the position is the backpack with three different directions which are East, Northeast and North.

where $\mathbb{E}(\cdot)$ is the expectation operation for each column of a matrix. Since $\mathbf{\Omega}$ is a symmetric matrix, it can be diagonalised as

$$\mathbf{\Omega} = \mathbf{Q}\mathbf{\Lambda}\mathbf{Q}^{\mathbf{T}} \tag{9.8}$$

where $\mathbf{Q}$ and $\mathbf{\Lambda}$ are eigenvector and eigenvalue matrices of $\mathbf{\Omega}$, respectively. Then, we rank the eigenvalues in descending order and reconstruct the egienvector matrix corresponding to their eigenvalues to obtain a new matrix $\tilde{\mathbf{Q}}$. The PCA transformation matrix can be expressed as

$$\mathbf{P} = \tilde{\mathbf{Q}}^{T} \tag{9.9}$$

The final PCA transformation result can be calculated as

$$\mathbf{G} = \mathbf{P}\mathbf{A}^{T} \tag{9.10}$$

where the first and second row of matrix $\mathbf{G}$ are the first and second principal components.

Once the PCA operation is completed, the direction effect can be eliminated by using the first and second principal components instead of the accelerations of x-axis and y-axis in the earth coordinate system. Figure 9.4 shows an example of the acceleration patterns before and after PCA analysis. After the PCA operation, the acceleration patterns become consistent for the same activity.

9.1.2 Feature Extraction

The $3D$ acceleration time series data after preprocessing is divided into windows. Then, time and frequency domain features are extracted from these data windows. Table 9.1 indicates the features applied in this work. Many researches have shown the effectiveness of these features [122–124].

9.1.3 Classification

Classifiers in [93, 125] based on deep neural network have been shown to have superior performance. But these approaches require a large dataset for training,

Domain	Features
Time	Absolute mean Variance Median absolute deviation Maximum Minimum Signal magnitude range Power Interquantile range
Frequency	Maximum Mean Skewness Kurtosis Power

TABLE 9.1: Selected features

which may not be feasible in real life. Some generic classifiers, i.e. KNN [126], DT [127], NN [128] and SVM [92], have been shown to be effective for human activity recognition with a reasonable size of the data.

9.2 Experimental Results and Discussions

9.2.1 Data Description

Three-dimensional acceleration data is collected from an Android application of a Google NEXUS 4 smartphone. Five subjects are involved in experiments with five activities of static, walking, running, going upstairs and going downstairs. The sampling frequency is $20Hz$, and the sliding window is 5 seconds with 50% overlap. Therefore, each segment contains 100 data points for three-dimension. Time and frequency domain features described in Table 9.1 are extracted for each segment.

9.2.2 Experimental Setup

Smartphone placements can be flexible for different subjects. In this work, we investigate three most commonly used placements of pants' pocket, shirt's pocket and backpack. Due to the size constraints for pants' pocket and shirt's pocket,

one orientation is chosen for each placement. In the placement of backpack, the orientation can be much more flexible. Thus, we choose three typical orientations shown in Figure 9.3 to investigate the orientation effect. To validate our proposed CT-PCA scheme, we apply leave-one-out cross validation technique. Precisely, we employ leave one orientation out cross validation in the placement of backpack. In this way, the data for testing is from an unseen orientation, which can validate the generalization performance of the algorithms. Meanwhile, we compare our proposed approach with two state-of-the-art methods in [92, 93]. In [92], the authors applied the magnitude to form augmented features to overcome orientation variations. And in [93], the authors leveraged on vertical component and the magnitude of horizontal components of transferred acceleration to eliminate orientation variations. Note that, the authors in [92, 93] did not perform leave one orientation out experiments. Instead, they mixed the data from all orientations for training and testing, which guarantees the high detection accuracies in their works. But this cannot verify the generalization performance of their approaches, because they did not show the performance of their approaches on the data from unseen orientations. Moreover, we also investigate the subject effect and placement effect by using leave one subject out and leave one location out experiments.

9.2.3 Orientation Independent Experiments

In the orientation-independent experiments, we applied the data collected from three different orientations in the backpack (see Figure 9.3) and employed the cross-validation technique. In details, we used the data from two orientations for training and the data from the remaining one unseen orientation for testing. Previously mentioned four generic classifiers, i.e. KNN, DT, NN, SVM, are employed to identify different activities. We also compared our proposed CT-PCA scheme with original, augmented [92] and bi-directional [93] methods.

TABLE 9.2 demonstrates the detection results of the four different methods. Our proposed CT-PCA method outperforms the other methods for the four generic classifiers on average results. The approach based on original signals performs the worst, which did not consider the varying orientation effects. Another approach using the magnitude to form augmented features [92] has limited improvements,

TABLE 9.2: Accuracy comparison for orientation-independent experiments with original, augmented, bi-directional and proposed methods in the placement of backpack (%). "O1+O2 → O3" means the use of the data from orientation 1 and 2 for training and the data from orientation 3 for testing.

Orientation	Methods	KNN	DT	NN	SVM
O1+O2 → O3	Original	71.48	65.09	67.43	71.33
	Augmented	74.10	71.61	68.69	74.67
	Bi-directional	90.51	89.45	90.61	91.33
	Proposed	90.52	91.04	91.74	93.56
O1+O3 → O2	Original	80.14	68.29	78.50	79.11
	Augmented	81.38	75.71	79.02	84.00
	Bi-directional	90.05	90.43	95.31	94.89
	Proposed	91.61	93.75	96.07	94.89
O2+O3 → O1	Original	62.69	43.40	41.09	58.44
	Augmented	64.59	43.65	41.27	56.22
	Bi-directional	90.98	88.18	95.47	95.56
	Proposed	92.40	93.12	96.09	96.22
Average	Original	71.44	58.92	62.34	69.63
	Augmented	73.36	63.66	62.99	71.63
	Bi-directional	90.67	89.36	93.80	93.93
	Proposed	**91.51**	**92.64**	**94.63**	**94.89**

because the unique properties on the three axes are merged when using the magnitude. The bi-directional approach separates the signal into vertical component and the magnitude of horizontal components [93], which did not take the properties of the signals on the orthogonal direction of the performed activity. For example, going upstairs or downstairs will have larger variance of signals on orthogonal directions of the performed activity than normal walking, because two feet always lay on different stairs during going upstairs or downstairs, which shall cause additional movements on the two sides. Note that the authors in [92, 93] did not perform leave one orientation out experiments to show the generalization ability of their algorithms. Our proposed method considers all the useful information on three directions, i.e. vertical direction, the direction of the performed activity on horizontal plane and its orthogonal direction. Thus, it has a superior performance over the other methods. Among the four different classification algorithms, the SVM algorithm with our proposed CT-PCA scheme performs the best, and has an average accuracy of 94.89%. This indicates the good generalization performance of our proposed approach on the data from unseen orientations.

Placement	Methods	KNN	DT	NN	SVM
P1+P2 → P3	Original	70.84	61.12	69.01	71.56
	Proposed	77.72	73.54	77.20	80.89
P1+P3 → P2	Original	61.53	65.10	59.93	65.78
	Proposed	66.16	63.82	70.09	74.00
P2+P3 → P1	Original	58.99	60.02	45.21	66.67
	Proposed	74.61	71.32	86.09	84.67
Average	Original	63.79	62.08	58.05	68.00
	Proposed	**72.83**	**69.56**	**77.79**	**79.85**

TABLE 9.3: Accuracy comparison for placement effect experiments (%). WO denotes the data without CT-PCA, and W denotes the data with CT-PCA.

9.2.4 The Impact of Placement Variations

To evaluate the impact of different placements, we test three common placements, i.e. pants' pocket, shirt's pocket, and backpack. Since we only collect the data of one orientation from pants' pocket and shirt's pocket, we only use the data from one orientation, i.e. O1 (see Figure 9.3(a)), in the placement of backpack to maintain consistency of data size in each placement. Leave one placement out cross validation is employed, which means using the data from one placement as testing dataset and the data from the remaining placements as training dataset. We also evaluate the performance of the proposed CT-PCA with regards to placement variations. Other settings are the same with the previous experiments.

Table 9.3 illustrates the classification accuracy under different conditions. We can find that the classification accuracy is relatively low, because different placements will generate different data characteristics. The classification performance with CT-PCA is only slightly better than that without CT-PCA. One reason is that CT-PCA cannot deal with the inherent signal difference caused by difference in placement. Another reason is that the orientation in each placement is similar which makes the effect of CT-PCA not remarkable. However, due to the slight difference of orientations in each placement, the classification accuracy with CT-PCA still has encouraging improvement.

Subject	Methods	KNN	DT	NN	SVM
Others → S1	Original	50.45	46.16	65.41	61.11
	Proposed	78.78	74.24	87.00	91.48
Others → S2	Original	59.28	53.80	69.88	69.75
	Proposed	79.40	60.93	83.36	84.81
Others → S3	Original	73.03	61.12	75.25	76.54
	Proposed	89.77	92.52	91.99	92.96
Others → S4	Original	87.24	74.53	94.31	92.59
	Proposed	94.55	92.59	97.63	100
Others → S5	Original	68.20	35.30	63.65	68.52
	Proposed	87.39	69.70	83.96	82.96
Average	Original	67.64	54.18	73.70	73.70
	Proposed	**85.78**	**78.00**	**88.79**	**90.44**

TABLE 9.4: Accuracy comparison for subject effect experiments (%). WO denotes the data without CT-PCA, and W denotes the data with CT-PCA.

9.2.5 The Impact of Subject Variations

To evaluate the effect of subject variation, we conduct a leave one subject out cross validation experiment, which means we use the data from any four subjects for training and the data from the remaining one subject for testing. We also test the performance of the proposed CT-PCA in terms of subject variations. Other experimental settings are the same with the previous experiments.

Table 9.4 shows the experiment results under different conditions. Since the behaviour of different subjects when performing different activities is quite different, most of the classification accuracies are not very high in leave one subject out experiments. Leaving S3 or S4 out experiment achieves relatively high classification accuracy. We can infer that their behaviour should be very similar. Therefore, in leaving one subject out experiment, the training data will always contain the data from at least one of them. Another observation is that the average classification accuracy with our proposed CT-PCA is higher than that without CT-PCA. Since the device orientation for different subjects varies slightly because of different clothing, our proposed CT-PCA can eliminate this orientation variations.

9.3 Summary

In this chapter, we proposed an orientation independent activity recognition system by using coordinate transformation and principle component analysis. We first presented a coordinate transformation method based on smartphone sensors to overcome the orientation variation problems in activity recognition. Then, a problem arose after this transformation, which is neglected by other researches. To solve this problem, we came up with a principle component analysis approach. In real experiments, we showed that our proposed approach significantly improves the detection accuracy in terms of orientation variations. Moreover, we also explored the performance of our proposed approach with regard to placement and subject variations and made a conclusion that our proposed approach achieves impressive effectiveness on placement and subject variations.

Chapter 10

Conclusion, Limitations and Future Works

10.1 Conclusion

In this thesis, we have considered the problem of occupant sensing that includes methods for occupant number, location and activity. We addressed the number of occupants (occupancy) in three aspects of modeling, estimation and prediction. For occupancy modeling, we presented two novel inhomogeneous Markov chain models under two scenarios of multi-occupant single-zone (MOSZ) and multi-occupant multi-zone (MOMZ). In the MOSZ scenario, we defined the state of Markov chain as the increment of occupancy in a zone. And in the MOMZ scenario, taking the interactions among occupants into consideration, we defined the state of Markov chain as a vector in which each component is the increment of occupancy in each zone. In this way, we can dramatically simplify the calculation of Markov transition probability matrices. Simulations have been conducted in two different environments for two scenarios of MOSZ and MOMZ. In the MOSZ scenario, we compared with a state-of-the-art approach, i.e. the agent-based model presented by [28]. Our proposed approach is simple to be implemented due to the low dimension of the Markov transition probability matrix at each time step, i.e. 3×3, and significantly outperforms the agent-based model. In the MOMZ scenario, our proposed approach also performed very well for each zone. These results can be used for the simulation of energy saving with various control strategies. In addition, the

occupancy dynamics revealed by the proposed occupancy models is able to improve the performance of real-time occupancy estimation.

For occupancy estimation, we proposed a fusion framework using environmental sensors. Data-driven models that include Extreme Learning Machine (ELM), Support Vector Machine (SVM), Artificial Neural Network (ANN), K-Nearest Neighbors (KNN), Linear Discriminant Analysis (LDA) and Classification And Regression Tree (CART) are employed to achieve an initial estimation of building occupancy. To select the best feature set, we performed an ELM-based wrapper method owing to the extremely fast learning speed of the ELM algorithm. Then, we fused the results of data-driven models with occupancy models which can extract occupancy patterns to improve the estimation accuracy. Experiments have been conducted in an office environment of a university campus. The results showed impressive improvements of estimation accuracy after using our proposed fusion framework. Moreover, two important parameters of time of first arrival (TOFA) and time of last departure (TOLD) have been defined for performance evaluation. The proposed fusion framework significantly decreased the detection errors of these two parameters. We also tested the detection accuracy of the presence and absence of the zone with our proposed fusion approach. The improvements of detection accuracy among different methodologies are in the range of $3-12\%$. After performing our fusion framework, the detection accuracy is around 93% with just the environmental sensors. These results are adequate for occupancy driven control. And the high detection accuracy for presence and absence is useful for determining the operation time of HVAC systems.

For occupancy prediction, we explored the prediction of regular occupancy level in commercial buildings using occupancy models and data mining approaches. The occupancy models included an inhomogeneous Markov chain (IMC) model and a multivariate Gaussian (MG) model, and the data mining approaches included three methodologies of Autoregressive Integrated Moving Average (ARIMA), ANN and Support Vector Regression (SVR). The experiments have been conducted using actual occupancy data under four prediction horizons which are 15 minutes ($15mins$), 30 minutes ($30mins$), 1 hour ($1h$) and 2 hours ($2h$). We can found that the prediction capabilities of the occupancy models are very limited as compared to the data mining approaches. In the prediction horizons of $15mins$ and $30mins$, the

linear data mining approach of ARIMA performed the best. In the prediction horizons of $1h$, the nonlinear data mining approach of SVR outperformed the others. And in the prediction horizons of $2h$, the simple diversity profile has a superior performance over the others. These conclusions gave a guideline on how to choose an applicable and efficient occupancy prediction model under different prediction horizons. Based on the short-term prediction results, one can perform pro-cooling or pre-heating strategies to construct a comfortable environment and save energy. Meanwhile, smart planning can be achieved with the long-term prediction results.

For occupant indoor localization, we proposed to fuse WiFi, smartphone sensors and landmarks using the Kalman filter which is light weight and feasible for a resource limited smartphone platform. For WiFi based localization that is used to provide an observation of occupant's position, we applied a weighted pass loss (WPL) algorithm which is simple to be implemented, instead of the labor intensive and time consuming WiFi fingerprinting approach. A pedestrian dead reckoning (PDR) approach was employed for smartphone sensors based localization. Moreover, we applied landmarks with known positions to restart the system. The landmarks can be detected based on the specific patterns of smartphone sensors. Real experiments have been conducted in two different scenarios of a research lab and a designed testbed. The results indicated that our proposed approach achieved significant improvements over the WiFi WPL approach and the PDR approach with landmarks. The overall localization accuracy is around $1m$ which is adequate for the control systems in buildings. Since WiFi scanning is power consuming, WiFi based approaches running on a battery limited smartphone platform may not be suitable for applications which require long term localization and tracking. Moreover, some buildings may have sparse deployments of WiFi Access Points (APs), which may dramatically degrade the performance of WiFi based approaches, and the installation of new WiFi APs are expensive. We proposed an iBeacon assisted indoor localization system using built-in smartphone inertial sensors. Based on the distribution of iBeacon measurements, we have defined a calibration range where the extended Kalman filter is formulated. Moreover, we have presented a weighted pass loss model to determine the initial position using RSS measurements in environments. To evaluate the performance of the proposed approach, real experiments have been conducted under two different environments, i.e. a research lab and an empty hall. With sparse deployment of iBeacons, we can significantly improve the localization accuracy. We have also evaluated the localization performance of the

proposed approach with respect to the number of iBeacons, and concluded that the optimal number of iBeacons can be determined depending on the required localization accuracy. For both WiFi enabled and WiFi denied environments, the indoor localization accuracies of around $1m$ indicate that localized cooling or heating can be performed to save energy. Moreover, other applications, such as lighting control, emergency evacuation and personalized services, can be performed with these results.

For occupant activity recognition, we presented an activity recognition system regardless of device orientation. A coordinate transformation and principal component analysis (CT-PCA) scheme was presented to eliminate the effect of orientation variations. Experimental results showed the effectiveness of the proposed approach in handling orientation variations for activity recognition. We also evaluated the influences of placement and subject variations. Our proposed CT-PCA approach also showed some promising improvements of classification accuracy in terms of placement and subject variations. The achieved high activity recognition accuracy regardless of device orientation makes real-time monitoring occupants' activity feasible. Then, real-time human comfort index can be estimated with occupants' activity information. Hence, a comfortable environment for occupants can be built with various control algorithms and strategies.

10.2 Limitations

For occupancy modeling, estimation and prediction, we mainly focus on regular occupancy. However, sometimes irregular occupancy caused by personal vacations, particular events and unpredictable emergencies, is also vital for the stability of the control systems in buildings. Due to the randomness of these irregular situations, the research of irregular occupancy is challenging, which requires further attention. For occupancy estimation, the occupancy pattern is utilized to improve the occupancy estimation accuracy. However, in the long run (say years), the venue may undergo a large change in terms of staff and facilities, thus changing the occupancy dynamics as well. If we still use the previous occupancy pattern, a good performance cannot be expected. One possible way to solve this problem is to use online learning. When the new data is available, we can online update the parameters of the occupancy model.

For indoor localization, we assume that each occupancy will take one smartphone all the time. This is not always true. Sometimes, the occupant may leave the smartphone on their desk, or the occupant may have two or more smartphones. In these cases, additional location estimation methods need to be combined for a better localization. Vision-based approach can be one possible way, but it can only be used in public areas without privacy concern. For activity recognition, the activities discussed in this thesis is limited to occupants' simple daily activities. More complicated activities such as working with a computer, meeting and having coffee are also meaningful. The detection of these complicated activities may require more advance sensors, such as wearable sensors or cameras.

10.3 Future Works

With the occupancy models that we developed, we intend to develop occupancy driven control algorithms to save energy and simulate different deployment scenarios using energy simulation tools such as EnergyPlus, DeST and TRNSYS. After that, we will implement the control algorithms in real deployment with real-time estimation of occupancy. Moreover, with the proposed occupancy prediction models, we can further improve the performance of the control system using occupancy predictions. The gap of energy consumption between simulation tools and real deployment will be analyzed and quantified. This can be useful as a guidance for new constructions which can only be assessed by performing simulations.

In real applications, the buildings mainly contain multiple floors. This is especially so in land scarce Singapore where most buildings have multiple floors. Multi-floor localization will therefore be meaningful. The barometer sensors can be a good candidate in detection of different floors based on the changes of air pressure with height. Detailed exploration is required. With accurate location information of occupants, location based control, e.g. lighting control, can be developed. It will not only be convenient for occupants, but also save energy.

We have already explored the detection of occupant's simple activity. Based on this information, real-time estimation of human comfort index can be achieved. Then, the feedback control of the HVAC system using real-time human comfort index can maximize energy saving while maintaining a desired environment for

occupants. Moreover, more complicated activities, e.g. using different appliances, need to be investigated. The detection of these activities can provide a clear map of energy consumption which is required to be optimized based on certain control strategies.

Author's Publications

Journal Articles

- **Chen, Zhenghua**, Rui Zhao, Qingchang Zhu, Mustafa K. Masood, Yeng Chai Soh and Kezhi Mao, "Building Occupancy Estimation with Environmental Sensors via CDBLSTM," *submitted to IEEE Transactions on Industrial Electronics (under review).*

- **Chen, Zhenghua**, Qingchang Zhu, Yeng Chai Soh and Le Zhang, "Robust Human Activity Recognition Using Smartphone Sensors via CT-PCA and Online SVM," *submitted to IEEE Transactions on Industrial Informatics (under review).*

- Qingchang Zhu, **Chen, Zhenghua** and Yeng Chai Soh, "Energy-related Activity Recognition based on Audio Signals using ELM-LRF," *submitted to IEEE Transactions on Systems, Man and Cybernetics: Systems (under review).*

- **Chen, Zhenghua**, Qingchang Zhu, Mustafa K. Masood and Yeng Chai Soh, "Environmental Sensors based Occupancy Estimation in Buildings via IHMM-MLR," accepted by *IEEE Transactions on Industrial Informatics.*

- Qingchang Zhu, **Chen, Zhenghua**, Mustafa K. Masood and Yeng Chai Soh,"Occupancy estimation with environmental sensing via non-iterative LRF feature learning in time and frequency domains" accepeted by *Energy and Buildings.*

- **Chen, Zhenghua**, Mustafa K. Masood and Yeng Chai Soh, "A fusion framework based occupancy estimation with environmental parameters in office buildings," *Energy and Buildings* 133 (2016): 790-798.

- **Chen, Zhenghua** and Yeng Chai Soh, "Comparing model-based and data-driven approaches for regular occupancy prediction in commercial buildings," *Journal of Building Performance Simulation*, (2016): 1-9.
- **Chen, Zhenghua**, Qingchang Zhu and Yeng Chai Soh, "Smartphone Inertial Sensor Based Indoor Localization and Tracking with iBeacon Corrections," *IEEE Transactions on Industrial Informatics* 12, no. 4 (2016): 1540-1549.
- **Chen, Zhenghua**, Jinming Xu and Yeng Chai Soh, "Modeling regular occupancy in commercial buildings using stochastic models," *Energy and Buildings* 103 (2015): 216-223.
- **Chen, Zhenghua**, Han Zou, Hao Jiang, Qingchang Zhu, Yeng Chai Soh, and Lihua Xie, "Fusion of WiFi, smartphone sensors and landmarks using the Kalman filter for indoor localization," *Sensors* 15, no. 1 (2015): 715-732.

Conference Proceedings

- Qingchang Zhu, **Chen, Zhenghua** and Yeng Chai Soh, "Using unlabeled acoustic data with locality-constrained linear coding for energy-related activity recognition in buildings," In *Automation Science and Engineering (CASE), 2015 IEEE International Conference on*, pp. 174-179. IEEE, 2015.
- **Chen, Zhenghua**, Qingchang Zhu, Hao Jiang, and Yeng Chai Soh, "Indoor localization using smartphone sensors and ibeacons," In *Industrial Electronics and Applications (ICIEA), 2015 IEEE 10th Conference on*, pp. 1723-1728. IEEE, 2015.
- Qingchang Zhu, **Chen, Zhenghua** and Yeng Chai Soh, "Smartphone-based Human Activity Recognition in buildings using Locality-constrained Linear Coding," In *Industrial Electronics and Applications (ICIEA), 2015 IEEE 10th Conference on*, pp. 214-219. IEEE, 2015.
- **Chen, Zhenghua** and Yeng Chai Soh, "Modeling building occupancy using a novel inhomogeneous Markov chain approach," In *Automation Science and Engineering (CASE), 2014 IEEE International Conference on*, pp. 1079-1084. IEEE, 2014.

Bibliography

[1] Sensor manager tutorial, 2015. `http://developer.android.com`.

[2] Liu Yang, Haiyan Yan, and Joseph C Lam. Thermal comfort and building energy consumption implications–a review. *Applied Energy*, 115:164–173, 2014.

[3] UNEP Sbci. Buildings and climate change: a summary for decision-makers. *United Nations Environmental Programme, Sustainable Buildings and Climate Initiative, Paris*, pages 1–62, 2009.

[4] Drury B Crawley, Linda K Lawrie, Frederick C Winkelmann, Walter F Buhl, Y Joe Huang, Curtis O Pedersen, Richard K Strand, Richard J Liesen, Daniel E Fisher, Michael J Witte, et al. Energyplus: creating a new-generation building energy simulation program. *Energy and Buildings*, 33 (4):319–331, 2001.

[5] Da Yan, Jianjun Xia, Waiyin Tang, Fangting Song, Xiaoliang Zhang, and Yi Jiang. Destan integrated building simulation toolkit part i: Fundamentals. In *Building Simulation*, volume 1, pages 95–110. Springer, 2008.

[6] SA Klein, WA Beckman, JW Mitchell, JA Duffie, NA Duffie, TL Freeman, JC Mitchell, JE Braun, BL Evans, JP Kummer, et al. Trnsys 16–a transient system simulation program, user manual. *Solar Energy Laboratory. Madison: University of Wisconsin-Madison*, 2004.

[7] Yuvraj Agarwal, Bharathan Balaji, Rajesh Gupta, Jacob Lyles, Michael Wei, and Thomas Weng. Occupancy-driven energy management for smart building automation. In *Proceedings of the 2nd ACM Workshop on Embedded Sensing Systems for Energy-Efficiency in Building*, pages 1–6. ACM, 2010.

[8] Thananchai Leephakpreeda. Adaptive occupancy-based lighting control via grey prediction. *Building and environment*, 40(7):881–886, 2005.

[9] P Hoes, JLM Hensen, MGLC Loomans, B De Vries, and D Bourgeois. User behavior in whole building simulation. *Energy and Buildings*, 41(3):295–302, 2009.

[10] Jan Širokỳ, Frauke Oldewurtel, Jiří Cigler, and Samuel Prívara. Experimental analysis of model predictive control for an energy efficient building heating system. *Applied Energy*, 88(9):3079–3087, 2011.

[11] Frauke Oldewurtel, Alessandra Parisio, Colin N Jones, Dimitrios Gyalistras, Markus Gwerder, Vanessa Stauch, Beat Lehmann, and Manfred Morari. Use of model predictive control and weather forecasts for energy efficient building climate control. *Energy and Buildings*, 45:15–27, 2012.

[12] Shri Goyal, Herbert A Ingley, and Prabir Barooah. Zone-level control algorithms based on occupancy information for energy efficient buildings. In *American Control Conference (ACC), 2012*, pages 3063–3068. IEEE, 2012.

[13] Jiakang Lu, Tamim Sookoor, Vijay Srinivasan, Ge Gao, Brian Holben, John Stankovic, Eric Field, and Kamin Whitehouse. The smart thermostat: using occupancy sensors to save energy in homes. In *Proceedings of the 8th ACM Conference on Embedded Networked Sensor Systems*, pages 211–224. ACM, 2010.

[14] Yongjun Sun, Shengwei Wang, Fu Xiao, and Gongsheng Huang. A study of pre-cooling impacts on peak demand limiting in commercial buildings. *HVAC&R Research*, 18(6):1098–1111, 2012.

[15] Wilhelm Kleiminger, Friedemann Mattern, and Silvia Santini. Predicting household occupancy for smart heating control: A comparative performance analysis of state-of-the-art approaches. *Energy and Buildings*, 85:493–505, 2014.

[16] Simon SK Kwok and Eric WM Lee. A study of the importance of occupancy to building cooling load in prediction by intelligent approach. *Energy Conversion and Management*, 52(7):2555–2564, 2011.

[17] Robert K Harle and Andy Hopper. The potential for location-aware power management. In *Proceedings of the 10th international conference on Ubiquitous computing*, pages 302–311. ACM, 2008.

[18] Nan Li, Burcin Becerik-Gerber, Lucio Soibelman, and Bhaskar Krishnamachari. Comparative assessment of an indoor localization framework for building emergency response. *Automation in Construction*, 57:42–54, 2015.

[19] Haris Doukas, Konstantinos D Patlitzianas, Konstantinos Iatropoulos, and John Psarras. Intelligent building energy management system using rule sets. *Building and environment*, 42(10):3562–3569, 2007.

[20] KL Ku, JS Liaw, MY Tsai, and TS Liu. Automatic control system for thermal comfort based on predicted mean vote and energy saving. *Automation Science and Engineering, IEEE Transactions on*, 12(1):378–383, 2015.

[21] Danni Wang, Clifford C Federspiel, and Francis Rubinstein. Modeling occupancy in single person offices. *Energy and buildings*, 37(2):121–126, 2005.

[22] Jessen Page, Darren Robinson, Nicolas Morel, and J-L Scartezzini. A generalised stochastic model for the simulation of occupant presence. *Energy and buildings*, 40(2):83–98, 2008.

[23] Gandherva Gunathilak, Aiswarya Prasannakumar, Negin Nazarian, and Homa Naeimi. A generalized event driven framework for building occupancy (wip). In *Proceedings of the Symposium on Simulation for Architecture & Urban Design*, page 26. Society for Computer Simulation International, 2013.

[24] Chuang Wang, Da Yan, and Yi Jiang. A novel approach for building occupancy simulation. *Building simulation*, 4(2):149–167, 2011.

[25] Ian Richardson, Murray Thomson, and David Infield. A high-resolution domestic building occupancy model for energy demand simulations. *Energy and Buildings*, 40(8):1560–1566, 2008.

[26] Varick L Erickson, Yiqing Lin, Ankur Kamthe, Rohini Brahme, Amit Surana, Alberto E Cerpa, Michael D Sohn, and Satish Narayanan. Energy efficient building environment control strategies using real-time occupancy measurements. In *Proceedings of the First ACM Workshop on Embedded Sensing Systems for Energy-Efficiency in Buildings*, pages 19–24. ACM, 2009.

[27] Varick L Erickson, Miguel Á Carreira-Perpiñán, and Alberto E Cerpa. Observe: Occupancy-based system for efficient reduction of hvac energy. In *Information Processing in Sensor Networks (IPSN), 2011 10th International Conference on*, pages 258–269. IEEE, 2011.

[28] Chenda Liao, Yashen Lin, and Prabir Barooah. Agent-based and graphical modelling of building occupancy. *Journal of Building Performance Simulation*, 5(1):5–25, 2012.

[29] Zheng Yang and Burcin Becerik-Gerber. Modeling personalized occupancy profiles for representing long term patterns by using ambient context. *Building and Environment*, 78:23–35, 2014.

[30] Christopher M Stoppel and Fernanda Leite. Integrating probabilistic methods for describing occupant presence with building energy simulation models. *Energy and Buildings*, 68:99–107, 2014.

[31] Kaiyu Sun, Da Yan, Tianzhen Hong, and Siyue Guo. Stochastic modeling of overtime occupancy and its application in building energy simulation and calibration. *Building and Environment*, 79:1–12, 2014.

[32] Robert H Dodier, Gregor P Henze, Dale K Tiller, and Xin Guo. Building occupancy detection through sensor belief networks. *Energy and buildings*, 38(9):1033–1043, 2006.

[33] Varick L Erickson, Stefan Achleitner, and Alberto E Cerpa. Poem: Power-efficient occupancy-based energy management system. In *Proceedings of the 12th international conference on Information processing in sensor networks*, pages 203–216. ACM, 2013.

[34] Timilehin Labeodan, Wim Zeiler, Gert Boxem, and Yang Zhao. Occupancy measurement in commercial office buildings for demand-driven control applicationsa survey and detection system evaluation. *Energy and Buildings*, 93: 303–314, 2015.

[35] Jie Zhao, Bertrand Lasternas, Khee Poh Lam, Ray Yun, and Vivian Loftness. Occupant behavior and schedule modeling for building energy simulation through office appliance power consumption data mining. *Energy and Buildings*, 82:341–355, 2014.

[36] Nan Li, Gulben Calis, and Burcin Becerik-Gerber. Measuring and monitoring occupancy with an rfid based system for demand-driven hvac operations. *Automation in construction*, 24:89–99, 2012.

[37] Bharathan Balaji, Jian Xu, Anthony Nwokafor, Rajesh Gupta, and Yuvraj Agarwal. Sentinel: occupancy based hvac actuation using existing wifi infrastructure within commercial buildings. In *Proceedings of the 11th ACM Conference on Embedded Networked Sensor Systems*, page 17. ACM, 2013.

[38] Giorgio Conte, Massimo De Marchi, Alessandro Antonio Nacci, Vincenzo Rana, and Donatella Sciuto. Bluesentinel: a first approach using ibeacon for an energy efficient occupancy detection system. In *BuildSys@ SenSys*, pages 11–19, 2014.

[39] Bing Dong, Burton Andrews, Khee Poh Lam, Michael Höynck, Rui Zhang, Yun-Shang Chiou, and Diego Benitez. An information technology enabled sustainability test-bed (itest) for occupancy detection through an environmental sensing network. *Energy and Buildings*, 42(7):1038–1046, 2010.

[40] Zheng Yang, Nan Li, Burcin Becerik-Gerber, and Michael Orosz. A systematic approach to occupancy modeling in ambient sensor-rich buildings. *Simulation*, 90(8):960–977, 2014.

[41] Aftab Khan, James Nicholson, Sebastian Mellor, Daniel Jackson, Karim Ladha, Cassim Ladha, Jon Hand, Joseph Clarke, Patrick Olivier, and Thomas Plötz. Occupancy monitoring using environmental & context sensors and a hierarchical analysis framework. *Embedded Systems for Energy-Efficient Buildings (BuildSys)*, pages 90–9, 2014.

[42] Luis M Candanedo and Véronique Feldheim. Accurate occupancy detection of an office room from light, temperature, humidity and co 2 measurements using statistical learning models. *Energy and Buildings*, 112:28–39, 2016.

[43] Robert Frodl and Thomas Tille. A high-precision ndir gas sensor for automotive applications. *IEEE Sensors Journal*, 6(6):1697–1705, 2006.

[44] James Scott, AJ Bernheim Brush, John Krumm, Brian Meyers, Michael Hazas, Stephen Hodges, and Nicolas Villar. Preheat: controlling home heating using occupancy prediction. In *Proceedings of the 13th international conference on Ubiquitous computing*, pages 281–290. ACM, 2011.

[45] Ardeshir Mahdavi and Farhang Tahmasebi. Predicting people's presence in buildings: An empirically based model performance analysis. *Energy and Buildings*, 86:349–355, 2015.

[46] Geoffrey Grimmett and David Stirzaker. *Probability and random processes*. Oxford university press, 2001.

[47] In Jae Myung. Tutorial on maximum likelihood estimation. *Journal of Mathematical Psychology*, 47(1):90–100, 2003.

[48] Philip Delff Andersen, Anne Iversen, Henrik Madsen, and Carsten Rode. Dynamic modeling of presence of occupants using inhomogeneous markov chains. *Energy and Buildings*, 69:213–223, 2014.

[49] Thomas M Cover and Joy A Thomas. *Elements of information theory*. John Wiley & Sons, 2012.

[50] Guang-Bin Huang, Qin-Yu Zhu, and Chee-Kheong Siew. Extreme learning machine: theory and applications. *Neurocomputing*, 70(1):489–501, 2006.

[51] Guang-Bin Huang, Hongming Zhou, Xiaojian Ding, and Rui Zhang. Extreme learning machine for regression and multiclass classification. *Systems, Man, and Cybernetics, Part B: Cybernetics, IEEE Transactions on*, 42(2):513–529, 2012.

[52] Vladimir Vapnik. *The nature of statistical learning theory*. Springer Science & Business Media, 2013.

[53] Ronald A Fisher. The use of multiple measurements in taxonomic problems. *Annals of eugenics*, 7(2):179–188, 1936.

[54] Petros Xanthopoulos, Panos M Pardalos, and Theodore B Trafalis. Linear discriminant analysis. In *Robust Data Mining*, pages 27–33. Springer, 2013.

[55] Wei-Yin Loh. Classification and regression trees. *Wiley Interdisciplinary Reviews: Data Mining and Knowledge Discovery*, 1(1):14–23, 2011.

[56] Khee Poh Lam, Michael Höynck, Rui Zhang, Burton Andrews, Yun-Shang Chiou, Bing Dong, and Diego Benitez. Information-theoretic environmental features selection for occupancy detection in open offices. In *Eleventh International IBPSA Conference, edited by PA Strachan, NJ Kelly and M Kummert*, pages 1460–1467. Citeseer, 2009.

[57] Tobore Ekwevugbe, Neil Brown, and Vijay Pakka. Real-time building occupancy sensing for supporting demand driven hvac operations. In *13th International Conference for Enhanced Building Operations, Montreal, Quebec*, 2013.

[58] Ron Kohavi and George H John. Wrappers for feature subset selection. *Artificial intelligence*, 97(1):273–324, 1997.

[59] Mustafa K Masood, Yeng Chai Soh, and Victor W-C Chang. Real-time occupancy estimation using environmental parameters. In *Neural Networks (IJCNN), 2015 International Joint Conference on*, pages 1–8. IEEE, 2015.

[60] Zhenghua Chen, Jinming Xu, and Yeng Chai Soh. Modeling regular occupancy in commercial buildings using stochastic models. *Energy and Buildings*, 103:216–223, 2015.

[61] M Sanjeev Arulampalam, Simon Maskell, Neil Gordon, and Tim Clapp. A tutorial on particle filters for online nonlinear/non-gaussian bayesian tracking. *Signal Processing, IEEE Transactions on*, 50(2):174–188, 2002.

[62] Zheng Yang, Nan Li, Burcin Becerik-Gerber, and Michael Orosz. A multisensor based occupancy estimation model for supporting demand driven hvac operations. In *Proceedings of the 2012 Symposium on Simulation for Architecture and Urban Design*, page 2. Society for Computer Simulation International, 2012.

[63] Christopher JC Burges. A tutorial on support vector machines for pattern recognition. *Data mining and knowledge discovery*, 2(2):121–167, 1998.

[64] Ilkka Virtanen and Paavo Yli-Olli. Forecasting stock market prices in a thin security market. *Omega*, 15(2):145–155, 1987.

[65] Javier Contreras, Rosario Espinola, Francisco J Nogales, and Antonio J Conejo. Arima models to predict next-day electricity prices. *Power Systems, IEEE Transactions on*, 18(3):1014–1020, 2003.

[66] Sangsoo Lee and Daniel Fambro. Application of subset autoregressive integrated moving average model for short-term freeway traffic volume forecasting. *Transportation Research Record: Journal of the Transportation Research Board*, (1678):179–188, 1999.

[67] Ardeshir Mahdavi and Farhang Tahmasebi. The deployment-dependence of occupancy-related models in building performance simulation. *Energy and Buildings*, 2015.

[68] Farhang Tahmasebi and Ardeshir Mahdavi. The sensitivity of building performance simulation results to the choice of occupants presence models: a case study. *Journal of Building Performance Simulation*, pages 1–11, 2015.

[69] Paramvir Bahl and Venkata N Padmanabhan. Radar: An in-building rf-based user location and tracking system. In *INFOCOM 2000. Nineteenth Annual Joint Conference of the IEEE Computer and Communications Societies. Proceedings. IEEE*, volume 2, pages 775–784. Ieee, 2000.

[70] Moustafa Youssef and Ashok Agrawala. The horus wlan location determination system. In *Proceedings of the 3rd international conference on Mobile systems, applications, and services*, pages 205–218. ACM, 2005.

[71] Nan Li, Burcin Becerik-Gerber, Bhaskar Krishnamachari, and Lucio Soibelman. A bim centered indoor localization algorithm to support building fire emergency response operations. *Automation in Construction*, 42:78–89, 2014.

[72] Nan Li, Burcin Becerik-Gerber, and Lucio Soibelman. Iterative maximum likelihood estimation algorithm: leveraging building information and sensing infrastructure for localization during emergencies. *Journal of Computing in Civil Engineering*, 29(6):04014094, 2014.

[73] Wonho Kang and Youngnam Han. Smartpdr: Smartphone-based pedestrian dead reckoning for indoor localization. *Sensors Journal, IEEE*, 15(5):2906–2916, May 2015.

[74] F. Zampella, A.R. Jimenez Ruiz, and F. Seco Granja. Indoor positioning using efficient map matching, rss measurements, and an improved motion model. *Vehicular Technology, IEEE Transactions on*, 64(4):1304–1317, April 2015. ISSN 0018-9545.

[75] Frédéric Evennou and François Marx. Advanced integration of wifi and inertial navigation systems for indoor mobile positioning. *Eurasip journal on applied signal processing*, 2006:164–164, 2006.

[76] Helena Leppäkoski, Jussi Collin, and Jarmo Takala. Pedestrian navigation based on inertial sensors, indoor map, and wlan signals. *Journal of Signal Processing Systems*, 71(3):287–296, 2013.

[77] Hui Wang, Henning Lenz, Andrei Szabo, Joachim Bamberger, and Uwe D Hanebeck. Wlan-based pedestrian tracking using particle filters and low-cost mems sensors. In *Positioning, Navigation and Communication, 2007. WPNC'07. 4th Workshop on*, pages 1–7. IEEE, 2007.

[78] Wasiq Waqar, Yuanzhu Chen, and Andrew Vardy. Incorporating user motion information for indoor smartphone positioning in sparse wi-fi environments. In *Proceedings of the 17th ACM international conference on Modeling, analysis and simulation of wireless and mobile systems*, pages 267–274. ACM, 2014.

[79] Brian Ferris, Dieter Fox, and Neil D Lawrence. Wifi-slam using gaussian process latent variable models. In *IJCAI*, volume 7, pages 2480–2485, 2007.

[80] Heba Abdelnasser, Reham Mohamed, Ahmed Elgohary, Moustafa Farid Alzantot, He Wang, Souvik Sen, Romit Roy Choudhury, and Moustafa Youssef. Semanticslam: Using environment landmarks for unsupervised indoor localization. *IEEE Transactions on Mobile Computing*, 15(7):1770–1782, 2016.

[81] Han Zou, Lihua Xie, Qing-Shan Jia, and Hengtao Wang. Platform and algorithm development for a rfid-based indoor positioning system. *Unmanned Systems*, 2(03):279–291, 2014.

[82] Stephane Beauregard and Harald Haas. Pedestrian dead reckoning: A basis for personal positioning. In *Proceedings of the 3rd Workshop on Positioning, Navigation and Communication*, pages 27–35, 2006.

[83] Gabriel Girard, Stéphane Côté, Sisi Zlatanova, Yannick Barette, Johanne St-Pierre, and Peter Van Oosterom. Indoor pedestrian navigation using foot-mounted imu and portable ultrasound range sensors. *Sensors*, 11(8):7606–7624, 2011.

[84] Antonio Ramón Jiménez Ruiz, Fernando Seco Granja, Jose Carlos Prieto Honorato, and Jorge I Guevara Rosas. Accurate pedestrian indoor navigation by tightly coupling foot-mounted imu and rfid measurements. *Instrumentation and Measurement, IEEE Transactions on*, 61(1):178–189, 2012.

[85] Seungwoo Lee, Byounggeun Kim, Hoon Kim, Rhan Ha, and Hojung Cha. Inertial sensor-based indoor pedestrian localization with minimum 802.15. 4a configuration. *Industrial Informatics, IEEE Transactions on*, 7(3):455–466, 2011.

[86] He Wang, Souvik Sen, Ahmed Elgohary, Moustafa Farid, Moustafa Youssef, and Romit Roy Choudhury. No need to war-drive: Unsupervised indoor localization. In *Proceedings of the 10th International Conference on Mobile Systems, Applications, and Services*, MobiSys '12, pages 197–210, New York, NY, USA, 2012. ACM. ISBN 978-1-4503-1301-8. doi: 10.1145/2307636.2307655. URL `http://doi.acm.org/10.1145/2307636.2307655`.

[87] Ling Bao and Stephen S Intille. Activity recognition from user-annotated acceleration data. In *Pervasive computing*, pages 1–17. Springer, 2004.

[88] Stephen J Preece, John Yannis Goulermas, Laurence PJ Kenney, and David Howard. A comparison of feature extraction methods for the classification of dynamic activities from accelerometer data. *Biomedical Engineering, IEEE Transactions on*, 56(3):871–879, 2009.

[89] Jennifer R Kwapisz, Gary M Weiss, and Samuel A Moore. Activity recognition using cell phone accelerometers. *ACM SigKDD Explorations Newsletter*, 12(2):74–82, 2011.

[90] Davide Figo, Pedro C Diniz, Diogo R Ferreira, and João MP Cardoso. Preprocessing techniques for context recognition from accelerometer data. *Personal and Ubiquitous Computing*, 14(7):645–662, 2010.

[91] Akram Bayat, Marc Pomplun, and Duc A Tran. A study on human activity recognition using accelerometer data from smartphones. *Procedia Computer Science*, 34:450–457, 2014.

[92] Lin Sun, Daqing Zhang, Bin Li, Bin Guo, and Shijian Li. Activity recognition on an accelerometer embedded mobile phone with varying positions

and orientations. In *Ubiquitous intelligence and computing*, pages 548–562. Springer, 2010.

[93] Dapeng Tao, Yonggang Wen, and Richang Hong. Multi-column bi-directional long short-term memory for mobile devices-based human activity recognition. *IEEE Internet of Things Journal*, 2016.

[94] Yunus Emre Ustev, Ozlem Durmaz Incel, and Cem Ersoy. User, device and orientation independent human activity recognition on mobile phones: challenges and a proposal. In *Proceedings of the 2013 ACM conference on Pervasive and ubiquitous computing adjunct publication*, pages 1427–1436. ACM, 2013.

[95] Haodong Guo, Ling Chen, Gencai Chen, and Mingqi Lv. Smartphone-based activity recognition independent of device orientation and placement. *International Journal of Communication Systems*, 2015.

[96] Han Zou, Hengtao Wang, Lihua Xie, and Qing-Shan Jia. An rfid indoor positioning system by using weighted path loss and extreme learning machine. In *Cyber-Physical Systems, Networks, and Applications (CPSNA), 2013 IEEE 1st International Conference on*, pages 66–71. IEEE, 2013.

[97] John S Seybold. *Introduction to RF propagation*. John Wiley & Sons, 2005.

[98] John J Craig. *Introduction to robotics: mechanics and control*. Pearson-/Prentice Hall Upper Saddle River, NJ, USA:, 2005.

[99] Android developers, 2014. `http://developer.android.com/index.html`.

[100] Moustafa Alzantot and Moustafa Youssef. Uptime: Ubiquitous pedestrian tracking using mobile phones. In *Wireless Communications and Networking Conference (WCNC), 2012 IEEE*, pages 3204–3209. IEEE, 2012.

[101] Paul D Groves. *Principles of GNSS, inertial, and multisensor integrated navigation systems*. Artech House, 2013.

[102] Harvey Weinberg. Using the adxl202 in pedometer and personal navigation applications. *Analog Devices AN-602 application note*, 2002.

[103] Amit Pande, Yunze Zeng, Aveek K Das, Prasant Mohapatra, Sheridan Miyamoto, Edmund Seto, Erik K Henricson, and Jay J Han. Energy expenditure estimation with smartphone body sensors. In *Proceedings of the 8th International Conference on Body Area Networks*, pages 8–14. ICST (Institute for Computer Sciences, Social-Informatics and Telecommunications Engineering), 2013.

[104] M Sanjeev Arulampalam, Simon Maskell, Neil Gordon, and Tim Clapp. A tutorial on particle filters for online nonlinear/non-gaussian bayesian tracking. *Signal Processing, IEEE Transactions on*, 50(2):174–188, 2002.

[105] Robert J Elliott, Lakhdar Aggoun, and John B Moore. *Hidden Markov Models*. Springer, 1994.

[106] Greg Welch and Gary Bishop. An introduction to the kalman filter, 1995.

[107] Fan Li, Chunshui Zhao, Guanzhong Ding, Jian Gong, Chenxing Liu, and Feng Zhao. A reliable and accurate indoor localization method using phone inertial sensors. In *Proceedings of the 2012 ACM Conference on Ubiquitous Computing*, pages 421–430. ACM, 2012.

[108] Henri Nurminen. Position estimation using rss measurements with unknown measurement model parameters. 2012.

[109] Subhankar Dhar and Upkar Varshney. Challenges and business models for mobile location-based services and advertising. *Communications of the ACM*, 54(5):121–128, 2011.

[110] R. Faragher and R. Harle. Location fingerprinting with bluetooth low energy beacons. *Selected Areas in Communications, IEEE Journal on*, PP(99):1–1, 2015. ISSN 0733-8716.

[111] Estimote beacons, 2015. `http://estimote.com/`.

[112] Paul Martin, Bo-Jhang Ho, Nicholas Grupen, Samuel Muñoz, and Mani Srivastava. An ibeacon primer for indoor localization: demo abstract. In *Proceedings of the 1st ACM Conference on Embedded Systems for Energy-Efficient Buildings*, pages 190–191. ACM, 2014.

[113] Hui Wang, Henning Lenz, Andrei Szabo, Joachim Bamberger, and Uwe D Hanebeck. Wlan-based pedestrian tracking using particle filters and low-cost mems sensors. In *Positioning, Navigation and Communication, 2007. WPNC'07. 4th Workshop on*, pages 1–7. IEEE, 2007.

[114] Angus FC Errington, Brian LF Daku, and Arnfinn F Prugger. Initial position estimation using rfid tags: A least-squares approach. *Instrumentation and Measurement, IEEE Transactions on*, 59(11):2863–2869, 2010.

[115] Oliver Woodman and Robert Harle. Rf-based initialisation for inertial pedestrian tracking. In *Pervasive Computing*, pages 238–255. Springer, 2009.

[116] William Wei-Liang Li, Ronald Iltis, Moe Z Win, et al. A smartphone localization algorithm using rssi and inertial sensor measurement fusion. In *Global Communications Conference (GLOBECOM), 2013 IEEE*, pages 3335–3340. IEEE, 2013.

[117] Zhi-An Deng, Ying Hu, Jianguo Yu, and Zhenyu Na. Extended kalman filter for real time indoor localization by fusing wifi and smartphone inertial sensors. *Micromachines*, 6(4):523–543, 2015.

[118] Fredrik Gustafsson, Fredrik Gunnarsson, Niclas Bergman, Urban Forssell, Jonas Jansson, Rickard Karlsson, and Per-Johan Nordlund. Particle filters for positioning, navigation, and tracking. *Signal Processing, IEEE Transactions on*, 50(2):425–437, 2002.

[119] James Diebel. Representing attitude: Euler angles, unit quaternions, and rotation vectors. *Matrix*, 58:15–16, 2006.

[120] Surapa Thiemjarus. A device-orientation independent method for activity recognition. In *Body Sensor Networks (BSN), 2010 International Conference on*, pages 19–23. IEEE, 2010.

[121] A study on instance-based learning with reduced training prototypes for device-context-independent activity recognition on a mobile phone. In *Body Sensor Networks (BSN), 2013 IEEE International Conference on*, pages 1–6. IEEE, 2013.

[122] Amin Rasekh, Chien-An Chen, and Yan Lu. Human activity recognition using smartphone. *Texas A&M Univ., Tech. Rep*, 2011.

[123] Davide Anguita, Alessandro Ghio, Luca Oneto, Xavier Parra, and Jorge L Reyes-Ortiz. A public domain dataset for human activity recognition using smartphones. In *European Symposium on Artificial Neural Networks, Computational Intelligence and Machine Learning, ESANN*, 2013.

[124] Davide Anguita, Alessandro Ghio, Luca Oneto, Xavier Parra, and Jorge L Reyes-Ortiz. Human activity recognition on smartphones using a multiclass hardware-friendly support vector machine. In *Ambient Assisted Living and Home Care*, pages 216–223. Springer, 2012.

[125] Mohammad Abu Alsheikh, Dusit Niyato, Shaowei Lin, Hwee-Pink Tan, and Zhu Han. Mobile big data analytics using deep learning and apache spark. *IEEE Network*, 30(3):22–29, 2016.

[126] Aiguo Wang, Guilin Chen, Jing Yang, Shenghui Zhao, and Chih-Yung Chang. A comparative study on human activity recognition using inertial sensors in a smartphone. *IEEE Sensors Journal*, 16(11):4566–4578, 2016.

[127] Hassan Ghasemzadeh and Roozbeh Jafari. Physical movement monitoring using body sensor networks: A phonological approach to construct spatial decision trees. *IEEE Transactions on Industrial Informatics*, 7(1):66–77, 2011.

[128] Jhun-Ying Yang, Jeen-Shing Wang, and Yen-Ping Chen. Using acceleration measurements for activity recognition: An effective learning algorithm for constructing neural classifiers. *Pattern recognition letters*, 29(16):2213–2220, 2008.